A New Generation of Hsp90 Inhibitors: Addressing Isoform Selectivity and Heat Shock Induction

By

Adam S. Duerfeldt

Submitted to the graduate degree program in Medicinal Chemistry and the graduate faculty of The University of Kansas in partial fulfillment of the requirements for the degree of Doctor of Philosophy

Committee:

_____
Brian S. J. Blagg, Ph.D
Committee Chair

_____
Thomas E. Prisinzano, Ph.D

_____
Jon A. Tunge, Ph.D

_____
Michael F. Rafferty, Ph.D

_____
Jeff P. Krise, Ph.D

Date defended: August 26th, 2011

The Dissertation Committee for Adam S. Duerfeldt certifies that this is the approved version of the following dissertation:

A New Generation of Hsp90 Inhibitors: Addressing Isoform Selectivity and Heat Shock Induction

_____

Brian S. J. Blagg, Ph.D
Committee Chair

Date approved: September 8, 2011

Abbreviations:

17-AAG = 17-allylamino-17-demethoxygeldanamycin
17-AAGH_2 = 17-allylamino-17-demethoxygeldanamycin hydroquinone hydrochloride
17-CEAG = 17-chloroethyl-17-demethoxygeldanamycin
17-CEAGH_2 = 17-chloroethyl-17-demethoxygeldanamycin hydroquinone
17-DMAG = 17-dimethylamino-17-demethoxygeldanamycin

ADP = adenosine diphosphate
Aha1 = Hsp90 co-chaperone (ATPase activator)
Akt = serine/threonine protein kinase
Ala = alanine
$AlCl_3$ = aluminum trichloride
AMP = adenosine monophosphate
AR = androgen receptor
Arg = arginine
Asn = asparagine
Asp = aspartic acid
AT13387 = Astex Therapeutics' lead small molecule Hsp90 inhibitor
ATP = adenosine triphosphate

CDK = cyclin-dependent kinase
CL = charged linker
CNF1010 = Conforma Therapeutics' small molecule Hsp90 inhibitor
CNF2020 = Conforma Therapeutics' small molecule Hsp90 inhibitor
CoQ = co-enzyme Q
cRDA = *cis*-radamide, compound **20**
CTD = *C*-terminal domain
CYP = cytochrome P450
Cys = cysteine

DCM = methylene chloride
dGrp94 = canine Grp94
dGrp94N = canine Grp94 N-terminal truncate
DMAP = 4-dimethylaminopyridine
DMF = dimethylformamide
DMSO = dimethylsulfoxide
DTT = dithiothreitol

EDCI = 1-ethyl-3-(3-dimethylaminopropyl)carbodiimide hydrochloride
eNOS = endothelial nitric oxide synthase
ER = endoplasmic reticulum
ERAD = endoplasmic reticulum-associated degradation
ES936 = NQO1 specific inhibitor
EtOH = ethanol

GDA = geldanamycin
GHKL = Family of ATPases consisting of DNA Gyrase, Hsp90, Histidine Kinase, and Mut L
Gln = glutamine
Glu = glutamic acid
Gly = glycine
GR = glucocorticoid receptor
Grp94 = glucose-regulated protein 94 kDa

H_2 = hydrogen
HBL-100 = human breast cancer cell line
HEK293 = kidney cancer cell line
Her2 = human epidermal growth factor receptor-2
hERG = human ether-á-go-go potassium ion channel
H. fuscoatra = Humicola fuscoatra
HIF = hypoxia-inducible factor
His = histidine
Hop = Hsp70/Hsp90 organizing protein
HPLC = high-performance liquid chromatography
H. sapiens = Homo sapiens
HSE = heat shock element
HSF = heat shock factor
HSP = heat shock protein family
Hsp = heat shock protein
HSR = heat shock response
hHsp90 = human Hsp90
hHsp90N = human Hsp90 N-terminal truncate
hTERT = human telomerase reverse transcriptase
HWE = Horner–Wadsworth–Emmons

KU-NG-1 = lead Grp94 inhibitor, compound **29**
KW-2478 = Kyowa Hakko Kirin's lead small molecule Hsp90 inhibitor

IC_{50} = inhibitory concentration eliciting half-maximal response
IFN-γ = interferon gamma
IGF = insulin-like growth factor
IL-12 = interleukin-12
Ile = isoleucine
IP = immunophilin
IRS = insulin receptor substrate
ITC = isothermal titration calorimetry

Kit = tyrosine protein kinase

LDA = lithium diisopropylamide
Leu = leucine
LiOH = lithium hydroxide

Lys = lysine

MAP = mitogen-activated protein
MCF-7 = estrogen receptor negative breast cancer cell line
*m*CPBA = *meta*-chloroperoxybenzoic acid
MD = middle domain
MDA-468 = human breast cancer cell line (NQO1-null)
MDA-468 (NQO1) = human breast cancer cell line NQO1 overexpressing
MDA-MB-231 = human breast cancer cell line
MDA-MB-453 = human metastatic breast cancer cell line
MeOH = methanol
Met = methionine
MET = hepatocyte growth factor receptor
MMP = matrix metalloproteinase
MPC-3100 = Myriad Pharmaceuticals' lead small molecule Hsp90 inhibitor
mRNA = messenger RNA
MTD = maximum tolerated dose

$NaClO_2$ = sodium chlorite
NADH = reduced nicotineamide-adenine dinucleotide
NaH = sodium hydride
NaH_2PO_4 = sodium dihydrogen phosphate
$NaIO_4$ = sodium periodate
NCI = National Cancer Institute
NECA = 5'-N-ethylcarboxamidoadenosine
NH_4HCO_3 = ammonium bicarbonate
NO = nitric oxide
NQO1 = NAD(P)H:quinone oxidoreductase
NSCLC = non-small cell lung cancer
NTD = *N*-terminal domain
NVP-AUY922 = Novartis' lead small molecule Hsp90 inhibitor

OsO_4 = osmium tetroxide

p23 = chaperone associated protein 23 kDa
p53 = tumor suppressor p53
Pd/C = palladium on carbon
P-gp = P-glycoprotein
Phe = phenylalanine
PI3K = phosphoinositide 3-kinase
Pro = proline

Raf = serine/threonine protein kinase
RDA = radamide
RDC = radicicol
$Rh(OAc)_2$ = rhodium acetate dimer

RIP = ribosome inhibiting protein
RNA = ribonucleic acid

Sba1 = yHsp90 co-chaperone (decreases ATPase activity)
SBDD = structure-based drug design
S. cerevisiae = *Saccharomyces cerevisiae*
Ser = serine
siRNA = small interfering RNA
SkBR3 = estrogen receptor positive breast cancer cell line
$SnCl_2$ = tin (II) chloride
SNX-5422 = Serenex's lead small molecule Hsp90 inhibitor
STA-9090 = Synta Pharmaceuticals' lead small molecule Hsp90inhibitor
Sti1 = yHsp90 co-chaperone (increases ATPase activity)

T47D = estrogen dependent human breast cancer cell line
TBAF = tetra-n-butylammonium fluoride
TBS = *tert*-butyldimethylsilyl
t-BuOH = *tert*-butanol
TFQ = tryptophan fluorescence quenching
THF = tetrahydrofurn
Thr = threonine
TK3 = non-receptor tyrosine kinase
TLR = Toll-like receptor
TNF = tumor necrosis factor
TNFR = tumor necrosis factor receptor
TRAP-1 = tumor necrosis factor receptor-associated protein
Trp = tryptophan
Tyr = tyrosine

UPR = unfolded protein response

Val = valine
VEGF = vascular endothelial growth factor
VEGFR = vascular endothelial growth factor receptor
v-Src = viral sarcoma oncoprotein

WX514 = GDA based Hsp90 selective inhibitor

XL888 = Exelixis' lead small molecule Hsp90 inhibitor

yHsp90 = yeast Hsp90 homolog

Abstract: The 90 kDa heat shock proteins (Hsp90) are molecular chaperones that are upregulated in response to cellular stress and are responsible for the conformational maturation, activation and/or stability of more than 200 client proteins. Many of these clients are oncogenic and facilitate the progression of cancer. Disruption of Hsp90's inherent ATPase activity renders the chaperone inactive, leading to degradation of substrates and ultimately, apoptosis. Consequently, Hsp90 has become a highly sought after anti-cancer target and numerous pharmaceutical companies and academic labs are expending efforts to develop novel methods to regulate the Hsp90-mediated protein folding process.

Included within the Hsp90 family are four isoforms, each of which exhibits a unique cellular localization, expression, function and clientele. Hsp90α (inducible) and Hsp90β (constitutive) both localize to the cytoplasm and share similar functions; however, recent studies have identified isoform specific substrates. Tumor necrosis factor receptor-associated protein (TRAP-1) is the Hsp90 isoform localized to the mitchondria and to date, no specific clients or selective inhibitors have been identified. The fourth isoform is glucose-regulated protein 94 kDa (Grp94), which is localized to the endoplasmic reticulum and is responsible for the maturation and stability of specific secreted and membrane bound proteins. Currently identified Hsp90 inhibitors exhibit *pan*-inhibition, resulting in the disruption of all four isoforms' ability to bind and hydrolyze ATP. This activity is believed responsible for the undesired toxicities related to Hsp90 inhibition in the clinic, as proteins that are critical to cardio function and the central nervous system are dependent upon yet to be determined Hsp90 isoforms.

Another detriment arising from N-terminal Hsp90 inhibition is induction of the pro-survival, heat shock response. Specifically, induction of the target, Hsp90, has resulted in therapeutic resistance and complications with dosing and administration protocols.

Presented herein is rationale for the development of Hsp90 isoform selective inhibitors and the first irreversible inhibitor of Hsp90 that mitigates induction of Hsp90; thus, providing key advancements towards addressing the detriments associated with Hsp90 inhibitors currently under clinical investigation.

Acknowledgments

The last 5-years have been an incredibly enjoyable experience; one resulting in friendships, collaborations, personal-growth, successes and failures. Although graduate school revolves around proving oneself competent to execute research independently, numerous people have played an intricate role in my evolution as a scientist and as a person. These are the people I owe a great debt of gratitude.

Firstly, I would like to thank my advisor Dr. Brian Blagg whose enthusiasm for science made the lab an enjoyable place to be. More than anything, I appreciate Brian's mentoring approach, as he taught me to think independently and outside-the-box. In addition, Brian has not only been a fantastic mentor, but also a colleague, friend, and confidant. I wish Brian the best of luck and look forward to a continued friendship and collegiality. With that said, I must also thank the Blagg lab members both past and present, who have been instrumental in my development as a person and as a scientist. I must give a special thank you to Laura Peterson who has served as my teammate on the Grp94 project, has been an excellent resource for scientific discussions, and an incredible friend. Also, a special thank you to Gary Brandt, who provided invaluable scientific insight throughout the years and a vat of Organic Chemistry knowledge, of which I'm still jealous of.

Secondly, I need to thank my committee members, Dr. Thomas Prisinzano, Dr. Jon Tunge, Dr. Michael Rafferty, and Dr. Jeff Krise. I thank them for not only serving on my committee, but also for providing excellent examples of what it takes to be a successful academician and scientist. Other members of the Medicinal Chemistry Department that deserve a special thank you are Norma Henley and Jane Buttenhoff, whose hard work and organization have made the administrative side of graduate school an absolute breeze.

Outside of those involved in the scientific realm of my graduate-school career, I must thank the funding mechanisms that support me. Thank you to IAMI and the Self Graduate Fellowship programs for extracurricular training that has made me a well-rounded academic. I thoroughly enjoyed the experiences of both fellowships and will remain involved with both as a supportive alumnus.

I need to also thank Scott Weir for his mentorship and introducing me to The University of Kansas Medicinal Chemistry Department. Scott's support has been a source of confidence and he will continue to be a valuable mentor as my career progresses.

Lastly, I must thank those outside the world of The University of Kansas, my family and friends. I have met a lot of inspiring people during my time in Lawrence, Kansas who have provided enough memories and friendships to last a life time. I must give a special thank you to Katie, who has provided unbelievable support as I finished my PhD requirements.

And to my family, I will forever be in debt for the amount of support they have provided. My family has been my biggest support mechanism in every aspect of life and to say I owe everything to them is an understatement.

I dedicate this work to Timothy Yates Heggen (1983-2002) and Evan Korynta:

Whose fight has inspired and motivated me more than they will ever know.

Table of Contents

List of Sections:

Chapter I
An Introduction to Hsp90 and Hsp90 Inhibitors Under Clinical Evaluation

I.1 Molecular Chaperones ---- 1

I.2 Heat Shock Protein 90 kDa ---- 2

I.2.1 Architecture and Energy Requirements of Hsp90 ---- 3

I.2.2 Hsp90 Isoforms ---- 5

Cytosolic Hsp90α and Hsp90β ---- 5

Mitochondrial TRAP-1 ---- 6

Endoplasmic Reticulum Localized Grp94 ---- 7

I.2.3 Natural Product Inhibitors of Hsp90 ---- 8

I.3 Clinical Candidate Profiles ---- 12

I.3.1 Ansamycin-derived Inhibitors ---- 12

I.3.2 Benzamide Inhibitors ---- 15

I.3.3 Purine Inhibitors ---- 16

I.3.4 Resorcinylic Inhibitors ---- 17

I.3.5 Other Inhibitors ---- 18

I.4 Biological Concerns with Hsp90 Inhibition ---- 18

I.4.1 Resistance ---- 19

Mutations ---- 19

Heat Shock Response ---- 21

Aberrant Function of Co-chaperones ---- 22

I.4.2 Genetic Polymorphisms ---- 23

I.4.3 Downstream Biological Effects ---------- 25

I.5 Concluding Remarks: The Next Generation of Hsp90 Inhibitors ---------- 26

I.6 References ---------- 29

Chapter II
***cis*-Radamide Analogs: Conformationally Constrained Chimeric N-terminal Hsp90 Inhibitors**

II.1 Rationale for the Development of *cis*-Amide Inhibitors ---------- 45

II.2 Synthesis of *cis*-Radamide Analogs ---------- 48

II.3 Biological Evaluation of *cis*-Radamide Analogs ---------- 51

II.3.1 Anti-proliferative Activity ---------- 51

II.3.2 Inhibition of Hsp90 ATPase Activity ---------- 51

II.3.3 Western Blot Analyses ---------- 52

II.4 Interaction of *cis*-Radamide with Hsp90 and Grp94 ---------- 53

II.4.1 Co-crystal Structure of cRDA Bound to Hsp90 ---------- 53

II.4.2 Binding Affinity of cRDA for Hsp90 and Grp94 ---------- 56

II.5 Concluding Remarks ---------- 57

II.6 Methods and Experimentals ---------- 58

II.7 References ---------- 70

Chapter III
Design and Synthesis of Proposed Grp94 Selective Inhibitors

III.1 Introduction to Grp94 ---------- 75

III.2 Structure ---------- 76

III.3 Cellular Functions of Grp94 ---------- 77

III.4 Known Ligands: Non-Selective and Selective ---------- 78

III.4.1 Endogenous Ligand: ATP ---------- 79

III.4.2 Geldanamycin ---------- 81

III.4.3 Isoform Selective Inhibitor: N-ethylcarboxamidoadenosine---------- 84

III.5 Proposal of Grp94 Selective Inhibitors ---------- 86

III.5.1 Quinone Substitution ---------- 87

III.5.2 Incorporation of a *cis*-Amide Bioisostere ---------- 89

III.6 Synthesis of Proposed Grp94 Selective Inhibitors ---------- 91

III.6.1 Synthesis of *des*-Quinone Analogs ---------- 92

III.6.2 Synthesis of Imidazole Bioisosteric Analogs ---------- 92

III.7 Concluding Remarks---------- 92

III.8 Methods and Experimentals ---------- 93

III.9 References---------- 103

Chapter IV
Biological Evaluation of Proposed Grp94 Selective Inhibitors

IV.1 Biological Roles of Grp94: Implications for Grp94 Inhibition ---------- 109

IV.1.1 Grp94 and Cancer ---------- 109

IV.1.2 Grp94 and Inflammation ---------- 111

IV.2 Biological Evaluation of Grp94 Selective Inhibitors---------- 112

IV.2.1 Anti-proliferative Activity ---------- 112

IV.2.2 Inhibition of Toll-Trafficking: A Grp94 Functional Assay ---------- 113

des-Quinone Analogs ---------- 114

Imidazole *cis*-Amide Bioisostere Analogs ---------- 116

IV.3 Biological Profile of KU-NG-1 ---------- 119

IV.3.1 Western Blot Confirmation for Lack of Hsp90 Inhibition ---------- 119

IV.3.2 NCI Cell Panel Profile---------- 120

IV.3.3 Binding Data for KU-NG-1 ---------- 122

IV.4 Future Directions and Concluding Remarks ---------- 124

IV.5 Methods and Experimentals ---------- 126

IV.6 References ---------- 127

Chapter V
The Design, Synthesis and Biological Evaluation
of a Pro-mustard Irreversible Alkylator of Hsp90

V.1 Rationale for an Irreversible Hsp90 Alkylator ---------- 133

V.2 Design of 17-CEAG ---------- 134

V.3 Synthesis of 17-CEAG ---------- 136

V.4 Biological Evaluation of 17-CEAG ---------- 136

V.4.1 NQO1 Reduction Dependence ---------- 137

V.4.2 Anti-proliferative Activity ---------- 138

V.4.3 Western Blot Analyses ---------- 140

V.5 Future Studies and Concluding Remarks ---------- 142

V.6 Methods and Experimentals ---------- 143

V.7 References ---------- 144

List of Figures:

Chapter I
An Introduction to Hsp90 and Hsp90 Inhibitors Under Clinical Evaluation

Figure 1: Six Hallmarks of Cancer ---- 3

Figure 2: Hsp90 Protein Folding Cycle ---- 4

Figure 3: Natural Product Inhibitors of Hsp90 ---- 8

Figure 4: Natural Product Interactions with Hsp90 ---- 10

Figure 5: 17-amino Substituted Ansamycins ---- 13

Figure 6: Benzamide Inhibitor: SNX-5422 ---- 15

Figure 7: Purine Inhibitor: CNF2024 (BIIB021) ---- 17

Figure 8: Resorcinylic Inhibitor: NVP-AUY922 ---- 17

Figure 9: Consequences of *H. fuscoatra* L34I Mutation ---- 19

Chapter II
***cis*-Radamide Analogs: Conformationally Constrained**
Chimeric N-terminal Hsp90 Inhibitors

Figure 10: Example N-terminal Hsp90 Inhibitors ---- 45

Figure 11: Conformational Comparison of RDC ---- 46

Figure 12: Conformational Comparison of GDA ---- 47

Figure 13: Chimeric N-terminal Hsp90 Inhibitors ---- 48

Figure 14: Mechanism of Coupled ATPase Activity ---- 51

Figure 15: Western Blots of Representative *cis*-RDA Analogs ---- 53

Figure 16: Co-crystal Structures of RDA and cRDA ---- 54

Figure 17: Resorcinylic Interactions of RDA and cRDA with Hsp90 ---- 54

Figure 18: RDA Quinone Interactions with yHsp90N ---- 55

Figure 19: cRDA Quinone Intereactions with hHsp90N ---- 55

Figure 20: TFQ Binding Affinity Curves for RDA and cRDA ---------- 56

Chapter III
Design and Synthesis of Proposed Grp94 Selective Inhibitors

Figure 21: Human Grp94 Expression Profile---------- 76

Figure 22: Sequence Alignment of dGrp94 and hHsp90α---------- 77

Figure 23: Known Grp94 Client Proteins ---------- 78

Figure 24: ADP Clash with Gly196 of Grp94---------- 79

Figure 25: Lid Region Comparison of ADP Bound yHsp90N and dGrp94N ---------- 80

Figure 26: Comparison of Isoform N-terminal Binding Domain Electrostatics---------- 81

Figure 27: apo-Grp94 Gly196/GDA Clash ---------- 82

Figure 28: GDA·dGrp94N Co-crystal Structure ---------- 83

Figure 29: Structure of WX514---------- 83

Figure 30: Structure of NECA ---------- 84

Figure 31: NECA Interactions with Grp94 ---------- 85

Figure 32: RDA·yHsp90 and RDA·dGrp94N Co-crystal Structure Comparison ---------- 87

Figure 33: Quinone Interactions Between RDA, yHsp90N and dGrp94N---------- 87

Figure 34: Proposed *des*-Quinone Analogs ---------- 88

Figure 35: Proposed Imidazole Linker Evaluation ---------- 89

Figure 36: Proposed Imidazole Analogs Based Upon **29**---------- 90

Figure 37: Proposed Alkyl Imidazoles ---------- 91

Chapter IV
Biological Evaluation of Proposed Grp94 Selective Inhibitors

Figure 38: Toll-trafficking Assay ---------- 114

Figure 39: Confocal Comparison of Functional Grp94 and Grp94 Targeted siRNA------- 114

Figure 40: *des*-Quinone Analogs ---------- 115

Figure 41: Confocal Microscopy Results for **26** ---------- 115

Figure 42: Imidazole Linker Lengths ---------- 116

Figure 43: Confocal Microscopy Results for **29** (KU-NG-1) ---------- 117

Figure 44: Imidazole Analogs Based Upon **29** ---------- 117

Figure 45: Alkyl Imidazoles ---------- 119

Figure 46: Western Blot Analysis of KU-NG-1 ---------- 119

Figure 47: NCI 60-cell Panel Cytotoxicity Results of KU-NG-1 ---------- 121

Figure 48: ITC Binding Curves for KU-NG-1 ---------- 123

Figure 49: TFQ Binding Curves for KU-NG-1 ---------- 123

Chapter V
The Design, Synthesis and Biological Evaluation
of a Pro-mustard Irreversible Alkylator of Hsp90

Figure 50: HSF-1 Mediated Induction of the HSR ---------- 133

Figure 51: Structure of 17-CEAG ---------- 135

Figure 52: NQO1 Mediated Reduction of 17-CEAG ---------- 135

Figure 53: 17-CEAG and 17-AAG Overlay ---------- 136

Figure 54: HPLC Evidence for NQO1 Mediated Reduction of 17-CEAG ---------- 137

Figure 55: Affect of ES936 on NQO1 Reduction of 17-CEAG ---------- 138

Figure 56: HPLC Analysis of NQO1 Mediated 17-CEAG Reduction in Cells ---------- 139

Figure 57: Western Blot Analyses of 17-CEAG ---------- 140

Figure 58: Western Blot Densitometry for 17-AAG ---------- 141

Figure 59: Western Blot Densitometry for 17-CEAG ---------- 141

List of Schemes:

Chapter II
***cis*-Radamide Analogs: Conformationally Constrained Chimeric N-terminal Hsp90 Inhibitors**

Scheme 1: Retrosynthetic Analysis for *cis*-RDA Analogs ---------- 48

Scheme 2: Synthesis of *cis*-Amide Phosphonate---------- 49

Scheme 3: Synthesis of Homologated Aldehydes ---------- 49

Scheme 4: Fragment Coupling and Deprotection---------- 50

Chapter III
Design and Synthesis of Proposed Grp94 Selective Inhibitors

Scheme 5: Synthetic Route to *des*-Quinone Analogs ---------- 92

Scheme 6: Synthetic Route to 1,2-Imidazole Analogs ---------- 92

Chapter V
The Design, Synthesis and Biological Evaluation of a Pro-mustard Irreversible Alkylator of Hsp90

Scheme 7: Synthesis of 17-CEAG ---------- 136

List of Tables:

Chapter I
An Introduction to Hsp90 and Hsp90 Inhibitors Under Clinical Evaluation

Table 1: Principle Heat Shock Proteins ---------- 2

Table 2: Reported Hsp90 Mutations and Biological Consequences ---------- 20

Table 3: Aberrant Co-chaperone Affects ---------- 22

Chapter II
***cis*-Radamide Analogs: Conformationally Constrained**
Chimeric N-terminal Hsp90 Inhibitors

Table 4: Anti-proliferative and ATPase Activity of *cis*-RDA Analogs ---------- 51

Chapter III
Design and Synthesis of Proposed Grp94 Selective Inhibitors

Table 5: Surflex Binding Scores for Analogs **28**–**32** ---------- 89

Chapter IV
Biological Evaluation of Proposed Grp94 Selective Inhibitors

Table 6: MTS Anti-proliferative and Toll-trafficking Results for Analogs **25**–**43** ---------- 113

Table 7: Binding Affinity Data for KU-NG-1 ---------- 122

Chapter V
The Design, Synthesis and Biological Evaluation
of a Pro-mustard Irreversible Alkylator of Hsp90

Table 8: Anti-proliferative Data for 17-CEAG ---------- 139

A New Generation of Hsp90 Inhibitors: Addressing Isoform Selectivity and Heat Shock Induction

Chapter I

An Introduction to Hsp90 and Hsp90 Inhibitors Under Clinical Evaluation

I.1 Molecular Chaperones

The ability of organisms to maintain a cellular environment consistent with vitality and well-being is referred to as homeostasis. Multiple pathways regulate cellular homeostasis, many of which consist of feedback mechanisms that are critical to maintaining a viable cellular environment. One of the most important aspects of cellular homeostasis is the ability to maintain the conformation of intracellular proteins, which encompasses their folding, stability, activation, trafficking and degradation. This maintenance is provided by a group of unrelated protein families referred to as molecular chaperones.[1-6]

As essential components of cellular viability, molecular chaperones respond to cellular stress, and mitigate the effects of extra- or intra-cellular stressors. Molecular chaperones interact with unfolded or partially folded proteins, to expedite the formation of biologically active structures, or remove the denatured substrates *via* degradation mechanisms. Proteins that depend upon or interact with molecular chaperones are termed clients, and each molecular chaperone interacts with a unique set of clients, with some chaperones exhibiting more selectivity than others.[3, 5] One class of molecular chaperone that has recently received significant attention is the heat shock protein family (HSP). Consistent with the name of this class, HSP expression is increased upon cellular stress, including elevated temperatures. However, induction can also result upon toxic insult,[7] inflammation,[8] hypoxia,[9] infection,[10] and/or nutrient starvation.[11] The increase of HSPs is a major constituent of the heat shock response (HSR), which is activated through the transcription factor, heat shock factor-1 (HSF-1), and the heat shock element (HSE), resulting in gene upregulation.[12]

The HSP family consists of multiple members that are named according to their molecular weight. For example, Hsp90 refers to a subset of heat shock proteins with a molecular weight of ~90 kDa. The principle HSPs are presented in Table 1. The upregulation of HSPs in response to cellular stressors has led to their implication in the progression of many disease states, highlighting their potential chemotherapeutic utility.[4, 13, 14]

Table 1: Principle heat shock proteins.

Family	Localization	Function(s)
Small Hsps (12-43 kDa)	cytosol	general chaperone, co-factor
Hsp60	mitochondria, cytosol, extracellular	mitochondrial protein folding
Hsp70	cytosol, lysosome, mitochondria	protein folding
Hsp90	cytosol, mitochondria, endoplasmic reticulum, extracellular	protein folding, activation, stabilization, cell signaling
Hsp100	mitochondria	solubilization of protein aggregates

I.2 Heat Shock Protein 90 kDa

Heat shock protein 90 kDa (Hsp90) is one of the most abundant ATPases in eukaryotic organisms, comprising ~1-2% of total cellular protein under non-stressed conditions.[15, 16] Upon introduction of stress, intracellular Hsp90 is increased to ~4-6% of total protein concentration.[16] In unstressed cells, Hsp90 exists in a latent state and aids homeostasis through transient protein folding assistance, intracellular transport, maintenance and degradation. Under stressed conditions, especially in malignancies, Hsp90 is upregulated to handle the increased demand of client proteins for the conformationally viable states induced by the chaperone. Furthermore, in stressed conditions, Hsp90 exists in a heteroprotein complex that exhibits higher affinity for ATP.[17] Thus, the prevalence of a high-affinity state, an addiction of cancer cells to oncogenic client proteins, and a greater dependency upon Hsp90 have supported Hsp90 inhibition as a novel chemotherapeutic target for the treatment of cancer.[18-21] In addition, Hsp90 is responsible

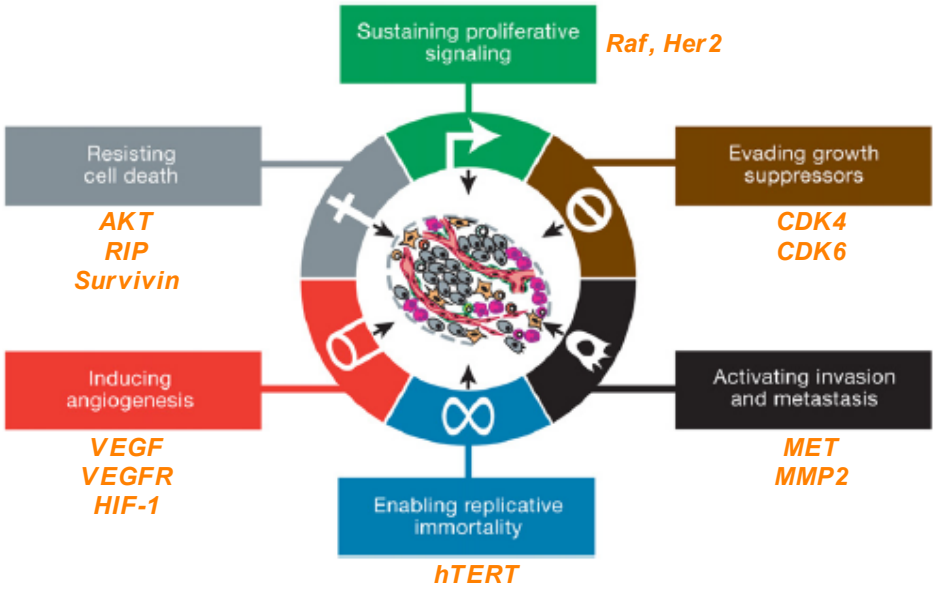

Figure 1. Six hallmarks of cancer. Example Hsp90 clients involved in each hallmark are listed in orange.[23]

for clientele that maintain critical roles in all six hallmarks of cancer (Figure 1).[22-24] Therefore, Hsp90 inhibition results in simultaneous disruption of all six events that are necessary for oncogenesis.[25]

I.2.1 *Architecture and Energy Requirements of Hsp90*

Hsp90 chaperones exist as homodimers, with each monomer consisting of an N-terminal regulatory domain (NTD), a charged linker (CL), a middle domain (MD) and a C-terminal dimerization domain (CTD) (Figure 2).[16] Hsp90 chaperone activity is linked to an ATP-driven conformational change within the NTD, leading to the closure of a helix-loop-helix "lid" over the ATP binding pocket.[26] This lid closure allows for a transient NTD dimerization that stabilizes alignment of the catalytic residues from the NTD and MD of the protein, resulting in ATP hydrolysis.[27]

Hsp90 is a member of the GHKL superfamily, which consists of DNA Gyrase, Hsp90, Histidine Kinase and Mut L. This superfamily contains a Bergerat-type ATP-binding domain

that binds nucleotides in a bent conformation, which is in contrast to other ATPases that bind nucleotides in a linear fashion. Mut L and Histidine kinase represent the other two members of this class expressed in the human genome.[28] Thus, Hsp90 inhibitors exhibit excellent selectivity due to the unique binding geometry not accommodated by other ATPases.

As shown in Figure 2, nascent polypeptides are delivered to the Hsp90 homodimer *via* heat shock proteins 70 kDa (Hsp70) and 40 kDa (Hsp40) along with Hsp70/Hsp90 organizing protein (Hop).[29] Upon transfer of the substrate (client) to Hsp90 (**1.2**),[30] client-dependent immunophilins and co-chaperones associate with the complex to form the activated heteroprotein complex (**1.3**).[27] This activated complex exhibits a high affinity for N-terminal ligands, including ATP and competitive inhibitors.[17] Upon binding ATP, N-terminal dimerization (**1.4**) occurs,[26] followed by the binding of p23, which facilitates the hydrolysis of ATP to ADP (**1.5**).[31] This hydrolysis provides the requisite energy for client folding, which yields the biologically active client (**1.6**), and releases Hsp90 (**1.1**) for future catalytic turnover.[27, 32] Introduction of a

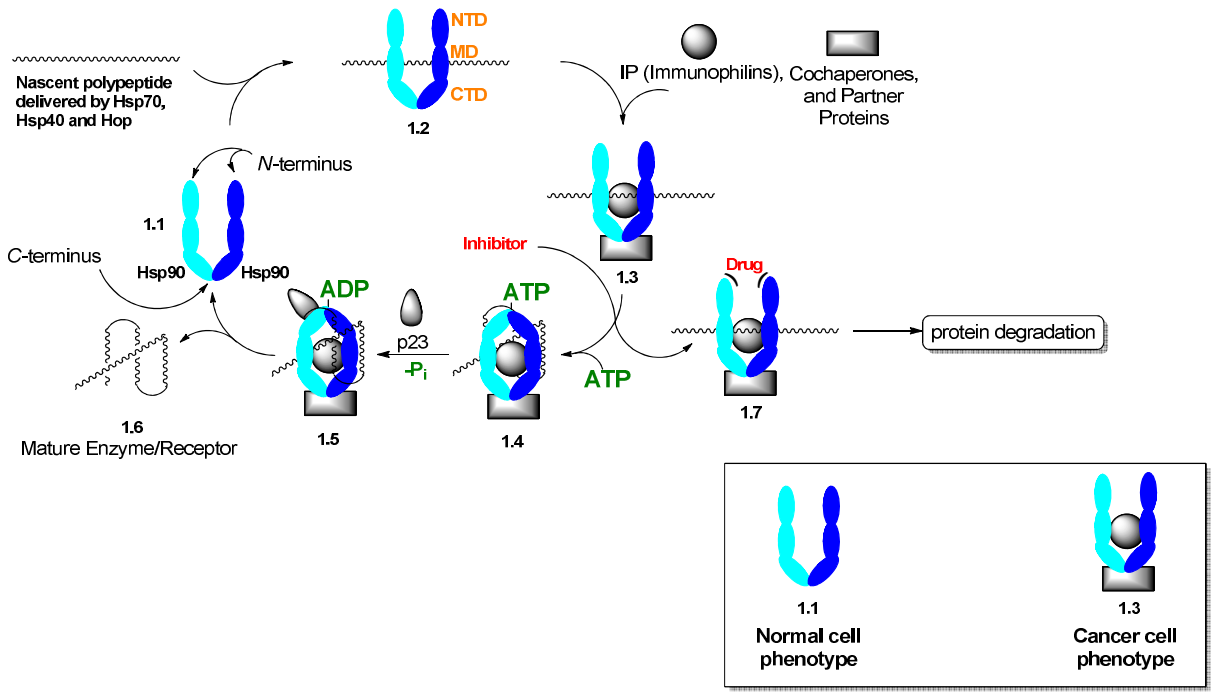

Figure 2. Hsp90 protein folding cycle.[32]

competitive ATP-inhibitor, arrests the substrate bound complex (**1.7**), resulting in ubiquitinylation of the client and subsequent degradation *via* the proteasome.[33, 34]

I.2.2 *Hsp90 Isoforms*

Four isoforms of Hsp90 are expressed in the human genome including cytoplasmic Hsp90α (inducible) and Hsp90β (constitutive); tumor necrosis factor receptor-associated protein (TRAP-1), which is localized to the mitochondria; and glucose-regulated protein (Grp94), which is localized to the endoplasmic reticulum.[35, 36] Similarities between the isoforms include 1) native existence as obligate homodimers; 2) dependence upon ATP-binding and hydrolysis; 3) a characteristic Bergerat-fold N-terminal ATP-binding pocket and 4) similar architecture including a NTD, MD and CTD.[37] However, amongst the isoforms differences have been observed, which has led to investigations aimed at elucidating the biological roles of each isoform.

Cytosolic Hsp90α and Hsp90β

Cytosolic Hsp90 has received the most attention from the Hsp90 research community. Numerous crystal and co-crystal structures have been solved for the cytosolic forms of Hsp90 and the list of identified clients continues to grow. Substrates of cytosolic Hsp90 encompass a vast array of proteins necessary for cellular function including protein kinase signaling proteins (Her2, Raf, Akt), mutated signaling proteins (p53, Kit, TK3), transcription factors (steroid hormone receptors: GR, AR), angiogenic factors (HIF–1α), telomerase, and cell-cycle regulators (CDK4 and CDK6).[22] As such, cytosolic Hsp90 is responsible for the conformational maturation of enzymes implicated in all six hallmarks of cancer (Figure 1). Thus, it was hypothesized that inhibition of cytosolic Hsp90 would result in simultaneous disruption of all six hallmarks of cancer, providing a ‘magic bullet’ chemotherapeutic target. However, no Hsp90 inhibitor has been approved by the FDA at present.

Hsp90α and Hsp90β exhibit ~95 % sequence homology at the ATP-binding region,[36] which has limited the potential for designing Hsp90α versus Hsp90β isoform selective inhibitors. With the lack of isoform specific inhibitors, it has been difficult to identify isoform dependent clients. However, function and expression profiles of the two paralogs have been analyzed through siRNA techniques. Constitutively active Hsp90β maintains key roles in early embryonic development, germ cell maturation, cytoskeletal stabilization, cellular transformation, signal transduction and long-term cell adaptation. In contrast, the inducible form, Hsp90α, is essential for the promotion of growth, cell cycle regulation and stress-induced cytoprotection.[37] Specific cellular functions of the two isoforms, suggest that each interacts with a unique subset of client proteins and co-chaperones. As a consequence, the client proteins and co-chaperones proposed to interact with "cytosolic Hsp90" are undergoing more thorough investigation to identify which isoforms they interact with. For this reason, the abbreviation, Hsp90 is accepted to encompass both cytosolic isoforms and will be used in this manner for the remainder of this dissertation.

Mitchondrial TRAP-1

Tumor necrosis factor (TNF) receptor-associated protein 1 (TRAP-1) was discovered upon its interaction with the intracellular domain of type 1 TNF receptor (TNFR-1).[38] Subsequent characterization of TRAP-1 showed ~35% identity and ~50% overall similarity with cytosolic Hsp90, and a ~70% similarity of the N-terminal ATP binding domain.[38, 39] Furthermore, several known N-terminal inhibitors of cytosolic Hsp90 (discussed in-depth in section I.2.3) also competitively inhibit ATP binding to TRAP-1.[40] In addition, every amino acid shown *via* mutational analysis to be essential for ATP binding to Hsp90 is conserved in the TRAP-1 N-terminal ATP-binding pocket.[35, 36] Thus, due to the structural conservation at the N-

terminal binding pocket, no TRAP-1 selective small molecule inhibitor has been developed to date.

Structurally, TRAP-1 lacks the charged linker connecting the N-terminal and middle domains noted in cytosolic Hsp90. Furthermore, TRAP-1 only exhibits ~23% identity with cytosolic Hsp90 in the C-terminal domain[35] and lacks the MEEVD tetratricopeptide repeat region responsible for the interactions with many co-chaperones. Thus, it is not surprising that TRAP-1 fails to interact with cytosolic Hsp90 co-chaperones including tumor suppressor p23 and Hop.[39] Therefore, it is hypothesized that TRAP-1 exhibits unique cellular functions and interacts with a specific set of client proteins and co-chaperones distinct from those that interact with cytosolic Hsp90. Identification of TRAP-1 selective inhibitors would be instrumental in delineating the biological function of this Hsp90 isoform. However, to date, no solution, crystal or co-crystal structures have been solved for TRAP-1, which has made structure-based ligand design difficult.

Endoplasmic Reticulum Localized Grp94

Glucose-regulated protein 94 kDa (Grp94) was first reported in 1977 upon the observation that its induction coincided with glucose deprivation.[41] Subsequent studies have revealed additional functions of Grp94 leading to alternative names such as gp96 and endoplasmin.[42] Unlike TRAP-1, co-crystal structures of Grp94 have been solved; however, no selective small molecule inhibitors have been developed.

Structurally, Grp94 exhibits ~50% overall identity with cytosolic Hsp90 in the N-terminal domain; nonetheless, the amino acids required for ligand binding are completely conserved.[43] The primary sequence for Grp94, however, contains a 3–5 species-dependent amino acid insertion, which has been shown to perturb the tertiary structure of the N-terminal

ATP-binding pocket.[43] This perturbation may provide an opportunity for ligand selectivity and is therefore hypothesized for use in the design of selective inhibitors. As with TRAP-1, Grp94 also lacks the TPR domain required for interaction with cytosolic Hsp90 co-chaperones, which suggests Grp94 operates under a unique regulatory mechanism and interacts with a distinct set of client proteins.[44, 45]

Recently, Grp94 has garnered considerable attention for its involvement in the biological maturation of secretory and membrane proteins including Toll-like receptors, integrins and growth factors.[46] Furthermore, Grp94 has been implicated in apoptosis protection,[47] cancer progression,[48] immunomodulation[46] and drug resistance.[49] Thus, Grp94 has garnered the attention of the Hsp90 community as a novel target for diseases ranging from cancer to immunological conditions. Grp94 is discussed in detail in Chapter III.

I.2.3 *Natural Product Inhibitors of Hsp90*

Known inhibitors of Hsp90 ATPase activity (Figure 3) include the natural products geldanamycin (GDA) and radicicol (RDC). Geldanamycin, a benzoquinone ansamycin antibiotic, was first isolated from the broth of *Streptomyces hygroscopicus* during the 1970s.[50] The first antitumor activity for GDA was reported nearly 20 years later, and the mode of action was believed to result from tyrosine kinase inhibition, due to its ability to reverse v-Src transformed cells into normal phentoypes.[51, 52] Subsequent studies revealed GDA to bind the N-terminal ATP-binding site of Hsp90, resulting in disruption of v-Src's maturation.[53]

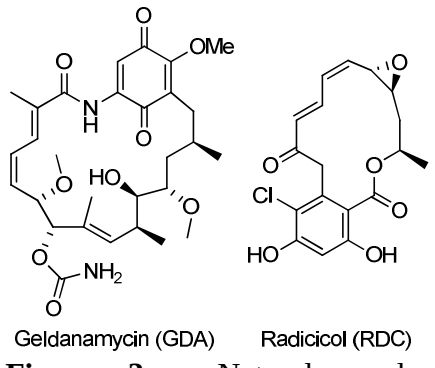

Figure 3. Natural product inhibitors of Hsp90.

Radicicol, a natural product that maintains antifungal properties, was originally isolated from the

fungus *Monosporium bonorden* in 1953.[54] Subsequent studies revealed RDC to be a potent inhibitor of Hsp90 through competitive inhibition of the N-terminal ATP-binding domain.[55, 56] The identification of GDA and RDC as potent natural product inhibitors of the Hsp90 N-terminal binding domain has been instrumental towards the delineation of the biological functions manifested by Hsp90 and for the facilitation of small molecule Hsp90 inhibitor development.

The co-crystal structures of adenosine nucleotides, GDA and RDC with Hsp90 have been solved, and have elucidated the key interactions of each ligand in the N-terminal nucleotide-binding pocket (Figure 4). The co-crystal structure of GDA bound to Hsp90 revealed the quinone moiety of GDA to occupy the diphosphate region of the binding pocket and to provide five hydrogen-bonding interactions with the protein (**B**, Figure 4).[57] In contrast, the 2,4-diphenol of RDC occupies the binding region normally occupied by the adenine ring of ATP, producing three important hydrogen-bonding interactions with Hsp90 (**C**, Figure 4). The chlorine atom in RDC projects into a large hydrophobic cavity that is surrounded by aromatic amino acids.[57] Unlike the quinone ring of GDA, only one hydrogen bond is formed between the oxirane of RDC and the phosphate-binding region.[57] Although GDA and RDC show no obvious structural compatibility with Hsp90's endogenous ligand, ATP, each natural product binds with high affinity through a network of specific hydrogen bonding interactions. Thus, both natural products have served as templates for the design of Hsp90 inhibitors; even though the biological profile exhibited by GDA and RDC limits their clinical utility.

GDA produces toxicity unrelated to Hsp90 inhibition and suffers from poor solubility.[58-61] Quinones are redox-active and recent studies have shown GDA to be a substrate for P-450 reductases.[62, 63] Upon reduction by these enzymes, GDA is converted to a semiquinone and upon

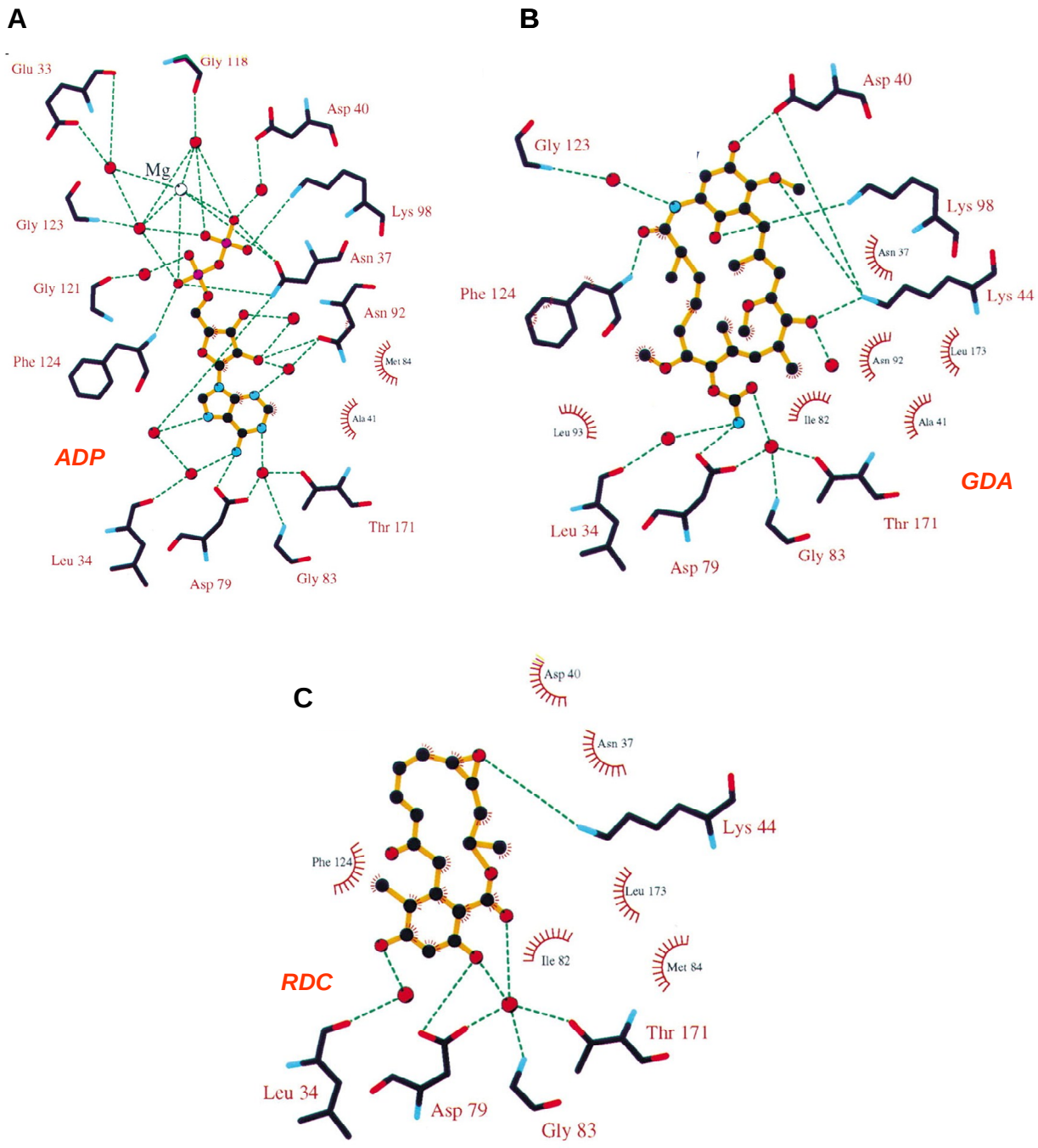

Figure 4. Schematic depictions of ligand interactions with the N-terminal domain of Hsp90. A) ADP, B) GDA, and C) RDC.[57]

exposure to oxygen, generates superoxide radicals.[62, 63] Superoxide radicals cause cell death in an Hsp90-independent manner. Therefore, new Hsp90 inhibitors lacking redox-active functionalities are being pursued to circumvent these effects.

In contrast to GDA, RDC lacks *in vivo* activity, despite its higher affinity for the N-terminal ATP-binding domain (GDA: K_d = 1.2 μM / RDC: K_d = 19 nM).[57] *In vivo*, the electrophilic nature of the α,β,γ,δ–unsaturated carbonyl moiety and the allylic epoxide result in rapid conversion to inactive compounds that have little or no affinity for Hsp90.[64, 65] Replacement of the epoxide ring of RDC with a cyclopropane moiety resulted in cycloproparadicicol, which displays potent activity against several cancer cell lines and is being investigated further.[65]

Although the clinical utility of GDA and RDC has been dismissed, the natural products have been instrumental in delineating selectivity of Hsp90 inhibitors towards malignant cells. Studies have shown that Hsp90 inhibitors accumulate in tumor cells and exhibit high differential selectivity.[17, 66] Recent immunoprecipitation experiments have demonstrated Hsp90 from malignant cells to exist in a heteroprotein complex consisting of client proteins and co-chaperones (**1.3**, Figure 2); whereas Hsp90 from normal cells was isolated as the uncomplexed homodimer (**1.1**, Figure 2).[17] The heteroprotein complex in tumor cells demonstrates ~100-fold higher affinity for the semi-synthetic GDA derivative, 17-AAG. Furthermore, upon incubation of the isolated heteroprotein complex with ATP, a significantly higher ATPase activity was measured than exhibited by homodimeric Hsp90; thus demonstrating that the heteroprotein complex not only exhibits higher affinity for N-terminal inhibitors but also for the natural substrate.[17] Subsequent studies revealed ATPase activity of the heteroprotein complex to be inhibited at lower concentrations of inhibitors than observed for homodimeric Hsp90.[17] These

results justify the differential selectivity manifested by N-terminal Hsp90 inhibitors for malignant cells over normal cells and demonstrate a promising therapeutic window.

I.3 Clinical Candidate Profiles

Co-crystal structures of Hsp90 bound to numerous ligands have been solved, which has led to structure-based ligand design efforts. These efforts have largely aimed at developing inhibitors for cytosolic Hsp90, as Hsp90α and Hsp90β have proven more prone to co-crystallization. As a result, small molecule inhibitors of Hsp90 are evaluated for inhibitory activity against the cytosolic forms of Hsp90; however, the results also suggest *pan*-inhibition against all Hsp90 isoforms.[61] At present no research group has been successful towards the rational design of isoform selective inhibitors.

I.3.1 Ansamycin-derived Inhibitors

Despite promising anti-tumor activity both *in vitro* and *in vivo*, clinical evaluation of GDA was halted due to metabolic instability, poor solubility and unfavorable toxicity profiles at therapeutically relevant doses. Furthermore, GDA is a P-glycoprotein (P-gp) substrate and is often effluxed from cells prior to eliciting its biological action.[67] Upregulation of P-gp pumps is recognized as a mechanism for drug resistance in transformed cells. Consequently, analogs based on the benzoquinone ansamycin scaffold have been pursued with the objective of improving physicochemical and pharmacological properties amenable to clinical use.

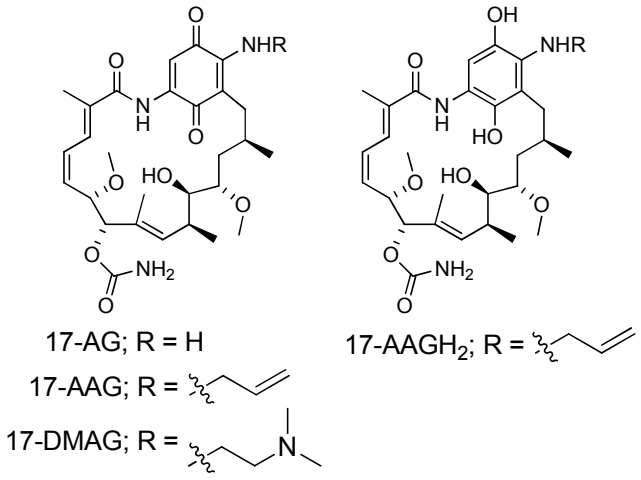

Figure 5. Ansamycin-based Hsp90 inhibitors

Optimization of the ansamycin scaffold has centered on the 17-position, as substitution at this position results in maintained or improved biological activity and superior physicochemical properties.[68, 69] The improved metabolic profile of these 17-amino substituted analogs is attributed, in part, to the enhanced electron-donating ability of the amino group, thus attenuating the electrophilicity of the quinone ring.[60, 61, 68] Furthermore, research has shown the 17-position to project towards the solvent upon Hsp90 binding, which allows for the incorporation of solubilizing appendages without affecting Hsp90 affinity.[70, 71] The ansamycin-based analogs under clinical evaluation (Figure 5) include 17-allylamino-17-demethoxygeldanamycin (17-AAG, tanespimycin, NSC330507, KOS953, CNF1010), 17-dimethylaminoethylamino-17-demethoxygeldanamycin (17-DMAG, alvespimycin, KOS1022), and the hydroquinone hydrochloride salt of 17-AAG (17-AAGH_2, retaspimycin hydrochloride, IPI-504).[60, 61]

The first ansamycin-derived analog to enter clinical trials was 17-AAG, which entered evaluation in 1999. 17-AAG exhibits antitumor activity in Her2-positive metastatic breast cancer; however, current clinical trials of 17-AAG are aimed at treating myelomas and lymphomas.[60, 61] Phase I and II clinical trials have been completed with 17-AAG using twice weekly and daily dosing schedules. Preliminary results were promising, however, a lack of clinical efficacy for 17-AAG in various phase II trials has dampened enthusiasm. Dose-

dependent hepatotoxicity and inadequate solubility have precluded the approval of 17-AAG.[60, 61] Therefore, numerous strategies have been pursued to increase bioavailability.

Evaluation of 17-AAG has demonstrated the compound is reduced by NAD(P)H:quinone oxidoreductase (NQO1), resulting in the hydroquinone metabolite 17-$AAGH_2$.[72, 73] Results from our laboratory[74] and others have shown that the hydroquinone ansamycin-based analogs exhibit superior binding affinity versus the quinone counterpart for Hsp90, as well as a slow k_{off} rate.[75, 76] Dependence of Hsp90 inhibitors upon NQO1 poses numerous liabilities, as NQO1 polymorphisms are common and NQO1 expression is a known mechanism for drug resistance.[77, 78] Thus, considering the metabolic fate of 17-AAG, resistance acquisition through NQO1 expression, and the superior affinity of hydroquinone analogs, researchers at Infinity Pharmaceuticals developed the hydroquinone hydrochloride salt, 17-$AAGH_2$ (IPI-504). Development of this analog eliminated dependence upon NQO1, therefore mitigating metabolic liabilities. Properties of this analog include high solubility in aqueous formulations, and improved Hsp90 inhibitory and tumor cell toxicity profiles when compared to 17-AAG.[60, 61] Although 17-$AAGH_2$ is still undergoing phase I/II clinical evaluation, one trial terminated prematurely citing "a higher than anticipated mortality rate among patients enrolled in the treatment arm." Current clinical evaluation is ongoing and 17-$AAGH_2$ is being evaluated for the treatment of non-small cell lung cancer (NSCLC), melanomas, and solid tumors as well as in combination therapy with the proteasome inhibitor, bortezomib.[60, 61]

In parallel to formulation and mechanistic studies of 17-AAG, 17-DMAG was developed by Kosan, and incorporates a solubilizing dimethylamino-ethyl moiety that remains protonated at physiological pH.[60, 61] An improved physicochemical profile is believed responsible for the observed improvement in Hsp90 inhibitory activity and biological affect on numerous cancer cell

lines. Although 17-DMAG exhibits an identical binding mode to other ansamycins, it demonstrates superior chemical and metabolic stability, lower toxicity, higher solubility and bioavailability than both 17-AAG and GDA.[60, 61] 17-DMAG is now being evaluated in Phase I clinical trials for leukemias and advanced solid tumors.

Another ansamycin inhibitor of note is the unsubstituted amino analog, 17-AG, which has recently entered phase I evaluation and remains an intriguing lead compound. 17-AG is the major metabolite of 17-amino substituted ansamycins and maintains Hsp90 affinity and anti-cancer activity.[60, 61] In summary, ansamycin inhibitors of Hsp90 have advanced the furthest in clinical trials. However, numerous detriments still exist with this class of drugs including formulation/scheduling difficulties due to heat shock induction, non-ideal toxicity profiles, and synthetic accessibility. These detriments have resulted in efforts to identify small molecule, synthetically accessible Hsp90 inhibitors that exhibit improved properties.

I.3.2 Benzamide Inhibitors

Serenex developed an Hsp90-based ATP-affinity column to identify new inhibitors.[61, 79] Cell lysates were loaded onto the column, resulting in the capture of ~2000 ATP-binding proteins. Compounds were screened for their ability to selectively displace Hsp90 from the ATP-binding column, resulting in identification of small molecule benzamide inhibitors of Hsp90, which were subsequently acquired by Pfizer for development as chemotherapeutic agents.[61, 79]

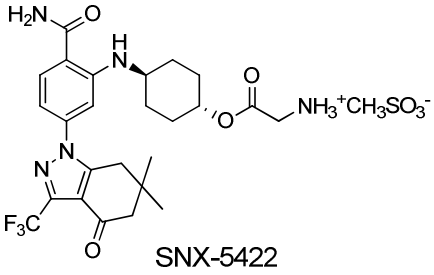

Figure 6. Benzamide inhibitor developed by Serenex/Pfizer.

The first benzamide inhibitor entered clinical trials in 2007. Although the lead compound exhibited variable bioavailability due to poor solubility and crystal polymorphisms, prodrugs were developed to mitigate such detriments. An orally bioavailable mesylate prodrug,

SNX-5422 (Figure 6), is currently under phase I clinical evaluation with preliminary studies focusing on the determination of the maximum tolerated dose (MTD), safety, and toxicity profiles.[61] Preclinical evaluation suggests a promising biological profile for this class of Hsp90 inhibitor and the ability to outperform ansamycin analogs in specific trials.[79] However, benzamide Hsp90 inhibitors, like ansamycins, continue to exhibit dose-dependent cardiotoxicity that has been attributed to the cardiac potassium human-ether-a-go-go (hERG) channel.[80] Furthermore, benzamide Hsp90 inhibitors are non-selective and bind Hsp90α, Hsp90β, Grp94 and TRAP-1.[61] The non-selective nature of benzamide inhibitors may be an insurmountable feature of this inhibitory class and may preclude FDA approval.

I.3.3 Purine Inhibitors

Utilizing structure-based drug design (SBDD), researchers at Memorial Sloan Kettering Institute developed small molecule Hsp90 inhibitors consisting of the adenine ring of ATP and an aromatic moiety.[61] SBDD studies resulted in a lead compound, PU3,[81] which was optimized independently by Conforma Therapeutics and later by Biogen Idec following acquisition. A pharmacophore model resulted from their optimization studies, which highlights three necessary features for the purine class of Hsp90 ATPase disruptors: 1) a necessary NH_2–C=N capable of binding the purine pocket of Hsp90, which mimics the same functionality in ATP; 2) an attached aromatic ring positioned six bonds away from the NH_2 group and 3) the presence of a purine moiety, which consists of optimally positioned basic nitrogen atoms to provide the requisite hydrogen bonding interactions.[61] Purine based analogs became the first fully synthetic Hsp90 inhibitors to enter clinical trials in 2005.

Clinical evaluation of purine-based Hsp90 inhibitors has resulted in optimism regarding this particular scaffold, as these inhibitors exhibit disease-modifying activity against malignancies with minimal off-target toxicities.[61] Two purine analogs, CNF1010 and CNF2024 (BIIB021, Figure 7), are currently under evaluation for the treatment of hematological and solid tumors. However, purine inhibitors retain detrimental heat shock induction and non-selective isoform binding profiles.[60, 61] Thus, as clinical evaluation progresses, it is hypothesized that similar scheduling difficulties and toxicities observed with other N-terminal Hsp90 inhibitors will also be found.

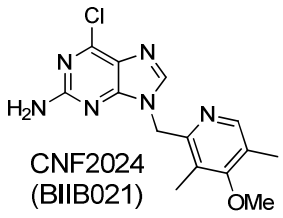

CNF2024
(BIIB021)

Figure 7. Purine inhibitor developed by Biogen Idec.

I.3.4 Resorcinylic Inhibitors

Following the lead of numerous other pharmaceutical companies, Vernalis initiated a structure-based approach towards the identification of small molecule Hsp90 inhibitors.[61, 82] Eventually, Vernalis and Novartis commenced in collaboration, leading to the identification of resorcinylic Hsp90 inhibitors. This series was optimized and decorated with solubilizing moieties, which produced NVP-AUY922 (Figure 8), and entered clinical trials in 2007 as an intravenous infusion.[82, 83] Currently, NVP-AUY922 is undergoing phase I/II clinical evaluation in combinatorial formulations and as a stand-alone agent against a variety of malignancies.[60, 61]

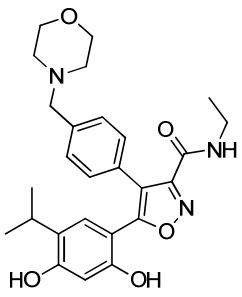

NVP-AUY922

Figure 8. Resorcinylic inhibitor developed by Novartis.

Resorcinylic inhibitors demonstrate minimal selectivity between cytosolic Hsp90 and either Grp94 or TRAP-1, ~10-fold and ~60-fold respectively.[61] However, detriments observed with other inhibitory scaffolds continue to plague this class, including heat shock induction and off-target toxicities.

Another company pursuing resorcinylic inhibitors is Synta Pharmaceuticals. The exact structure for Synta's lead compound, STA-9090,[84] has not been disclosed, however examination of the patent literature suggests the scaffold to contain a uniquely functionalized resorcinol.[85] Ongoing clinical evaluation for STA-9090 include phase I/II studies with one study utilizing co-administration with docetaxel, a microtubule stabilizing agent.[61] Published clinical results for STA-9090 have been limited; however, discussions with project leaders at the Hsp90 Symposium in 2010 revealed that similar detriments observed with other classes of Hsp90 inhibitors are also noted with STA-9090.

I.3.5 Other Inhibitors

The inability to gain FDA approval for any chemotherapeutic, that targets Hsp90, has not deterred competitors. Four other Hsp90 inhibitors have commenced clinical evaluation including Kyowa Hakko Kirin's KW-2478, Myriad Pharmaceuticals' MPC-3100, Exelixis' XL888, and Astex Therapeutics' AT13387.[60, 61, 85] All of the aforementioned inhibitors are orally available except KW-2478, which is administered intraveneously. None of the structures have been disclosed and little clinical data has been released. However, it can be hypothesized that each of these inhibitors will also suffer from the detriments manifested by other N-terminal Hsp90 inhibitors, as none have demonstrated novel profiles in preliminary disclosures.

I.4 Biological Concerns with Hsp90 Inhibition

Other than detriments observed in the clinical evaluation of Hsp90 inhibitors, numerous research groups have identified problematic resistance mechanisms and biological consequences relating to Hsp90 inhibition worthy of consideration.

I.4.1 *Resistance*

The ability of Hsp90 inhibitors to modulate multiple oncogenic pathways has launched many research endeavors to target this chaperone. As with the development of any class of chemotherapeutic agents, resistance is a concern and recent reports have validated the potential for acquired and intrinsic resistance to Hsp90 inhibitors.

Mutations

As discussed previously, Hsp90 N-terminal inhibitors act through competitive inhibition of the ATP-binding site, disrupting the ability of the chaperone complex to bind and hydrolyze ATP. Thus, the catalytic cycle is inhibited, which leads to client protein degradation and eventual cell death. Due to the competitive nature of Hsp90 inhibitors versus ATP, it was assumed that target mutation could be dismissed as a potential mechanism of resistance; as such mutations would alter the ability of the protein to bind ATP and therefore be deleterious to its function. This hypothesis was recently challenged through studies with *Humicola fuscoatra*, a fungus that produces RDC and exhibits resistance through a single point mutation (L34I).[86] This mutation is located within the N-

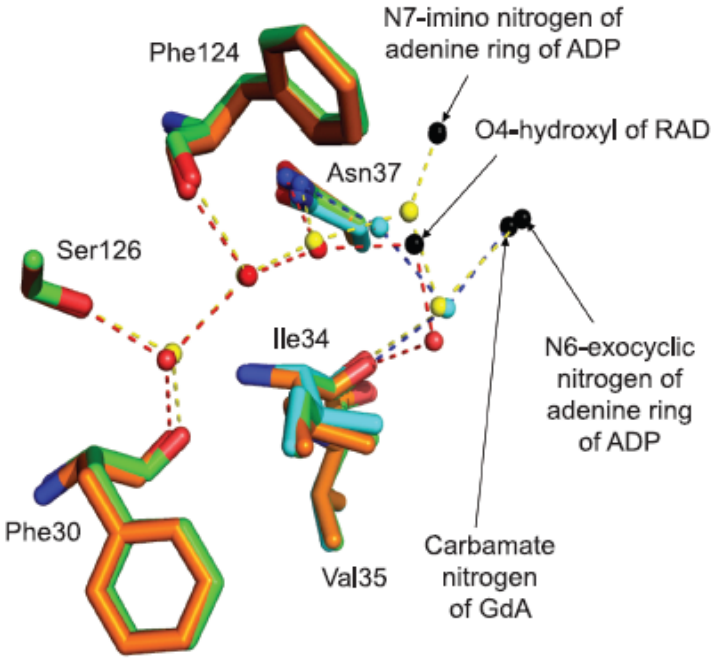

Figure 9. Comparison of the ligand interactions with L34I mutant Hsp90. Amino acids from the co-crystal structures are shown RDC (green), GDA (cyan), and ADP (orange). Water molecules for RDC (red), GDA (cyan), and ADP (Yellow) are shown as spheres.[86]

terminal nucleotide binding pocket and causes an increase in the hydration state of the binding domain (Figure 9). This mutation decreases the affinity of *H. fuscoatra* Hsp90 for RDC, while allowing both GDA and ATP to bind normally; however, it has yet to be determined whether such a mutation can arise with human Hsp90.[86]

Other mutations have been reported to allosterically alter the sensitivity of Hsp90 to inhibitors (Table 2). A yeast-based approach has identified a single point mutation in yeast Hsp90 (yHsp90; A107N) that can alter its affinity for both RDC and 17-AAG, without compromising ATP binding.[87] Expression of Hsp90α and Hsp90β with equivalent mutations, A121N for Hsp90α and A116N for Hsp90β, as the sole source of Hsp90 in the yeast system

Table 2. Reported mutations to Hsp90 orthologs and the associated affects.

Ortholog	Species	Mutation	Effect
yHsp90	*S. cerevisiae*	A107N	Stabilizes ATP lid closure; Decreases efficacy of RDC and 17-AAG; ATP binding unaffected
yHsp90	*S. cerevisiae*	T22I	Decreases efficacy of 17-AAG; Increases ATPase activity through Aha1 independent mechanism
Hsp90α	*H. sapiens*	A121N	Stabilizes ATP lid closure; Decreases efficacy of RDC and 17-AAG; ATP binding unaffected
Hsp90α	*H. sapiens*	I128T	Decreases efficacy of RDC and 17-AAG *in vivo*; ATP binding unaffected; Increases affinity for Aha1
Hsp90β	*H. sapiens*	A116N	Stabilizes ATP lid closure; Decreases efficacy of RDC and 17-AAG; ATP binding unaffected; Increases affinity of Aha1
Hsp90β	*H. sapiens*	I123T	Decreases efficacy of RDC and 17-AAG *in vivo*; ATP binding unaffected; Increases affinity for Aha1
Hsp90β	*H. sapiens*	T31I	Decreases efficacy of 17-AAG; Increases ATPase activity through Aha1 independent mechanism
Hsp90	*H. fuscoatra*	L34I	Increased hydration state; Decreases affinity for RDC; GDA and ATP binding unaffected

produced identical results. This alanine substitution favors closure of the ATP-lid over ATP stimulating N-terminal dimerization and association with Aha1, which increases ATPase activity. This increase in ATPase activity blocks the ability of inhibitors to bind.[87, 88] As shown in Table 2, this same Aha1 dependent mechanism of resistance has been linked to Hsp90α I128T and Hsp90β I123T mutations. Additionally, an Hsp90β T34I mutation has been identified that causes resistance to Hsp90 inhibition, however the mechanism, although allosteric in nature, appears to be Aha1 independent.[88] Like most chemotherapeutic agents, other mechanisms of resistance to Hsp90 inhibitors have been reported including target induction, alteration in drug influx or efflux, and expression modification to associated co-factors.[89]

Heat Shock Response

Another mechanism of resistance displayed towards Hsp90 inhibition involves the heat shock response (HSR). Administration of Hsp90 N-terminal inhibitors leads to the release of HSF-1, subsequent trimerization of HSF-1, phophorylation and translocation to the nucleus, wherein HSF-1 acts as a transcription factor that binds the heat shock element to induce the HSR. This induction results in the overexpression Hsp90, Hsp70, Hsp40 and Hsp27; all of which serve as anti-apoptotic chaperones that serve to protect the cell.[90-92] Induction of these pro-survival chaperones, especially Hsp90, has resulted in dosing and scheduling conflicts in patients. In addition, various cell lines exhibiting an increase in drug efflux and metabolism have been reported to correlate directly with heat shock induction. Using photoaffinity labels, Benchekroun and colleagues demonstrated the ansamycin analogs act as both substrates and inhibitors of P-gp pumps, suggesting drug accumulation may be affected.[67] Identification of Hsp90 inhibitors that fail to activate the HSR and do not interact with P-gp pumps is important to the progression of Hsp90 inhibitor development. Elimination of these attributes will likely aid in

the identification of amenable dosing and scheduling for oncology patients. Alternatively, strategies aimed at inhibiting Hsp90 and Hsp70 simultaneously or inhibiting the C-terminal putative binding domain may represent promising avenues to mitigate some of the aforementioned problems with current inhibitors.[93-95]

Aberrant Function of Co-chaperones

A myriad of partner proteins that interact with the Hsp90 machinery have been reported and it is well accepted that these co-chaperones work in collaboration to modulate the catalytic cycle.[22] Alteration of the expression of these interactors has suggested yet another mechanism for acquired resistance to Hsp90 inhibition (Table 3). One example is the overexpression of p23/Sba1, which is responsible for binding to and stabilizing the Hsp90·ATP complex.[96] Upon stabilization, hydrolysis is blocked, and consequently the active site of Hsp90 remains occupied, eliminating the ability of inhibitors to modulate ATP binding. Consequently, Cox and Miller have demonstrated that overexpression of p23/Sba1 leads to lower responses to N-terminal inhibitors. Furthermore, Forafonov *et al.* reported that in the absence of p23/Sba1, cells are more responsive to Hsp90 inhibition.[97] Additional studies have shown that mutants of p23/Sba1 are viable; suggesting that p23/Sba1 interactions with Hsp90 may provide the first evolutionary mechanism designed to protect cells from Hsp90 inhibition.[98] In total, resistance to Hsp90 inhibition has been reported to arise through numerous

Table 3. Hsp90 co-chaperones and the associated affects on the ATPase cycle.

Co-chaperone	Effect
HOP/Sti1	Decreases ATPase activity through partial blockade of N-terminal nucleotide binding pocket; Decreases efficacy of GDA and RDC
p23/Sba1	Binds to Hsp90/ATP complex, inhibiting ATPase actitivity; decreases efficacy of GDA and RDC
Aha1	Increases ATPase actitivity; decreases efficacy of GDA and RDC

mechanisms, and these mechanisms must be further detailed and continually monitored during clinical studies.

I.4.2 *Genetic Polymorphisms*

Apart from acquired resistance to Hsp90 inhibitors, intrinsically expressed genetic polymorphisms have also been identified. Two of these polymorphisms include NQO1 (DT-diaphorase) and cytochrome P450 3A4 (CYP3A4).[77] Although these polymorphisms seem to affect only certain ansamycin scaffolds, they deserve attention, as similar problems may arise with future Hsp90 inhibitors.[77] Numerous polymorphisms of Hsp90 have been identified; however these polymorphisms usually result in diminished Hsp90 activity.[99, 100] For this reason, only genetic polymorphisms of the enzymes responsible for the metabolism of select ansamycin analogs are discussed herein.

Cytochrome P450 3A4 is one of the most active mixed-function oxidase enzymes in the human genome. In fact, CYP3A4/CYP3A5 are responsible for ~36% of xenobiotic metabolism and the CYP3A subfamily is the most abundantly expressed CYP in the liver (30%) and intestine (70%).[101, 102] Research has identified CYP3A4 as one enzyme responsible for the metabolism of 17-AAG.[103] Genetic polymorphisms of CYP3A4 are common, as over 40 single nucleotide polymorphisms have been identified in the CYP3A4 gene within the promoter and/or coding regions. The variability in this metabolic enzyme must be monitored during clinical evaluations of ansamycin-based inhibitors of Hsp90, as dosing and scheduling protocols may need to be changed. Furthermore, CYP3A4 is known to be inhibited and/or induced by many substrates, including currently used chemotherapeutic agents, antibiotics, immunomodulators and anti-depressants, all of which are commonly prescribed to oncology patients.[101, 102] Taken together, the genetic variability of the enzyme paired with the potential for serious drug-drug interactions

suggests the development of small molecule inhibitors that lack interaction with CYP3A4 is important to the development of future Hsp90 inhibitors with clinical applications.

As discussed previously, outside of cytochromes P450 metabolism, research has shown the efficacy of 17-AAG to correlate directly with NQO1 gene expression *in vitro*.[73, 76] High expression of the NQO1 gene results in high levels of the DT-diaphorase enzyme, believed to be responsible for conversion of 17-AAG to a more efficacious hydroquinone, although the mechanism by which this occurs remains under investigation. Preliminary research suggests up to a ~32-fold increase in cellular sensitivity to 17-AAG in cells containing high levels of active DT-diaphorase. Intriguingly, this phenomenon was not observed for GDA, suggesting that this mechanism is not applicable to all ansamycin-based Hsp90 inhibitors. Furthermore, the correlation between NQO1 expression and 17-AAG efficacy is not observed *in vivo*.[104] The discrepancy between *in vitro* and *in vivo* dependence upon NQO1 expression should be considered when evaluating quinone containing Hsp90 inhibitors in preliminary biological evaluation. It is reported that 5−20% of the population is homozygous for the NQO1*2 polymorphism[72, 105] (diminished activity) and DT-diaphorase expression in human tumors is known to be variable,[106-108] suggesting that although dependence of 17-AAG upon NQO1 has yet to be noted *in vivo,* subsequent quinone containing Hsp90 inhibitors should be evaluated for metabolic activation *in vivo*.

In total, the variability of CYP3A4 and DT-diaphorase polymorphisms suggest the need to determine the levels of these enzymes and their effect on efficacy prior to administration of Hsp90 inhibitors. Furthermore, the ability to correlate enzyme effects *in vitro* and *in vivo* may help predict the efficacy and/or toxicity of inhibitors before administration. The design of inhibitors exhibiting activity independent of cytochromes P450 metabolism and intracellular

reductases especially CYP3A4 and DT-diaphorase, respectively, will likely enhance the predictability and widespread use of Hsp90 inhibitors.

I.4.3 *Downstream Biological Effects*

The effect of Hsp90 inhibitors on the cell cycle and the mechanisms by which inhibitors induce cytostasis and/or apoptosis is well understood.[18, 19, 109] However, recent research has shed light on unexpected biological events resulting from Hsp90 inhibition, leading to unanswered questions regarding downstream biological effects. It is well accepted that Hsp90 inhibition results in disruption of the Hsp90 protein folding machinery and subsequent client protein degradation *via* the ubiquitin-proteasome pathway, culminating in eventual cell death. However, detrimental downstream effects resulting from Hsp90 inhibition have recently surfaced. For example, although previous research suggests intracellular Hsp90 inhibition to be anti-metastatic in nature.[110] Price and colleagues report that inhibition of Hsp90 with 17-AAG upregulates osteoclast formation and augments bone metastasis.[111] This is not surprising, as it was previously reported that 17-AAG exhibits pronounced effects on gene expression in cancer cells, including upregulation of genes responsible for tumor cell survival and/or growth in bone.[112] Considering metastatic tumor growths cause the majority of deaths in cancer patients, and only ~20% of breast cancer patients survive longer than 5 years after bone metastasis is discovered,[111, 113] it provides an example as to why disease progression mechanisms must be further delineated.

Beyond specific disease progression, one must also look at the effects of Hsp90 inhibition on other tissues. Although the "magic bullet" theory introduced by Erlich was intuitive, no such compounds have come to fruition. Non-selective binding and localization to non-diseased tissues have and will continue to cause undesired toxicities for chemotherapeutic agents. Evidence shows that Hsp90 inhibition significantly alters dendritic cell function by reducing T-

cell proliferation and decreasing the ability of mature dendritic cells to present antigens.[114] Importantly, the data suggest that the Hsp90-protein-folding machinery is essential to dendritic cell function and patients enrolled in Hsp90 inhibitor clinical trials should be carefully monitored for immunosupression.

Another example of deleterious downstream effects resulting from Hsp90 inhibition is the alteration of glomerular filtration, as reported by Ramirez *et al.*.[115] Multiple reports have established that Hsp90 is responsible for regulating nitric oxide (NO) synthesis, which is dependent upon endothelial nitric oxidase synthase (eNOS).[116-119] Due to the eNOS regulation on glomerular filtration rate, Ramirez and colleagues investigated the effect of acute Hsp90 inhibition with RDC on the eNOS pathway and glomerular filtration rate. The study suggests that RDC induced Hsp90 inhibition leads to decreases in eNOS phosphorylation, eNOS dimer/monomer ratio and in renal blood flow, therefore decreasing glomerular filtration rate, which can be associated with hypertension and metabolic syndrome.[115] Although eNOS is a known Hsp90-dependent client protein and these results are not too surprising, these effects should be monitored during clinical evaluation of Hsp90 inhibitors.

Needless to say, further studies are necessary to determine the downstream biological effects of Hsp90 inhibition in order to anticipate potential complications that may arise in clinical trials. Future studies on the biology of Hsp90 inhibition will help identify potential side-effects including immunosuppression, hypertension, liver toxicity, and kidney failure.

I.5 Concluding Remarks: The Next Generation of Hsp90 Inhibitors

Although cancer is generally defined as a malignant growth or tumor caused by uncontrolled cellular division, it is well accepted in the medical and scientific community that cancer is also an umbrella term encompassing more than 200 diseases. It has been noted that

each cancer exhibits a unique biological profile and distinct mechanism of progression. While the excitement surrounding Hsp90 research stems from the ability of Hsp90 inhibition to simultaneously disrupt all six hallmarks of cancer, many questions remain unanswered as to which cancer, which combination of therapies, and which patient population will be responsive to each Hsp90 inhibitory scaffold.

Until the recent advancement of various small molecule Hsp90 inhibitors into clinical trials, the majority of clinically relevant Hsp90 inhibitors have been ansamycin analogs. Efforts to improve upon synthetic feasibility, compound solubility, pharmacological profiles and physicochemical properties have inspired further small molecule development. Although all of the inhibitors in clinical trials bind and inhibit the ATPase activity of the N-terminal dimerization domain, each scaffold exhibits unique downstream effects and phenotypic changes in specific cancers. Reported structures of clinical candidates include ansamycin, benzamide, purine, and resorcinylic based scaffolds.

Clinical results have shown Hsp90 inhibitory scaffolds to exhibit unique efficacy profiles, suggesting specific scaffolds may be beneficial towards certain cancer types or that administration of multiple Hsp90 inhibitory scaffolds may act synergistically against malignant growths.[60, 61, 120] Furthermore, it is apparent that Hsp90 inhibitory scaffolds may prevent the ability of malignancies to develop resistance to commonly prescribed chemotherapeutic agents,[121, 122] suggesting the identification of a combination therapy may represent the most promising strategy to treat patients. This has been affirmed in the clinic as the efficacy of monotherapy with specific Hsp90 inhibitors, especially ansamycin based scaffolds, has been a disappointment; however combinatorial therapies have been promising.[60, 61, 122]

Identification of new Hsp90 inhibitory scaffolds and elucidation of each scaffold's biological profile will allow clinicians to more rapidly predict the proper indication and/or combination of therapies for each patient. Technological advancements now allow clinicians to screen for various biological markers and forecast disease progression, confirming the beginning of the personalized medicine era.

Development of new Hsp90 inhibitory scaffolds and further evaluation of current scaffolds may also make it possible to identify isoform selective inhibitors. Identification of such inhibitors may prove beneficial in eliminating potentially detrimental effects observed with *pan*-Hsp90 inhibition. Multiple isoforms of Hsp90 are found in the human genome and include Hsp90α (inducible; cytoplasmic), Hsp90β (constitutive; cytoplasmic), Grp94 (endoplasmic reticulum) and TRAP1 (mitochondrial). Each isoform may be responsible for the maturation of distinct client proteins. Thus, the ability to target one isoform selectively may enhance efficacy, therapeutic control and further elucidate the physiological role of each isoform. To date, little data exist suggesting isoform selectivity for any of the clinically relevant Hsp90 inhibitors. Identification of isoform selective inhibitors may allow for degradation of specific client proteins, which will further enhance selectivity and provide yet another class of Hsp90 inhibitors, potentially giving rise to a series of tunable chemotherapeutic agents.

Although the ability to identify Hsp90 inhibitory scaffolds is becoming trivial, understanding the biological responses inherent to each inhibitory class is difficult. Hsp90 has been validated as an anti-cancer target and clinical trials with various inhibitory scaffolds are ongoing. Both academic and pharmaceutical research teams continue to invest resources in Hsp90 modulatory projects, however, the bottleneck for development of Hsp90 inhibitors

remains focused on patient responses to Hsp90 inhibition and subsequent effects in gene expression levels.

Multiple Hsp90 inhibitory scaffolds have been identified and each scaffold appears to exhibit different binding modes and therefore different profiles of efficacy. Focus has shifted from semi-synthetic ansamycin analogs to scaleable small molecules exhibiting superior physicochemical and pharmacological properties. The utilization of competitive small molecule Hsp90 inhibitors should provide tools that elucidate mechanisms and downstream biological effects resulting from the administration of each scaffold. Through collaborative efforts between medicinal chemists, pharmaceutical chemists and pharmacologists, new small molecule Hsp90 inhibitors will undoubtedly progress towards clinical evaluation. The continual development of novel Hsp90 inhibitory scaffolds paired with strong biological and mechanistic studies will help decipher the complicated network associated with Hsp90 inhibition and bring personalized chemotherapy to the forefront of medicine.

I.6 References

1. Hartl, F. U.; Martin, J., Molecular chaperones in cellular protein folding. *Curr. Opin. Struct. Biol.* **1995,** 5, 92-102.

2. Hartl, F. U., Molecular chaperones in cellular protein folding. *Nature* **1996,** 381, 571-579.

3. Hartl, F. U.; Bracher, A.; Hayer-Hartl, M., Molecular chaperones in protein folding and proteostasis. *Nature* **2011,** 475, 324-332.

4. Almeida, M. B.; do Nascimento, J. L.; Herculano, A. M.; Crespo-Lopez, M. E., Molecular chaperones: Toward new therapeutic tools. *Biomed. Pharmacother.* **2011,** 65, 239-243.

5. Buchberger, A.; Bukau, B.; Sommer, T., Protein quality control in the cytosol and the endoplasmic reticulum: Brothers in arms. *Mol. Cell* **2010,** 40, 238-252.

6. Walter, S.; Buchner, J., Molecular chaperones--cellular machines for protein folding. *Angew Chem Int Ed Engl* **2002,** 41, (7), 1098-113.

7. Koller, M.; Hensler, T.; Konig, B.; Prevost, G.; Alouf, J.; Konig, W., Induction of heat-shock proteins by bacterial toxins, lipid mediators and cytokines in human leukocytes. *Zentralbl Bakteriol* **1993,** 278, 365-376.

8. Pockley, A. G., Heat shock proteins, inflammation, and cardiovascular disease. *Circulation* **2002,** 105, 1012-1017.

9. Benjamin, I. J.; Kroger, B.; Williams, R. S., Activation of the heat shock transcription factor by hypoxia in mammalian cells. *Proc. Natl. Acad. Sci. USA* **1990,** 87, 6263-6267.

10. Simon, M. C.; Kitchener, K.; Kao, H. T.; Hickey, E.; Weber, L.; Voellmy, R.; Heintz, N.; Nevins, J. R., Selective induction of human heat shock gene transcription by the adenovirus E1A gene products, including the 12S E1A product. *Mol. Cell Biol.* **1987,** 7, 2884-2890.

11. Hecker, M.; Schumann, W.; Volker, U., Heat-shock and general stress response in Bacillus subtilis. *Mol. Microbiol.* **1996,** 19, 417-428.

12. Morimoto, R. I., Cells in stress: Transcriptional activation of heat shock genes. *Science* **1993,** 259, 1409-1410.

13. Soti, C.; Nagy, E.; Giricz, Z.; Vigh, L.; Csermely, P.; Ferdinandy, P., Heat shock proteins as emerging therapeutic targets. *Br. J. Pharmacol.* **2005,** 146, 769-780.

14. Ciocca, D. R.; Calderwood, S. K., Heat shock proteins in cancer: diagnostic, prognostic, predictive, and treatment implications. *Cell Stress Chaperones* **2005,** 10, 86-103.

15. Lai, B. T.; Chin, N. W.; Stanek, A. E.; Keh, W.; Lanks, K. W., Quantitation and intracellular localization of the 85K heat shock protein by using monoclonal and polyclonal antibodies. *Mol. Cell Biol.* **1984,** 4, 2802-2810.

16. Csermely, P.; Schnaider, T.; Soti, C.; Prohaszka, Z.; Nardai, G., The 90-kDa molecular chaperone family: structure, function, and clinical applications. A comprehensive review. *Pharmacol. Ther.* **1998,** 79, 129-168.

17. Kamal, A.; Thao, L.; Sensintaffar, J.; Zhang, L.; Boehm, M. F.; Fritz, L. C.; Burrows, F. J., A high-affinity conformation of Hsp90 confers tumor selectivity on Hsp90 inhibitors. *Nature* **2003,** 425, 407-410.

18. Prodromou, C., Strategies for stalling malignancy: targeting cancer's addiction to Hsp90. *Curr. Top. Med. Chem.* **2009,** 9, 1352-1368.

19. Pearl, L. H.; Prodromou, C.; Workman, P., The Hsp90 molecular chaperone: An open and shut case for treatment. *Biochem. J.* **2008,** 410, 439-453.

20. Bagatell, R.; Whitesell, L., Altered Hsp90 function in cancer: A unique therapeutic opportunity. *Mol. Cancer Ther.* **2004,** 3, 1021-1030.

21. Taldone, T.; Gozman, A.; Maharaj, R.; Chiosis, G., Targeting Hsp90: Small-molecule inhibitors and their clinical development. *Curr. Opin. Pharmacol.* **2008,** 8, 370-374.

22. Picard, D., Website. *http://www.picard.ch/downloads/Hsp90interactors.pdf*.

23. Hanahan, D.; Weinberg, R. A., The hallmarks of cancer. *Cell* **2000,** 100, 57-70.

24. Hanahan, D.; Weinberg, R. A., Hallmarks of cancer: The next generation. *Cell* **2011,** 144, 646-674.

25. Bishop, S. C.; Burlison, J. A.; Blagg, B. S., Hsp90: A novel target for the disruption of multiple signaling cascades. *Curr. Cancer Drug Targets* **2007,** 7, 369-388.

26. Prodromou, C.; Panaretou, B.; Chohan, S.; Siligardi, G.; O'Brien, R.; Ladbury, J. E.; Roe, S. M.; Piper, P. W.; Pearl, L. H., The ATPase cycle of Hsp90 drives a molecular 'clamp' via transient dimerization of the N-terminal domains. *EMBO J.* **2000,** 19, 4383-4392.

27. Krukenberg, K. A.; Street, T. O.; Lavery, L. A.; Agard, D. A., Conformational dynamics of the molecular chaperone Hsp90. *Q. Rev. Biophys.* **2011,** 44, 229-255.

28. Dutta, R.; Inouye, M., GHKL, an emergent ATPase/kinase superfamily. *Trends Biochem. Sci.* **2000,** 25, 24-28.

29. Carrello, A.; Ingley, E.; Minchin, R. F.; Tsai, A.; Ratajczak, T., The common tetratricopeptide repeat acceptor site for steroid receptor-associated immunophilins and HOP is located in the dimerization domain of Hsp90. *J. Biol. Chem.* **1999,** 274, 2682-2689.

30. Southworth, D. R.; Agard, D. A., Client-loading conformation of the Hsp90 molecular chaperone revealed in the cryo-EM structure of the human Hsp90:Hop complex. *Mol. Cell* **2011,** 42, 771-781.

31. Chadli, A.; Bouhouche, I.; Sullivan, W.; Stensgard, B.; McMahon, N.; Catelli, M. G.; Toft, D. O., Dimerization and N-terminal domain proximity underlie the function of the molecular chaperone heat shock protein 90. *Proc. Natl. Acad. Sci. USA* **2000,** 97, 12524-12529.

32. Chaudhury, S.; Welch, T. R.; Blagg, B. S., Hsp90 as a target for drug development. *ChemMedChem* **2006,** 1, 1331-1340.

33. Phillips, J. J.; Yao, Z. P.; Zhang, W.; McLaughlin, S.; Laue, E. D.; Robinson, C. V.; Jackson, S. E., Conformational dynamics of the molecular chaperone Hsp90 in complexes with a co-chaperone and anticancer drugs. *J. Mol. Biol.* **2007,** 372, 1189-1203.

34. Blagosklonny, M. V., Hsp-90-associated oncoproteins: multiple targets of geldanamycin and its analogs. *Leukemia* **2002,** 16, 455-462.

35. Chen, B.; Zhong, D.; Monteiro, A., Comparative genomics and evolution of the HSP90 family of genes across all kingdoms of organisms. *BMC Genomics* **2006,** 7, 156.

36. Chen, B.; Piel, W. H.; Gui, L.; Bruford, E.; Monteiro, A., The HSP90 family of genes in the human genome: insights into their divergence and evolution. *Genomics* **2005,** 86, 627-637.

37. Sreedhar, A. S.; Kalmar, E.; Csermely, P.; Shen, Y.-F., Hsp90 isoforms: Functions, expression and clinical importance. *FEBS Lett.* **2004,** 562, 11-15.

38. Song, H. Y.; Dunbar, J. D.; Zhang, Y. X.; Guo, D.; Donner, D. B., Identification of a protein with homology to hsp90 that binds the type 1 tumor necrosis factor receptor. *J. Biol. Chem.* **1995,** 270, 3574-3581.

39. Felts, S. J.; Owen, B. A.; Nguyen, P.; Trepel, J.; Donner, D. B.; Toft, D. O., The hsp90-related protein TRAP1 is a mitochondrial protein with distinct functional properties. *J. Biol. Chem.* **2000,** 275, 3305-3312.

40. Landriscina, M.; Amoroso, M. R.; Piscazzi, A.; Esposito, F., Heat shock proteins, cell survival and drug resistance: the mitochondrial chaperone TRAP1, a potential novel target for ovarian cancer therapy. *Gynecol. Oncol.* **2010,** 117, 177-182.

41. Shiu, R. P.; Pouyssegur, J.; Pastan, I., Glucose depletion accounts for the induction of two transformation-sensitive membrane proteinsin Rous sarcoma virus-transformed chick embryo fibroblasts. *Proc. Natl. Acad. Sci. USA* **1977,** 74, 3840-3844.

42. Argon, Y.; Simen, B. B., GRP94, an ER chaperone with protein and peptide binding properties. *Semin. Cell Dev. Biol.* **1999,** 10, 495-505.

43. Soldano, K. L.; Jivan, A.; Nicchitta, C. V.; Gewirth, D. T., Structure of the N-terminal domain of GRP94. *J. Biol. Chem.* **2003,** 279, 48330-48338.

44. Dollins, D. E.; Warren, J. J.; Immormino, R. M.; Gewirth, D. T., Structures of GRP94-nucleotide complexes reveal mechanistic differences between the Hsp90 chaperones. *Mol. Cell* **2007,** 28, 41-56.

45. Randow, F.; Seed, B., Endoplasmic reticulum chaperone gp96 is required for innate immunity but not cell viability. *Nat. Cell Biol.* **2001,** 3, 891-896.

46. McLaughlin, M.; Vandenbroeck, K., The endoplasmic reticulum protein folding factory and its chaperones: new targets for drug discovery? *Br. J. Pharmacol.* **2011,** 162, 328-345.

47. Breckenridge, D. G.; Germain, M.; Mathai, J. P.; Nguyen, M.; Shore, G. C., Regulation of apoptosis by endoplasmic reticulum pathways. *Oncogene* **2003,** 22, 8608-8618.

48. Pan, Z.; Erkan, M.; Streit, S.; Friess, H.; Kleef, J., Silencing of GRP94 expression promotes apoptosis in pancreatic cancer cells. *Int. J. Oncol.* **2009,** 35, 823-828.

49. Fu, Y.; Lee, A. S., Glucose regulated proteins in cancer progression, drug resistance and immunotherapy. *Cancer Biol. Ther.* **2006,** 5, 741-744.

50. DeBoer, C.; Meulman, R. J.; Wnuk, R. J.; Peterson, D. H., Geldanamycin, a new antibiotic. *J. Antibiot.* **1970,** 23, 442-447.

51. Uehara, Y.; Hori, M.; Takeuchi, T.; Umezawa, H., Screening of agents which convert 'transformed morphology' of Rous sarcoma virus-infected rat kidney cells to 'normal morphology': identification of an active agent as herbimycin and its inhibition of intracellular src kinase. *Jpn. J. Cancer Res.* **1985,** 76, 672-675.

52. Uehara, Y.; Hori, M.; Takeuchi, T.; Umezawa, H., Phenotypic change from transformed to normal induced by benzoquinonoid ansamycins accompanies inactivation of p60src in rat kidney cells infected with Rous sarcoma virus. *Mol. Cell. Biol.* **1986,** 6, 2198-2206.

53. Whitesell, L.; Mimnaugh, E. G.; De Costa, B.; Myers, C. E.; Neckers, L. M., Inhibition of heat shock protein HSP90-pp60v-src heteroprotein complex formation by benzoquinone ansamycins: essential role for stress proteins in oncogenic transformation. *Proc. Natl. Acad. Sci. USA* **1994,** 91, 8324-8328.

54. Delmotte, P.; Delmotte-Plaque, J., A new antifungal substance of fungal origin. *Nature* **1953,** 171, 344.

55. Sharma, S. V.; Agatsuma, T.; Nakano, H., Targeting of the protein chaperone, HSP90, by the transformation suppressing agent, radicicol. *Oncogene* **1998,** 16, 2639-2645.

56. Schulte, T. W.; Akinaga, S.; Soga, S.; Sullivan, W.; Stensgard, B.; Toft, D.; Neckers, L. M., Antibiotic radicicol binds to the N-terminal domain of Hsp90 and shares important biological activities with geldanamycin. *Cell Stress Chaperones* **1998,** 3, 100-108.

57. Roe, S. M.; Prodromou, C.; O'Brien, R.; Ladbury, J. E.; Piper, P. W.; Pearl, L. H., Structural basis for inhibition of the Hsp90 molecular chaperone by the antitumor antibiotics radicicol and geldanamycin. *J. Med. Chem.* **1999,** 42, 260-266.

58. Supko, J. G.; Hickman, R. L.; Grever, M. R.; Malspeis, L., Preclinical pharmacologic evaluation of geldanamycin as an antitumor agent. *Cancer Chemother. Pharmacol.* **1995,** 36, 305-315.

59. Usmani, S. Z.; Bona, R.; Li, Z., 17 AAG for HSP90 inhibition in cancer--from bench to bedside. *Curr. Mol. Med.* **2009,** 9, 654-664.

60. Kim, Y. S.; Alarcon, S. V.; Lee, S.; Lee, M. J.; Giaccone, G.; Neckers, L.; Trepel, J. B., Update on Hsp90 inhibitors in clinical trial. *Curr. Top. Med. Chem.* **2009,** 9, 1479-1492.

61. Biamonte, M. A.; Van de Water, R.; Arndt, J. W.; Scannevin, R. H.; Perret, D.; Lee, W. C., Heat shock protein 90: Inhibitors in clinical trials. *J. Med. Chem.* **2010,** 53, 3-17.

62. Benchekroun, N. M.; Myers, C. E.; Sinha, B. K., Free radical formation by ansamycin benzoquinone in human breast tumor cells: implications for cytotoxicity and resistance. *Free Radic. Biol. Med.* **1994,** 17, 191-200.

63. Guo, W.; Reigan, P.; Siegel, D.; Ross, D., Enzymatic reduction and glutathione conjugation of benzoquinone ansamycin heat shock protein 90 inhibitors: relevance for toxicity and mechanism of action. *Drug Metab. Dispos.* **2008,** 36, 2050-2057.

64. Fukuyo, Y.; Hunt, C. R.; Horikoshi, N., Geldanamycin and its anti-cancer activities. *Cancer Lett.* **2010,** 290, 24-35.

65. Yamamoto, K.; Garbaccio, R. M.; Stachel, S. J.; Solit, D. B.; Chiosis, G.; Rosen, N.; Danishefsky, S. J., Total synthesis as a resource in the discovery of potentially valuable antitumor agents: cycloproparadicicol. *Angew. Chem., Int. Ed.* **2003,** 42, 1280-1284.

66. Chiosis, G.; Neckers, L., Tumor selectivity of Hsp90 inhibitors: The explanation remains elusive. *ACS Chem. Biol.* **2006,** 1, 279-284.

67. Benchekroun, M. N.; Schneider, E.; Safa, A. R.; Townsend, A. J.; Sinha, B. K., Mechanisms of resistance to ansamycin antibiotics in human breast cancer cell lines. *Mol. Pharmacol.* **1994,** 46, 677-684.

68. Porter, J. R.; Ge, J.; Lee, J.; Normant, E.; West, K., Ansamycin inhibitors of Hsp90: Nature's prototype for anti-chaperone therapy. *Curr. Top. Med. Chem.* **2009,** 9, 1386-1418.

69. Ge, J.; Normant, E.; Porter, J. R.; Ali, J. A.; Dembski, M. S.; Gao, Y.; Georges, A. T.; Grenier, L.; Pak, R. H.; Patterson, J.; Sydor, J. R.; Tibbitts, T. T.; Tong, J. K.; Adams, J.; Palombella, V. J., Design, synthesis, and biological evaluation of hydroquinone derivatives of 17-amino-17-demethoxygeldanamycin as potent, water-soluble inhibitors of Hsp90. *J. Med. Chem.* **2006,** 49, 4606-15.

70. Hollingshead, M.; Alley, M.; Burger, A. M.; Borgel, S.; Pacula-Cox, C.; Fiebig, H. H.; Sausville, E. A., In vivo antitumor efficacy of 17-DMAG (17-dimethylaminoethylamino-17-demethoxygeldanamycin hydrochloride), a water-soluble geldanamycin derivative. *Cancer Chemother. Pharmacol.* **2005,** 56, 115-125.

71. Tian, Z. Q.; Liu, Y.; Zhang, D.; Wang, Z.; Dong, S. D.; Carreras, C. W.; Zhou, Y.; Rastelli, G.; Santi, D. V.; Myles, D. C., Synthesis and biological activities of novel 17-aminogeldanamycin derivatives. *Bioorg. Med. Chem.* **2004,** 12, 5317-5329.

72. Kelland, L. R.; Sharp, S. Y.; Rogers, P. M.; Myers, T. G.; Workman, P., DT-Diaphorase expression and tumor cell sensitivity to 17-allylamino, 17-demethoxygeldanamycin, an inhibitor of heat shock protein 90. *J. Natl. Cancer Inst.* **1999,** 91, 1940-1949.

73. Guo, W.; Reigan, P.; Siegel, D.; Zirrolli, J.; Gustafson, D.; Ross, D., Formation of 17-allylamino-demethoxygeldanamycin (17-AAG) hydroquinone by NAD(P)H:quinone oxidoreductase 1: role of 17-AAG hydroquinone in heat shock protein 90 inhibition. *Cancer Res.* **2005,** 65, 10006-10015.

74. Shen, G.; Blagg, B. S. J., Radester, a novel inhibitor of the Hsp90 protein folding machinery. *Org. Lett.* **2005,** 7, 2157-2160.

75. Maroney, A. C.; Marugan, J. J.; Mezzasalma, T. M.; Barnakov, A. N.; Garrabrant, T. A.; Weaner, L. E.; Jones, W. J.; Barnakova, L. A.; Koblish, H. K.; Todd, M. J.; Masucci, J. A.; Deckman, I. C.; Galemmo, R. A., Jr.; Johnson, D. L., Dihydroquinone ansamycins: Toward resolving the conflict between low in vitro affinity and high cellular potency of geldanamycin derivatives. *Biochemistry* **2006,** 45, 5678-5685.

76. Guo, W.; Reigan, P.; Siegel, D.; Zirrolli, J.; Gustafson, D.; Ross, D., The bioreduction of a series of benzoquinone ansamycins by NAD(P)H:quinone oxidoreductase 1 to more potent heat

shock protein 90 inhibitors, the hydroquinone ansamycins. *Mol. Pharmacol.* **2006,** 70, 1194-1203.

77. Gaspar, N.; Sharp, S. Y.; Pacey, S.; Jones, C.; Walton, M.; Vassal, G.; Eccles, S.; Pearson, A.; Workman, P., Acquired resistance to 17-allylamino-17-demethoxygeldanamycin (17-AAG, tanespimycin) in glioblastoma cells. *Cancer Res.* **2009,** 69, 1966-1975.

78. Tew, K. D.; O'Brien, M.; Laing, N. M.; Shen, H., Coordinate changes in expression of protective genes in drug-resistant cells. *Chem. Biol. Interact.* **1998,** 111-112, 199-211.

79. Huang, K. H.; Veal, J. M.; Fadden, R. P.; Rice, J. W.; Eaves, J.; Strachan, J. P.; Barabasz, A. F.; Foley, B. E.; Barta, T. E.; Ma, W.; Silinski, M. A.; Hu, M.; Partridge, J. M.; Scott, A.; DuBois, L. G.; Freed, T.; Steed, P. M.; Ommen, A. J.; Smith, E. D.; Hughes, P. F.; Woodward, A. R.; Hanson, G. J.; McCall, W. S.; Markworth, C. J.; Hinkley, L.; Jenks, M.; Geng, L.; Lewis, M.; Otto, J.; Pronk, B.; Verleysen, K.; Hall, S. E., Discovery of novel 2-aminobenzamide inhibitors of heat shock protein 90 as potent, selective and orally active antitumor agents. *J. Med. Chem.* **2009,** 52, 4288-4305.

80. Dennis, A.; Wang, L.; Wan, X.; Ficker, E., hERG channel trafficking: Novel targets in drug-induced long QT syndrome. *Biochem. Soc. Trans.* **2007,** 35, 1060-1063.

81. Chiosis, G.; Timaul, M. N.; Lucas, B.; Munster, P. N.; Zheng, F. F.; Sepp-Lorenzino, L.; Rosen, N., A small molecule designed to bind to the adenine nucleotide pocket of Hsp90 causes Her2 degradation and the growth arrest and differentiation of breast cancer cells. *Chem. Biol.* **2001,** 8, 289-299.

82. Brough, P. A.; Aherne, W.; Barril, X.; Borgognoni, J.; Boxall, K.; Cansfield, J. E.; Cheung, K. M.; Collins, I.; Davies, N. G.; Drysdale, M. J.; Dymock, B.; Eccles, S. A.; Finch, H.; Fink, A.; Hayes, A.; Howes, R.; Hubbard, R. E.; James, K.; Jordan, A. M.; Lockie, A.; Martins,

V.; Massey, A.; Matthews, T. P.; McDonald, E.; Northfield, C. J.; Pearl, L. H.; Prodromou, C.; Ray, S.; Raynaud, F. I.; Roughley, S. D.; Sharp, S. Y.; Surgenor, A.; Walmsley, D. L.; Webb, P.; Wood, M.; Workman, P.; Wright, L., 4,5-diarylisoxazole Hsp90 chaperone inhibitors: potential therapeutic agents for the treatment of cancer. *J. Med. Chem.* **2008,** 51, 196-218.

83. Eccles, S. A.; Massey, A.; Raynaud, F. I.; Sharp, S. Y.; Box, G.; Valenti, M.; Patterson, L.; de Haven Brandon, A.; Gowan, S.; Boxall, F.; Aherne, W.; Rowlands, M.; Hayes, A.; Martins, V.; Urban, F.; Boxall, K.; Prodromou, C.; Pearl, L.; James, K.; Matthews, T. P.; Cheung, K. M.; Kalusa, A.; Jones, K.; McDonald, E.; Barril, X.; Brough, P. A.; Cansfield, J. E.; Dymock, B.; Drysdale, M. J.; Finch, H.; Howes, R.; Hubbard, R. E.; Surgenor, A.; Webb, P.; Wood, M.; Wright, L.; Workman, P., NVP-AUY922: A novel heat shock protein 90 inhibitor active against xenograft tumor growth, angiogenesis, and metastasis. *Cancer Res.* **2008,** 68, 2850-2860.

84. Wang, Y.; Trepel, J. B.; Neckers, L. M.; Giaccone, G., STA-9090, a small-molecule Hsp90 inhibitor for the potential treatment of cancer. *Curr. Opin. Investig. Drugs* **2010,** 11, 1466-1476.

85. Messaoudi, S.; Peyrat, J. F.; Brion, J. D.; Alami, M., Heat-shock protein 90 inhibitors as antitumor agents: a survey of the literature from 2005 to 2010. *Expert Opin. Ther. Pat.* **2011**.

86. Prodromou, C.; Nuttall, J. M.; Millson, S. H.; Roe, S. M.; Sim, T. S.; Tan, D.; Workman, P.; Pearl, L. H.; Piper, P. W., Structural basis of the radicicol resistance displayed by a fungal hsp90. *ACS Chem. Biol.* **2009,** 4, 289-297.

87. Millson, S. H.; Prodromou, C.; Piper, P. W., A simple yeast-based system for analyzing inhibitor resistance in the human cancer drug targets Hsp90[alpha]/[beta]. *Biochem. Pharmacol.* **2010,** 79, 1581-1588.

88. Zurawska, A.; Urbanski, J.; Matuliene, J.; Baraniak, J.; Klejman, M. P.; Filipek, S.; Matulis, D.; Bieganowski, P., Mutations that increase both Hsp90 ATPase activity in vitro and Hsp90 drug resistance in vivo. *Biochim. Biophys. Acta* **2010,** 1803, 575-583.

89. Duerfeldt, A. S.; Blagg, B. S. J., Hydrating for resistance to radicicol. *ACS Chem. Biol.* **2009,** 4, 245-247.

90. McCollum, A. K.; TenEyck, C. J.; Stensgard, B.; Morlan, B. W.; Ballman, K. V.; Jenkins, R. B.; Toft, D. O.; Erlichman, C., P-Glycoprotein-mediated resistance to Hsp90-directed therapy is eclipsed by the heat shock response. *Cancer Res.* **2008,** 68, 7419-7427.

91. Didelot, C.; Schmitt, E.; Brunet, M.; Maingret, L.; Parcellier, A.; Garrido, C., Heat shock proteins: Endogenous modulators of apoptotic cell death. *Handb. Exp. Pharmacol.* **2006**, 171-198.

92. Garrido, C.; Brunet, M.; Didelot, C.; Zermati, Y.; Schmitt, E.; Kroemer, G., Heat shock proteins 27 and 70: Anti-apoptotic proteins with tumorigenic properties. *Cell Cycle* **2006,** 5, 2592-2601.

93. Brodsky, J. L.; Chiosis, G., Hsp70 molecular chaperones: emerging roles in human disease and identification of small molecule modulators. *Curr. Top. Med. Chem.* **2006,** 6, 1215-1225.

94. Donnelly, A.; Blagg, B. S. J., Novobiocin and additional inhibitors of the Hsp90 C-terminal nucleotide-binding pocket. *Curr. Med. Chem.* **2008,** 15, 2702-2717.

95. Holzbeierlein, J. M.; Windsperger, A.; Vielhauer, G., Hsp90: a drug target? *Curr. Oncol. Rep.* **2010,** 12, 95-101.

96. Cox, M. B.; Miller, C. A., 3rd, Pharmacological and genetic analysis of 90-kDa heat shock isoprotein-aryl hydrocarbon receptor complexes. *Mol. Pharmacol.* **2003,** 64, 1549-1556.

97. Forafonov, F.; Toogun, O. A.; Grad, I.; Suslova, E.; Freeman, B. C.; Picard, D., p23/Sba1p protects against Hsp90 inhibitors independently of its intrinsic chaperone activity. *Mol. Cell Biol.* **2008,** 28, 3446-3456.

98. Fang, Y.; Fliss, A. E.; Rao, J.; Caplan, A. J., SBA1 encodes a yeast Hsp90 cochaperone that is homologous to vertebrate p23 proteins. *Mol. Cell Biol.* **1998,** 18, 3727-3734.

99. Passarino, G.; Cavalleri, G. L.; Stecconi, R.; Franceschi, C.; Altomare, K.; Dato, S.; Greco, V.; Luca Cavalli Sforza, L.; Underhill, P. A.; de Benedictis, G., Molecular variation of human HSP90alpha and HSP90beta genes in Caucasians. *Hum. Mutat.* **2003,** 21, 554-555.

100. Rahim, R. A.; Boyd, P. A.; Ainslie Patrick, W. J.; Burdon, R. H., Human heat shock protein gene polymorphisms and sudden infant death syndrome. *Arch. Dis. Child.* **1996,** 75, 451-452.

101. Anglicheau, D.; Legendre, C.; Beaune, P.; Thervet, E., Cytochrome P450 3A polymorphisms and immunosuppressive drugs: An update. *Pharmacogenomics* **2007,** 8, 835-849.

102. Bozina, N.; Bradamante, V.; Lovric, M., Genetic polymorphism of metabolic enzymes P450 (CYP) as a susceptibility factor for drug response, toxicity, and cancer risk. *Arh. Hig. Rada. Toksikol.* **2009,** 60, 217-242.

103. Egorin, M. J.; Rosen, D. M.; Wolff, J. H.; Callery, P. S.; Musser, S. M.; Eiseman, J. L., Metabolism of 17-(allylamino)-17-demethoxygeldanamycin (NSC 330507) by murine and human hepatic preparations. *Cancer Res.* **1998,** 58, 2385-2396.

104. Douglas, M.; Lim, A. R.; Porter, J. R.; West, K.; Pink, M. M.; Ge, J.; Wylie, A. A.; Tibbits, T. T.; Biggs, K.; Curtis, M.; Palombella, V. J.; Adams, J.; Fritz, C. C.; Normant, E., The

antiproliferative activity of the heat shock protein 90 inhibitor IPI-504 is not dependent on NAD(P)H:quinone oxidoreductase 1 activity in vivo. *Mol. Cancer Ther.* **2009,** 8, 3369-3378.

105. Kelsey, K. T.; Ross, D.; Traver, R. D.; Christiani, D. C.; Zuo, Z. F.; Spitz, M. R.; Wang, M.; Xu, X.; Lee, B. K.; Schwartz, B. S.; Wiencke, J. K., Ethnic variation in the prevalence of a common NAD(P)H quinone oxidoreductase polymorphism and its implications for anti-cancer chemotherapy. *Br. J. Cancer* **1997,** 76, 852-854.

106. Robertson, N.; Stratford, I. J.; Houlbrook, S.; Carmichael, J.; Adams, G. E., The sensitivity of human tumour cells to quinone bioreductive drugs: what role for DT-diaphorase? *Biochem. Pharmacol.* **1992,** 44, 409-412.

107. Belinsky, M.; Jaiswal, A. K., NAD(P)H:quinone oxidoreductase1 (DT-diaphorase) expression in normal and tumor tissues. *Cancer Metastasis Rev.* **1993,** 12, 103-117.

108. Fitzsimmons, S. A.; Workman, P.; Grever, M.; Paull, K.; Camalier, R.; Lewis, A. D., Reductase enzyme expression across the national cancer institute tumor cell line panel: Correlation with sensitivity to mitomycin C and EO9. *J. Natl. Cancer Inst.* **1996,** 88, 259-269.

109. Hostein, I.; Robertson, D.; DiStefano, F.; Workman, P.; Clarke, P. A., Inhibition of signal transduction by the Hsp90 inhibitor 17-allylamino-17-demethoxygeldanamycin results in cytostasis and apoptosis. *Cancer Res.* **2001,** 61, 4003-4009.

110. Tsutsumi, S.; Beebe, K.; Neckers, L., Impact of heat-shock protein 90 on cancer metastasis. *Future Oncol.* **2009,** 5, 679-688.

111. Price, J. T.; Quinn, J. M.; Sims, N. A.; Vieusseux, J.; Waldeck, K.; Docherty, S. E.; Myers, D.; Nakamura, A.; Waltham, M. C.; Gillespie, M. T.; Thompson, E. W., The heat shock protein 90 inhibitor, 17-allylamino-17-demethoxygeldanamycin, enhances osteoclast formation

and potentiates bone metastasis of a human breast cancer cell line. *Cancer Res.* **2005,** 65, 4929-4938.

112. Clarke, P. A.; Hostein, I.; Banerji, U.; Stefano, F. D.; Maloney, A.; Walton, M.; Judson, I.; Workman, P., Gene expression profiling of human colon cancer cells following inhibition of signal transduction by 17-allylamino-17-demethoxygeldanamycin, an inhibitor of the hsp90 molecular chaperone. *Oncogene* **2000,** 19, 4125-4133.

113. Yin, J. J.; Pollock, C. B.; Kelly, K., Mechanisms of cancer metastasis to the bone. *Cell Res.* **2005,** 15, 57-62.

114. Bae, J.; Mitsiades, C.; Tai, Y. T.; Bertheau, R.; Shammas, M.; Batchu, R. B.; Li, C.; Catley, L.; Prabhala, R.; Anderson, K. C.; Munshi, N. C., Phenotypic and functional effects of heat shock protein 90 inhibition on dendritic cell. *J. Immunol.* **2007,** 178, 7730-7737.

115. Ramirez, V.; Mejia-Vilet, J. M.; Hernandez, D.; Gamba, G.; Bobadilla, N. A., Radicicol, a heat shock protein 90 inhibitor, reduces glomerular filtration rate. *Am. J. Physiol. Renal Physiol.* **2008,** 295, F1044-1051.

116. Garcia-Cardena, G.; Fan, R.; Shah, V.; Sorrentino, R.; Cirino, G.; Papapetropoulos, A.; Sessa, W. C., Dynamic activation of endothelial nitric oxide synthase by Hsp90. *Nature* **1998,** 392, 821-824.

117. Pritchard, K. A., Jr.; Ackerman, A. W.; Gross, E. R.; Stepp, D. W.; Shi, Y.; Fontana, J. T.; Baker, J. E.; Sessa, W. C., Heat shock protein 90 mediates the balance of nitric oxide and superoxide anion from endothelial nitric-oxide synthase. *J. Biol. Chem.* **2001,** 276, 17621-17624.

118. Xu, H.; Shi, Y.; Wang, J.; Jones, D.; Weilrauch, D.; Ying, R.; Wakim, B.; Pritchard, K. A., Jr., A heat shock protein 90 binding domain in endothelial nitric-oxide synthase influences enzyme function. *J. Biol. Chem.* **2007,** 282, 37567-37574.

119. Yetik-Anacak, G.; Xia, T.; Dimitropoulou, C.; Venema, R. C.; Catravas, J. D., Effects of hsp90 binding inhibitors on sGC-mediated vascular relaxation. *Am. J. Physiol. Heart Circ. Physiol.* **2006,** 291, H260-268.

120. Janin, Y. L., ATPase inhibitors of heat-shock protein 90, second season. *Drug Discov. Today* **2010,** 15, 342-353.

121. Solit, D. B.; Basso, A. D.; Olshen, A. B.; Scher, H. I.; Rosen, N., Inhibition of heat shock protein 90 function down-regulates Akt kinase and sensitizes tumors to Taxol. *Cancer Res.* **2003,** 63, 2139-2144.

122. Xiao, L.; Rasouli, P.; Ruden, D. M., Possible effects of early treatments of hsp90 inhibitors on preventing the evolution of drug resistance to other anti-cancer drugs. *Curr. Med. Chem.* **2007,** 14, 223-232.

Chapter II

cis-Radamide Analogs: Conformationally Constrained Chimeric N-terminal Hsp90 Inhibitors

II.1 Rationale for the Development of *cis*-Amide Inhibitors

The 90 kDa heat shock proteins (Hsp90) are ATP-dependent molecular chaperones that are overexpressed in response to cellular stress and necessary for the folding, activation, stabilization and/or rematuration of polypeptides.[1-4] Two natural products depicted in Figure 10, geldanamycin[5] (GDA) and radicicol[6] (RDC), bind competitively to the Hsp90 N-terminal binding pocket, resulting in degradation of Hsp90-dependent client proteins *via* the ubiquitin-proteasome pathway.[7] Hsp90 clientele play key roles in multiple hallmarks of cancer,[8] therefore, inhibition of the Hsp90 protein folding machinery results in simultaneous disruption of numerous mechanisms of oncogenesis.[9, 10] Consequently, not only has Hsp90 emerged as a promising anti-cancer target,[11] but GDA and RDC have proven to represent excellent models for which the development of new Hsp90 inhibitors can be pursued for drug development and mechanistic investigations.[12]

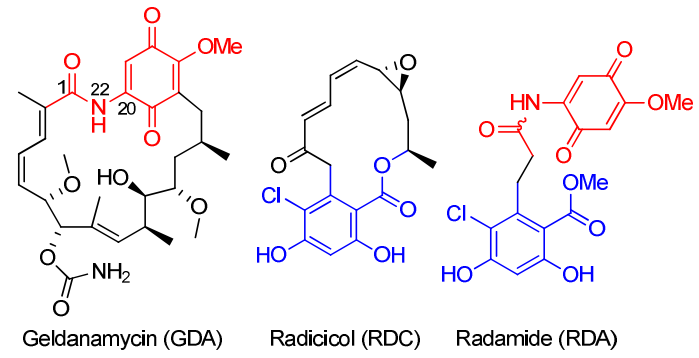

Figure 10. Structures of N-terminal Hsp90 inhibitors. GDA and RDC are natural product inhibitors and RDA is a chimeric inhibitor developed in the Blagg laboratory.

Although RDC and GDA both bind the Hsp90 N-terminal ATP Bergerat-fold with high affinity, their modes of binding and inhibitory activities are different. Radicicol exists in a bent conformation whether bound or unbound to Hsp90 (Figure 11) and produces a favorable entropy of 8.3 cal/mol upon binding.[13] Not surprisingly, the predisposition of RDC to the bent conformation is believed to be a contributing factor towards its similar activity in both cellular and recombinant assays.[13, 14] Even though RDC is the most potent *in vitro* natural product inhibitor of Hsp90 identified to date, its metabolic liabilities and physiologic instability preclude RDC's use therapeutically. Thiols such as dithiothreitol (DTT) inactivate RDC, suggesting physiological inactivation by endogenous antioxidants such as glutathione.[15]

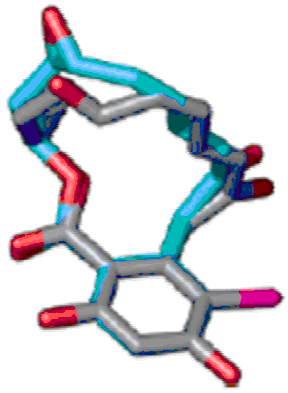

Figure 11. Solid-state structure of RDC (gray) overlapped with the Hsp90 bound conformation (cyan).

Numerous analogs of RDC, which address the instability of the electrophilic epoxide and α,β,γ,δ-unsaturated ketone moieties, have been prepared and evaluated for Hsp90 inhibitory activity.[16, 17] Studies by Moulin *et al.* utilizing molecular dynamics simulations suggested a correlation between the conformation of RDC analogs and potency.[14] Despite the syntheses of various analogs that exhibit greater stability, potency, and retain a bioactive ground-state conformation, no RDC-based analogs are currently under clinical evaluation. In contrast, considerable effort has been devoted towards the development of GDA-based semi-synthetics as chemotherapeutics.[18]

In contrast to the bent, *cis*-amide conformation of GDA when bound to Hsp90, both solution and crystal structures have demonstrated that this natural product exists in an extended,

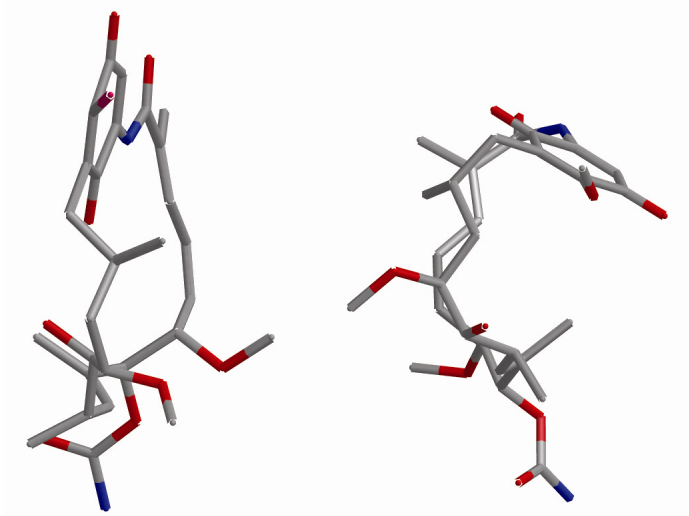

Figure 12. Solution structure of GDA (left) and the Hsp90 bound structure (right).

trans-amide conformation in the ground state (Figure 12).[19] Multiple studies have shown that prior to binding Hsp90, GDA must undergo two conformational changes; the ansa ring must rotate over the benzoquinone moiety and the amide bond must isomerize from *trans* to *cis* by rotation about C_1–N_{22} and C_{20}–N_{22} (Figure 10).[20] The first event is reported to occur spontaneously; however, isomerization of the amide bond is suggested to be Hsp90-dependent.[20] Accordingly, isothermal titration calorimetry (ITC) experiments have shown that GDA exhibits an entropic penalty of −6.4 cal/mol upon binding Hsp90.[21, 22]

As a consequence of these thermodynamic data, Jez and coworkers hypothesized that GDA analogs containing a predisposed *cis*-amide bond will result in ~1000 fold increase in Hsp90 affinity through reduction of entropic penalties.[23] Such postulations have inspired subsequent studies aimed at determining the effect of *trans/cis* isomerization of the GDA-amide moiety.[24-26] However, to the best of our knowledge, no analogs had been synthesized that exhibited a predisposed *cis*-amide functionality.

Recently, chimeric inhibitors of Hsp90 were disclosed that contained both the quinone ring from GDA and the resorcinol moiety of RDC in an attempt to mimic the hydrogen-bonding interactions exemplified by the two natural products when bound to the Hsp90 N-terminal nucleotide-binding pocket (Figure 13).[27] Although this approach produced novel scaffolds for

Hsp90 inhibition, none of the reported analogs exhibited conformational characteristics observed by the natural products when bound to Hsp90.[27-29] Analysis of the *seco* derivative, radamide (RDA), revealed the potential to introduce conformational aspects of both natural products when bound to Hsp90, specifically a bent conformation and a ground-state *cis*-amide moiety. Furthermore, of the three classes of chimeric inhibitors developed in our laboratory, RDA represented the most synthetically accessible scaffold for which to incorporate the desired conformational characteristics. The compounds developed have been classified as *cis*-RDA analogs.

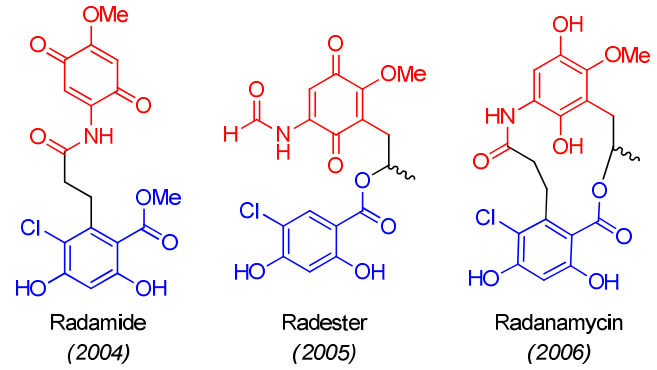

Figure 13. Chimeric Hsp90 inhibitors developed in the Blagg Laboratory.

II.2 Synthesis of *cis*-Radamide Analogs

Retrosynthetically, we envisioned the desired analogs to be obtained via a Horner–Wadsworth–Emmons (HWE) olefination reaction between cyclic phosphonate **1** and homologated aldehydes, **2** and **3** (Scheme 1). Compound **1** was proposed to result from tandem reduction/intramolecular cyclization of compound **4**, which could be obtained from commercially available 4-benzyloxy-3-methoxybenzaldehyde in 4 steps. Aldehydes **2** and **3** could be prepared

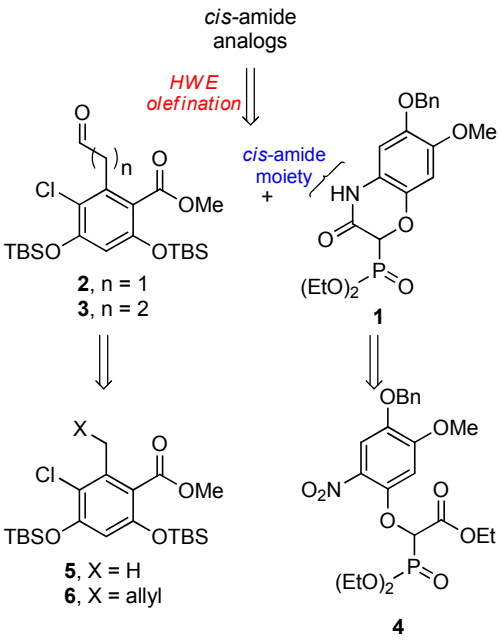

Scheme 1. Retrosynthetic analysis for the synthesis of *cis*-amide chimeric analogs.

directly from **5**[28] and **6,** respectively.

Commencing with commercially available 4-benzyloxy-3-methoxy benzaldehyde (**7**, Scheme 2), phenol **8** was formed via a Dakin oxidation. Treatment of **8** with diazophosphonate **9**, enlisting a rhodium carbenoid mediated O-H insertion, resulted in the phenolic ether **10**. Regioselective nitration of **10** was accomplished utilizing mild ammonium nitrate and trifluoroacetic anhydride conditions. Refluxing **4** with tin(II) chloride resulted in not only reduction of the nitro group to the corresponding aniline, but also cyclization to give the desired key intermediate, **1**.

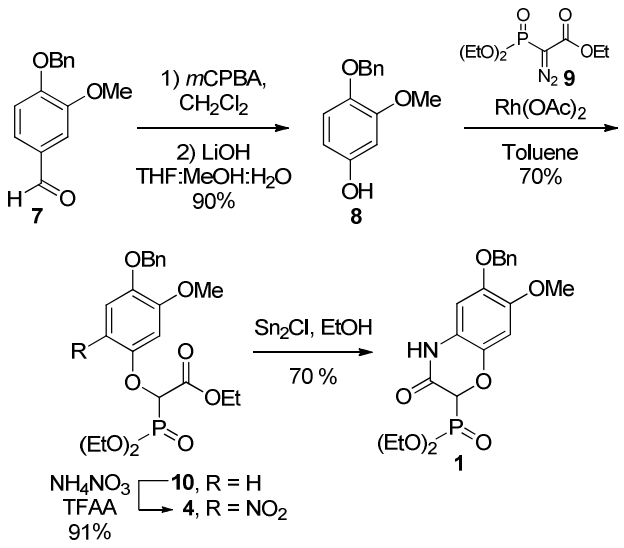

Scheme 2. Synthesis of *cis*-amide cyclic phosphonate.

The protected resorcinylic precursors were prepared by treatment of **5** with lithium diisopropylamide at -78°C to generate the benzylic anion, which was quenched upon addition of dimethylformamide to afford the aldehyde product, **2**, or with allyl bromide to give **6** (Scheme 3). Oxidation of **6** with osmium tetroxide gave the corresponding diol, which was cleaved in situ with sodium periodate to yield the homologated aldehyde, **3**.

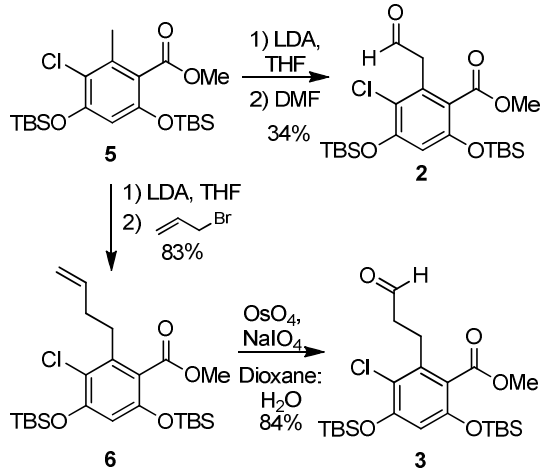

Scheme 3. Synthesis of homologated aldehydes.

With the synthons in hand, the fragments

were joined via a Horner–Wadsworth–Emmons olefination reaction and subsequent removal of the *tert*-butyl-dimethylsilyl protecting groups with tetrabutylammonium fluoride provided compounds **11–14** (Scheme 4).

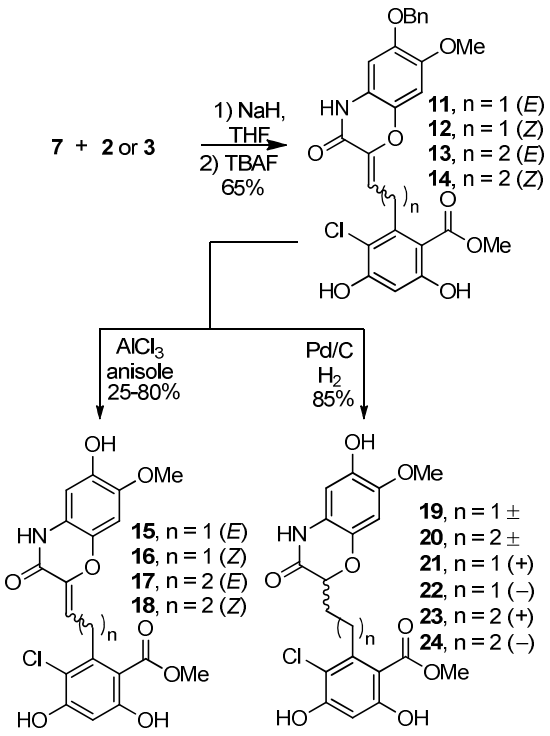

Scheme 4. Fragment coupling and deprotection.

Originally, we were only interested in the saturated analogs, but realized the olefinated intermediates exhibited higher conformational rigidity than the saturated analogs. Thus, we attempted to selectively remove the benzyl ether in the presence of the unsaturated amide with procedures reported in literature including $FeCl_3$, $Pd(OAc)_2/Et_3SiH/Et_3N$, and NaI/TMSCl. However, none of these conditions afforded the desired products. Eventually, conditions employing aluminum(III) chloride in anisole effectively cleaved the benzyl ether without alteration of the α,β-unsaturated amide to afford compounds **15–18 (**Scheme 4).

Standard hydrogenation conditions with palladium on carbon under hydrogen atmosphere yielded racemic products **19** and **20**, which were subjected to chiral HPLC to afford the enantiopure analogs, **21**–**24** (Scheme 4).

Table 4. Anti-proliferative and ATPase activity of *cis*-amide analogs. IC_{50} values expressed as μM concentrations unless otherwise noted.

Compound	MCF-7	SKBr3	ATPase
15	3.2 ± 0.1	1.8 ± 0.1	2.4 ± 0.1
16	78.9 ± 11.3	57.1 ± 8.4	–
17	1.5 ± 0.1	1.2 ± 0.1	1.6 ± 0.0
18	9.8 ± 1.9	15.9 ± 4.1	–
19	4.8 ± 1.1	7.3 ± 0.2	–
20	6.3 ± 0.9	7.8 ± 0.2	–
21	3.6 ± 0.1	2.1 ± 0.2	1.5 ± 0.1
22	14.9 ± 0.2	15.4 ± 0.8	–
23	2.7 ± 0.5	2.1 ± 0.7	1.2 ± 0.0
24	78.0 ± 4.4	15.4 ± 0.8	–
Radamide	18.6 ± 0.9	23.7 ± 1.7	5.9
GDA	9.8 ± 0.1 nM	8.5 ± 1.1 nM	2.5 ± 0.4
RDC	47.7 ± 2.6 nM	37.5 ± 4.0 nM	0.4 ± 0.0

IC_{50} = concentration needed to produce 50% inhibition

II.3 Biological Evaluation of *cis*-Radamide Analogs

II.3.1 *Anti-proliferation Activity*

Anti-proliferation studies with compounds **15–24** were conducted against MCF-7 and SKBr3 breast cancer cell lines. As shown in Table 4, the *E*-olefin is more active than the *Z*-olefin for both linker lengths and the (+)-enantiomer is more active than the (–)-enantiomer. Rationale for the observed results will be provided in section II.4.1.

II.3.2 *Inhibition of Hsp90 ATPase Activity*

To evaluate this series for inhibition of ATPase activity,[30] recombinant yeast Hsp90 (yHsp90) was overexpressed in *Escherichia coli* and purified.[31] The purified protein was incubated with ATP in the presence of **15**, **17**, **21**, and **23** following the assay protocol previously

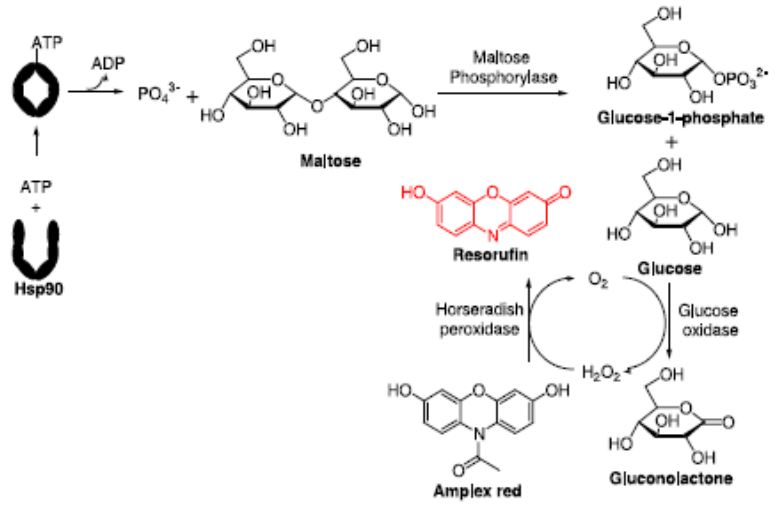

Figure 14. Mechanism of coupled ATPase assay.[30]

developed in our laboratory**.** As depicted in Figure 14, inorganic phosphate is produced upon Hsp90 mediated ATP hydrolysis. Maltose phosphorylase subsequently mediates the phosphorylation of maltose and cleavage of the glycosidic linkage to produce glucose-1-phosphate and free glucose. The free glucose is oxidized by glucose oxidase in the presence of molecular oxygen to produce hydrogen peroxide (H_2O_2) and gluconolactone. The resulting H_2O_2, is utilized by horseradish peroxidase to reduce Amplex Red, which is present in the assay media, to resorufin, which can be measured spectroscopically. However, in the presence of an Hsp90 inhibitor, Hsp90's ATPase activity is inhibited and inorganic phosphate is not produced, thus the catalytic cycle responsible for resorufin production is circumvented. This provides a method to measure inhibition of Hsp90's inherent ATPase activity through measurement of resorufin absorption at 563 nm.

As shown in Table 4, the ATPase IC_{50} values correlated to those observed in the anti-proliferation studies, suggesting equipotency of these analogs for the heteroprotein complex present in transformed cells and the purified homodimeric species employed in the ATPase assay.

II.3.3 *Western Blot Analyses*

To confirm the anti-proliferative nature of these compounds resulted from Hsp90 inhibition, representative compounds **17** and **23** were incubated with MCF-7 cells for 24 h and Western blot analyses were performed with the cell lysates (Figure 15). As expected, the immunoblots confirmed concentration-dependent degradation of Hsp90-dependent client proteins, Her2 and Raf at concentrations reflective of the corresponding anti-proliferative IC_{50} values, thus linking cell viability to Hsp90 inhibition. Western blot analyses also demonstrated induction of the heat shock response, as indicated by induction of Hsp70, which is a common

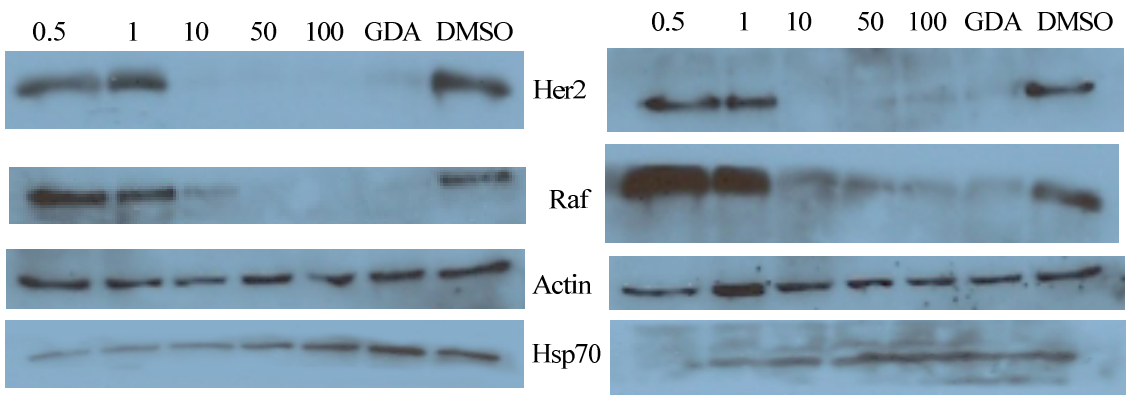

Figure 15. Western blot analyses of compounds **17** (left) and **23** (right). Concentrations denoted in μM.

downstream affect resulting from N-terminal Hsp90 inhibition. Actin is not an Hsp90 client protein, therefore its concentration is unaffected by the compounds and can be used as a loading control.

II.4 Interaction of cis-Radamide with Hsp90 and Grp94

II.4.1 *Co-crystal Structure of cRDA Bound to Hsp90*

Preliminary biological studies with *cis*-RDA analogs confirmed a characteristic Hsp90 inhibitory profile. Since the *cis*-RDA class of chimeric Hsp90 inhibitors represented a new class of conformationally constrained N-terminal inhibitors, compound **20** (cRDA) was sent to Dr. Daniel Gewirth at the Hauptman–Woodward Medical Research Institute for co-crystallization studies. The racemic compound was chosen solely on the basis of the quantity of material needed. Inspired by the differences between the co-crystal structures for the *seco*-analog RDA with the N-terminal domains of both the yeast homolog of human Hsp90 (yHsp90N) and canine Grp94 (dGrp94N),[32] the Gewirth laboratory attempted to co-crystallize cRDA with both chaperones; however, only a co-crystal structure for cRDA bound to the N-terminus of human Hsp90α (hHsp90N) was successful (Figure 16).

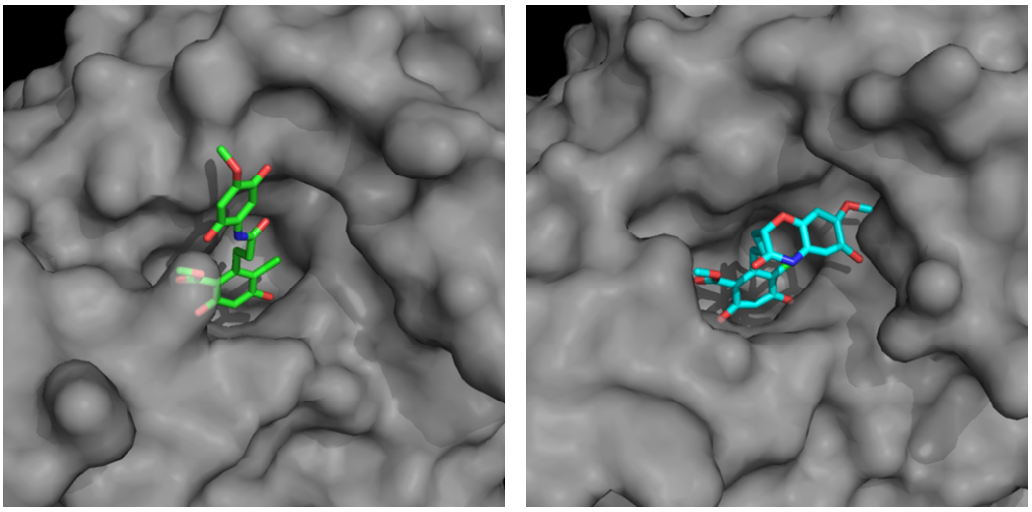

Figure 16. RDA (left, green) bound to yHsp90N and cRDA (right, blue) bound to hHsp90N.

As revealed in the next section, the inability to co-crystallize cRDA with Grp94 does not suggest lack of binding. It is well accepted in the Hsp90 structural biology community that Grp94 is inherently difficult to co-crystallize. This isoform is incredibly flexible and adopts numerous ligand dependent conformations. Thus obtaining co-crystal structures of ligands bound to Grp94 is arduous and often unsuccessful. Nevertheless, comparison of RDA and cRDA with yHsp90N and hHsp90N, respectively, provides valuable insights.

In both RDA and cRDA (unpublished) co-crystal structures, the resorcinol ring makes a direct hydrogen-bonding interaction with the carboxylate of the aspartic acid residue (Asp79 in yHsp90) required for ATP binding, thus inhibiting the ability of ATP to bind (Figure 17).[32] This orientation is

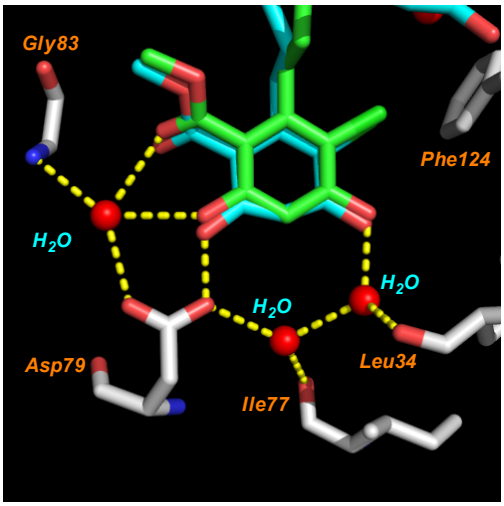

Figure 17. Resorcinylic hydrogen-bonding network of RDA (green) and cRDA (blue) with yHsp90N labeled amino acids.

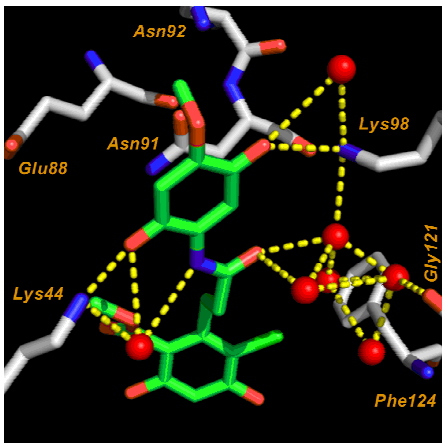

Figure 18. Quinone interactions of RDA with yHsp90N.

consistent with all of the resorcinylic inhibitors to date. Furthermore, the chlorine functionality on both inhibitors projects towards a hydrophobic pocket containing Phe124, while the methyl ester participates in a water mediated hydrogen-bonding network with Asp79 and the backbone of Gly83.[32]

The difference in co-crystal structures becomes evident when examining the amide portion of both inhibitors. The quinone moiety of RDA projects towards the solvent (Figure 18) and makes direct hydrogen-bonding interactions with Lys44 and Lys98.[32] Water-mediated contacts between Lys44, Glu88, Asn91, Asn92 and Lys98 and the quinone are also observed. An additional water-mediated hydrogen bond network is also observed between the amide-linker and Lys98, Gly121 and the Phe124 backbone.[32] These hydrogen-bonding networks elicit a *trans*-amide conformation of RDA when bound to the Hsp90 N-terminal ATP-binding pocket, further exemplifying the inability of the chimeric *seco* analogs to bind in a manner observed by either natural product inhibitor of Hsp90.

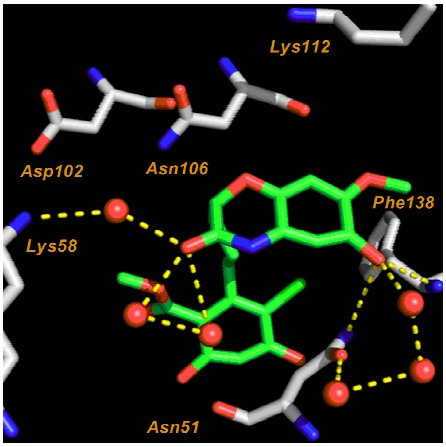

Figure 19. Quinone mimic interactions of cRDA with hHsp90N.

In contrast to the linear conformation exhibited by RDA, cRDA binds the Hsp90 N-terminal ATP-binding pocket in a bent conformation indicative of the constraint induced *via* the *cis*-amide moiety and the appending stereocenter (Figure 19). This binding mode, provides an explanation for the differences in anti-proliferative

activity exhibited by +/– enantiomers or *E/Z* olefins (Table 4), as a specific geometry is necessary for binding the Hsp90 N-terminal binding pocket. This binding orientation results in direct hydrogen-bonding contacts between the cRDA phenol and the backbone of Phe138 (Phe124 in yHsp90) and Asn51 (Asn37 in yHsp90). An additional water-mediated hydrogen-bonding network occurs between the amide carbonyl of cRDA and Lys58 (Lys44 in yHsp90). No obvious interactions are observed between cRDA and Asp102, Asn 105, Asn106 or Lys112 (Glu88, Asn91, Asn92 and Lys98 in yHsp90); all of which are amino acids that interact with the quinone region of RDA. Therefore, the binding mode of cRDA provides a unique set of interactions with Hsp90 and yields a novel scaffold exploitable for inhibitor design.

II.4.2 *Binding Affinity of cRDA for Hsp90 and Grp94*

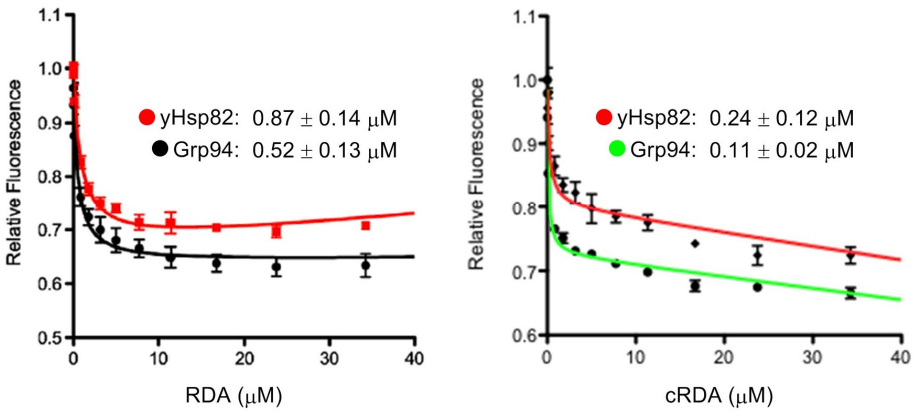

Figure 20. Tryptophan fluorescence titration for binding of RDA and cRDA to full-length yHsp90 and dGrp94.

Although Gewirth and colleagues were unable to isolate high quality crystals of cRDA bound to Grp94, they were able to determine the binding affinity of cRDA to both full-length yHsp90 and dGrp94 through tryptophan fluorescence quenching (TFQ) analysis. Proteins generally exhibit intrinsic fluorescence, which is predominantly derived from tryptophan residues. Research has shown that upon binding N-terminal ligands, Hsp90 undergoes conformational changes that results in tryptophan fluorescence quenching.[33] Thus, TFQ has

been validated as a method to measure the binding affinity of Hsp90 N-terminal ligands. The binding affinity values for cRDA were determined to be 0.24 ± 0.12 μM for yHsp90 and 0.11 ± 0.02 μM for dGrp94. A comparison of these values to the *seco*-analog RDA values (0.87 ± 0.14 μM for yHsp90 and 0.52 ± 0.13 μM for dGrp94), shows ~4-fold increase in affinity for both Hsp90 isoforms (Figure 20**)**. These results suggest that both Hsp90 and Grp94 are sensitive to ligand conformation, which provides an avenue for the design of isoform selective inhibitors.

II.5 Concluding Remarks

In conclusion, we have designed, synthesized, and provided biological data for a series of analogs that not only contain hydrogen bonding moieties exhibited by GDA and RDC, but also exhibit the conformational biases adopted by the natural products when bound to Hsp90 *via* inclusion of a bent conformation and a *cis*-amide moiety. In accord with Jez and co-workers,[23] introduction of a *cis*-amide moiety increased Hsp90 inhibitory activity (~10 fold), compared to RDA. As indicated by the biological results, introduction of both the *cis*-amide and the bent conformation to the chimeric inhibitors does not influence activity against purified recombinant Hsp90; however, the activity against cancer cells increased ~10-fold with respect to the *seco* derivative, RDA. These results coincide with the hypotheses posed by multiple groups, who suggest a mechanistic difference between the heteroprotein complex and purified recombinant Hsp90. In addition, the data demonstrates the heteroprotein complex is more sensitive to amide isomerization and conformational predisposition.

Examination of the co-crystal structures of RDA[32] and cRDA bound to Hsp90 homologs shows different binding modes of the quinone portions. RDA binds Hsp90 in a linear conformation resulting in hydrogen bonding interactions with the lid of the Hsp90 N-terminal ATP-binding pocket,[32] whereas cRDA folds towards an α-helix at the front of the pocket forming

a unique set of hydrogen-bonding interactions. The unique binding mode of cRDA coupled with the binding affinity data for this inhibitor with yHsp90 and dGrp94 led us to development of selective Grp94 inhibitors.

II.6 Methods and Experimentals

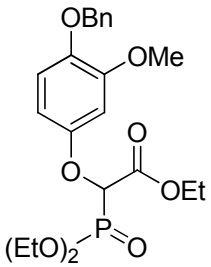

Ethyl 2-(4-(benzyloxy)-3-methoxyphenoxy)-2-(diethoxyphosphoryl)acetate (10): Rhodium (II) acetate (1 mol%) was added to a solution of **8** (2.90 g, 12.61 mmol) and **9** (1.58 g, 6.32 mmol) dissolved in anhydrous toluene (50 mL) at rt. The suspension was warmed to 90 °C for 18 h under argon atmosphere. The cooled solution was poured over a plug of celite and concentrated in vacuo. Flash chromatography (SiO_2, 20% EtOAc in Et_2O) gave **10** (2.00 g, 70%) as a colorless amorphous solid: ^{1}H NMR ($CDCl_3$, 400 MHz) δ 7.45 – 7.31 (m, 5H), 6.77 (d, *J* = 8.8, 1H), 6.67 (d, *J* = 2.9, 1H), 6.31 (dd, *J* = 2.9, 8.8, 1H), 5.09 (s, 2H), 4.97 (d, *J* = 18.8, 1H), 4.36 – 4.26 (m, 6H), 3.88 (s, 3H), 1.39 (t, *J* = 7.1, 6H), 1.30 (t, *J* = 7.1, 3H); ^{13}C NMR ($CDCl_3$, 100 MHz) δ 166.6, 152.8 (d, *J* = 13.6), 150.8, 143.7, 137.2, 128.5 (2C), 127.8, 127.4 (2C), 114.9, 104.5, 102.1, 75.2 (d, *J* = 157.7), 71.8, 64.1 (d, *J* = 7.5), 64.0 (d, *J* = 6.3), 62.2, 55.6, 16.4 (d, *J* = 6.3), 16.4 (d, *J* = 5.0), 14.1; ESI-HRMS *m/z* 453.1667 ($M + H^+$, $C_{22}H_{29}O_8P$ requires 453.1678).

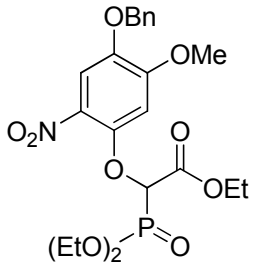

Ethyl 2-(4-(benzyloxy)-5-methoxy-2-nitrophenoxy)-2-(diethoxyphosphoryl)acetate (4): Compound **10** (0.96 g, 2.12 mmol) was dissolved in anhydrous THF (22 mL) and cooled to 0 °C under an argon atmosphere. Ammonium nitrate (0.25 g, 3.12 mmol) was added at once and trifluoroacetic anhydride (1.76 g, 8.38 mmol) was added dropwise to the stirred suspension. The resulting solution was warmed to 25 °C and stirred 1 h, before saturated aqueous $NaHCO_3$ (10 mL) was added. The resulting biphasic solution was poured into EtOAc (25 mL) and the aqueous layer washed with EtOAc (2 x 20 mL). The combined organic layers were combined, dried with Na_2SO_4, and concentrated. Flash chromatography (SiO_2, 20% EtOAc in Et_2O) gave **5** (0.95 g, 91%) as a yellow amorphous solid: ^{1}H NMR (400 MHz, CDCl3) δ 7.63 (s, 1H), 7.47 – 7.33 (m, 5H), 6.75 (s, 1H), 5.15 (s, 2H), 5.10 (d, *J* = 17.3, 1H), 4.42 – 4.28 (m, 6H), 3.93 (s, 3H), 1.44 – 1.36 (m, 6H), 1.31 (t, *J* = 7.1, 3H); ^{13}C NMR ($CDCl_3$, 100 MHz) δ 165.8, 154.9, 147.7 (d, *J* = 12.2), 143.3, 135.7 (2C), 132.5, 128.7 (2C), 128.4, 127.6, 110.9, 102.1, 77.2 (d, *J* = 155.4), 71.6, 64.7 (d, *J* = 6.3), 64.4 (d, *J* = 7.5), 62.5, 56.5, 16.4 (d, *J* = 5.0), 16.4 (d, *J* = 6.3), 14.1; ESI-HRMS *m/z* 496.1380 ($M - H^+$, $C_{22}H_{28}NO_{10}P$ requires 496.1373).

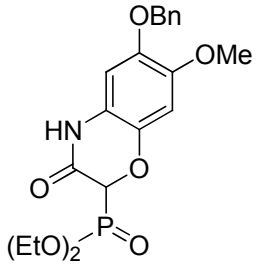

Diethyl 6-(benzyloxy)-7-methoxy-3-oxo-3,4-dihydro-2H-benzo[b][1,4]oxazin-2-ylphosphonate (1): Tin (II) chloride (2.50 g, 13.16 mmol) was added to a solution of **4** (0.97 g, 1.95 mmol) in absolute ethanol (2.5 mL) and the suspension was refluxed for 1 h before pouring into saturated aqueous $NaHCO_3$ (25 mL). Precipitate was filtered and washed with EtOAc (25 mL) and H_2O (25 mL). The filtrate was rinsed with EtOAc (3 x 15 mL) and the organic layers were combined, dried with Na_2SO_4, and concentrated. Recrystallization with EtOAc and hexanes gave **6** (0.59 g, 72%) as a white amorphous solid: ^{1}H NMR (400 MHz, $CDCl_3$) δ 8.71 (s, 1H), 7.46 – 7.30 (m, 5H), 6.65 (s, 1H), 6.43 (s, 1H), 5.02 (s, 2H), 5.00 (d, *J* = 16.2, 1H), 4.25 – 4.03 (m, 4H), 3.82 (s, 3H), 1.34 (t, *J* = 7.1, 3H), 1.24 (t, *J* = 7.1, 3H); ^{13}C NMR ($CDCl_3$, 100 MHz) δ 161.7 (d, *J* = 3.1), 146.5, 143.7, 136.8, 136.4 (d, *J* = 1.8), 128.6 (2C), 128.0, 127.5 (2C), 117.9, 103.8, 102.0, 74.1 (d, *J* = 151.5), 72.0, 63.8 (d, *J* = 6.3), 63.7 (d, *J* = 7.5), 56.4, 16.4 (d, *J* = 7.5), 16.3 (d, *J* = 5.0); ESI-HRMS *m/z* 420.1207 ($M - H^+$, $C_{20}H_{24}NO_7P$ requires 420.1212).

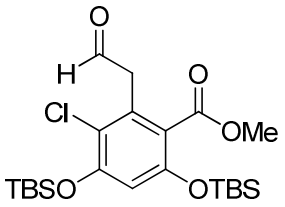

Methyl 4,6-bis(tert-butyldimethylsilyloxy)-3-chloro-2-(2-oxoethyl)benzoate (2): A 1.0 M solution of lithium diisopropylamide (3.7 mL, 3.71 mmol) was added dropwise to a solution of **5** (1.50 g, 3.37 mmol) dissolved in anhydrous THF (35 mL) at -78°C. After stirring 5 min under argon atmosphere, DMF (4.93 g, 67.45 mmol) was added at once under the solution level and the reaction stirred at -78°C for 10 min. The resulting solution was poured into saturated aqueous NH_4Cl (100 mL) previously cooled to 0°C. This mixture stirred at 0°C for 30 minutes. The product was extracted with EtOAc (50 mL) and the aqueous layer was washed with EtOAc (3 x 30 mL). The combined organic layers were washed with saturated aqueous NaCl, dried with

Na_2SO_4, and concentrated. Flash chromatography (SiO_2, 5% EtOAc in hexanes) gave **2** as a yellow oil (0.53 g, 34%): ^{1}H NMR ($CDCl_3$, 400 MHz) δ 9.65 (t, *J* = 1.5, 1H), 6.42 (s, 1H), 3.84 (s, 3H), 3.83 (d, *J* = 1.5, 2H), 1.05 (s, 9H), 0.98 (s, 9H), 0.27 (s, 6H), 0.24 (s, 6H); ^{13}C NMR ($CDCl_3$, 100 MHz) δ 195.3, 165.1, 151.1, 149.9, 128.7, 119.0, 117.3, 108.3, 49.9, 43.7, 23.2 (3C), 23.1 (3C), 16.0, 15.7, -6.7 (2C), -6.8 (2C); ESI-HRMS *m/z* 473.1940 (M + H^+, $C_{22}H_{37}ClO_5Si_2$ requires 473.1946).

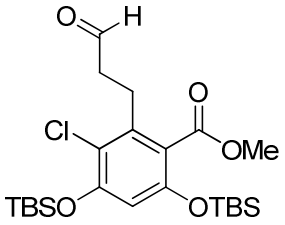

Methyl 4,6-bis(tert-butyldimethylsilyloxy)-3-chloro-2-(3-oxopropyl)benzoate (3): Osmium tetraoxide (96 µL) and sodium periodate (0.42 g, 1.96 mmol) were added consecutively to a solution of **6** (0.32 g, 0.66 mmol) in dioxane : H_2O (3 : 1) (10 mL) and the resulting solution stirred for 8 h. The precipitate was filtered and washed with EtOAc (20 mL). The filtrate was washed with H_2O (2 x 20 mL) and saturated aqueous NaCl (20 mL). The organic layer was collected, dried with Na_2SO_4, and concentrated in vacuo. Flash Chromatography (SiO_2, 5% EtOAc in hexanes) gave **3** as a colorless oil (0.27g, 84%): ^{1}H NMR ($CDCl_3$, 500 MHz) δ 9.59 (s, 1H), 6.11 (s, 1H), 3.63 (s, 3H), 2.73 (dd, *J* = 6.6, 9.3, 2H), 2.56 (dd, *J* = 6.5, 9.3), 0.81 (s, 9H), 0.74 (s, 9H), 0.02 (s, 6H), 0.00 (s, 6H); ^{13}C NMR ($CDCl_3$, 126 MHz) δ 201.0, 168.0, 153.1, 151.6, 137.7, 121.1, 118.4, 109.6, 52.3, 43.4, 25.6 (3C), 25.4 (3C), 24.7, 18.3, 18.0, -4.4 (2C), -4.4 (2C); ESI-HRMS *m/z* 487.2104 (M + H^+, $C_{23}H_{39}ClO_5Si_2$ requires 487.2103).

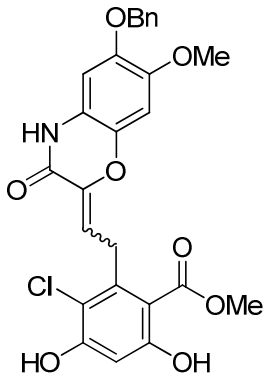

(*E*)-Methyl 2-(2-(6-(benzyloxy)-7-methoxy-3-oxo-3,4-dihydro-2H-benzo[b][1,4]oxazin-2-ylidene)ethyl)-3-chloro-4,6-dihydroxybenzoate (11): Sodium hydride (30.0 mg) was added to a suspension of **1** (0.26 g, 0.62 mmol) in anhydrous THF (6 mL) at 0 °C. The solution was warmed to 25 °C and stirred for 30 min under argon atmosphere before cooling to 0 °C. A 0.1M solution of **2** (0.35 g, 0.74 mmol) in anhydrous THF was canulated into the reaction mixture. The reaction was stirred at 0 °C for 30 min then warmed to 25 °C for 12 h. Tetrabutylammonium fluoride (2.5 mL, 2.47 mmol, 0.1 M solution in THF) was added dropwise and the reaction mixture stirred for 1 h. The reaction was quenched with saturated aqueous NH_4Cl and extracted with EtOAc (20 mL). The aqueous layer was rinsed with EtOAc (2 x 20 mL). The organic layers were combined, washed with saturated aqueous NaCl, dried with Na_2SO_4, and concentrated. Repeated flash chromatography (SiO_2, 30% EtOAc in hexanes) afforded the *cis* and *trans* (3:1) isomers giving **11** (0.16 g) and **12** (0.05g) in 67% overall yield: ^{1}H NMR (Acetone, 400 MHz) δ 9.58 (s, 1H), 7.48–7.32 (m, 5H), 6.72 (s, 1H), 6.66 (s, 1H), 6.53 (s, 1H), 5.55 (t, *J* = 6.8, 1H), 5.04 (s, 2H), 4.49 (d, *J* = 6.8, 2H), 3.89 (s, 3H), 3.80 (s, 3H); ^{13}C NMR (Acetone, 126 MHZ) δ 171.3, 162.1, 158.6, 158.3, 147.1, 144.7, 142.2, 142.1, 138.4, 137.4, 129.2 (2C), 128.7, 128.6 (2C), 119.1, 118.9, 115.2, 108.6, 104.1, 103.3, 102.1, 72.5, 56.8, 52.8, 31.1; ESI-HRMS 510.0938 ($M - H^+$, $C_{26}H_{22}ClNO_8$ requires 510.0956).

(*Z*)-Methyl 2-(2-(6-(benzyloxy)-7-methoxy-3-oxo-3,4-dihydro-2H-benzo[b][1,4]oxazin-2-ylidene)ethyl)-3-chloro-4,6-dihydroxybenzoate (12): ^{1}H NMR (Acetone, 400 MHz) δ 9.40 (s, 1H), 7.37–7.17 (m, 5H), 6.73 (s, 1H), 6.61 (s, 1H), 6.42 (s, 1H), 5.78 (t, *J* = 6.9, 1H), 4.93 (s, 2H), 3.97 (d, *J* = 6.9, 2H), 3.78 (s, 3H), 3.73 (s, 3H); ^{13}C NMR (Acetone, 126 MHZ) δ 171.3, 162.3, 158.8, 156.8, 147.1, 144.9, 143.4, 141.4, 138.4, 136.5, 129.2 (2C), 128.7, 128.6 (2C), 115.2, 112.4, 108.3, 104.2, 104.1, 103.3, 102.2, 72.4, 56.8, 53.0, 28.9; ESI-HRMS 510.0959 (M – H^+, $C_{26}H_{22}ClNO_8$ requires 510.0956).

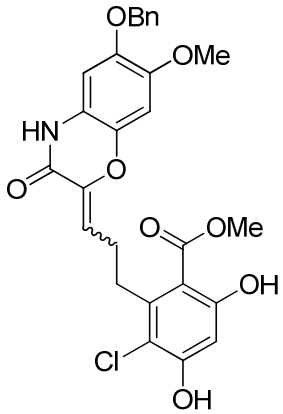

(*E*)-Methyl 2-(3-(6-(benzyloxy)-7-methoxy-3-oxo-3,4-dihydro-2H-benzo[b][1,4]oxazin-2-ylidene)propyl)-3-chloro-4,6-dihydroxybenzoate (13): Following the procedure to generate **11** and **12**, cyclophosphonate **1** (0.26 g, 0.62 mmol) was reacted with **3** (0.32 g, 0.66 mmol) in anhydrous THF (6 mL). Repeated flash chromatography (SiO_2, 30% EtOAc in hexanes) afforded the *cis* and *trans* (3:1) isomers giving **13** (0.15 g) and **14** (0.05 g) in 70% overall yield: ^{1}H NMR (Acetone, 400 MHz) δ 9.44 (s, 1H), 7.48–7.29(m, 5H), 6.69 (s, 1H), 6.69 (s, 1H), 6.49 (s, 1H), 5.72 (t, *J* = 8.0, 1H), 5.03 (s, 2H), 3.95 (s, 3H), 3.82 (s, 3H), 3.25–3.20 (m, 2H), 3.03–2.96 (m, 2H); ^{13}C NMR (Acetone, 126 MHZ) δ 171.6, 162.4, 158.6, 158.1, 147.1, 144.6, 143.5, 142.2, 138.4, 137.4, 129.2 (2C), 128.7, 128.6 (2C), 120.4, 119.2, 114.8, 108.1, 104.1, 103.0,

102.1, 72.5, 56.8, 52.8, 32.9, 27.4; ESI-HRMS 524.1115 (M – H^+, $C_{27}H_{24}ClNO_8$ requires 511.1112).

(*Z*)-Methyl 2-(3-(6-(benzyloxy)-7-methoxy-3-oxo-3,4-dihydro-2H-benzo[b][1,4]oxazin-2-ylidene)propyl)-3-chloro-4,6-dihydroxybenzoate (14): ^{1}H NMR (Acetone, 400 MHz) δ 9.48 (s, 1H), 7.50–7.29(m, 5H), 6.76 (s, 1H), 6.72 (s, 1H), 6.50 (s, 1H), 6.03 (t, *J* = 7.8, 1H), 5.06 (s, 2H), 3.98 (s, 3H), 3.83 (s, 3H), 3.30–3.20 (m, 2H), 2.63–2.57 (m, 2H); ^{13}C NMR (Acetone, 126 MHZ) δ 171.5, 158.7, 156.9, 147.0, 144.7, 143.8, 143.3, 138.4, 136.5, 129.2 (2C), 128.7 (2C), 128.6 (2C), 128.5, 118.7, 114.8, 113.9, 108.1, 104.2, 103.1, 102.1, 72.4, 56.8, 52.9, 32.0, 25.3; ESI-HRMS 524.1109 (M – H^+, $C_{27}H_{24}ClNO_8$ requires 511.1112).

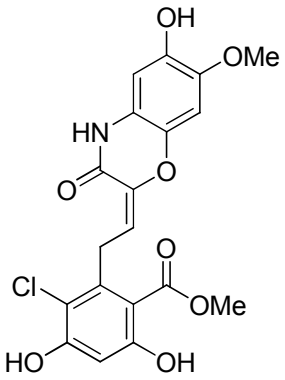

(*E*)-methyl 3-chloro-4,6-dihydroxy-2-(2-(6-hydroxy-7-methoxy-3-oxo-3,4-dihydro-2H-benzo[b][1,4]oxazin-2-ylidene)ethyl)benzoate (15): Aluminum (III) chloride (42.0 mg, 0.31 mmol) was added to a solution of **11** (40.0 mg, 0.08 mmol) in anhydrous anisole (10 mL) at 0 °C. This mixture was stirred at 0 °C and monitored closely by TLC. Upon complete conversion of **11**, MeOH (10 mL) was added and stirring continued while warming to 25°C. Concentration of the resulting solution followed by flash chromatography (SiO_2, 50% EtOAc in hexanes) gave **15** as a white amorphous solid (48.0 mg, 83%): ^{1}H NMR (Acetone, 400 MHz) δ 9.58 (s, 1H),

6.63 (s, 1H), 6.57 (s, 1H), 6.52 (s, 1H), 5.52 (t, *J* = 6.8, 1H), 4.48 (d, *J* = 6.8, 2H), 3.89 (s, 3H), 3.79 (s, 3H); ^{13}C NMR (Acetone, 126 MHZ) δ 171.2, 162.0, 158.7, 158.5, 144.0, 142.9, 142.3, 142.1, 136.0, 119.7, 118.6, 115.2, 108.6, 103.3, 103.1, 101.3, 56.8, 52.8, 31.1; ESI-HRMS 420.0486 (M – H$^+$, $C_{19}H_{16}ClNO_8$ requires 420.0486).

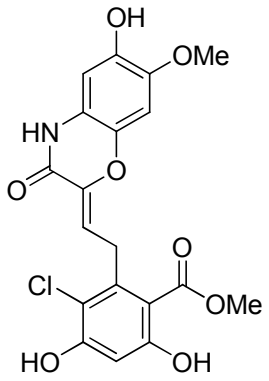

(Z)-methyl 3-chloro-4,6-dihydroxy-2-(2-(6-hydroxy-7-methoxy-3-oxo-3,4-dihydro-2H-benzo[b][1,4]oxazin-2-ylidene)ethyl)benzoate (16): Compound **12** (22.0 mg, 0.04 mmol) was subjected to the conditions used to generate **15**. Flash chromatography (SiO_2, 50% EtOAc in hexanes) gave **16** as a white amorphous solid (4.0 mg, 24%): ^{1}H NMR (Acetone, 400 MHz) δ 9.53 (s, 1H), 6.83 (s, 1H), 6.58 (s, 1H), 6.53 (s, 1H), 5.90 (t, *J* = 6.9, 1H), 4.10 (d, *J* = 6.9, 2H), 3.90 (s, 3H), 3.86 (s, 3H); ^{13}C NMR (Acetone, 126 MHZ) δ 171.5, 162.6, 159.9, 157.0, 144.1, 143.5, 143.1, 141.3, 135.1, 119.3, 115.7, 112.4, 107.4, 103.4, 103.3, 101.4, 56.9, 52.8, 29.0; ESI-HRMS 420.0496 (M – H$^+$, $C_{19}H_{16}ClNO_8$ requires 420.0486).

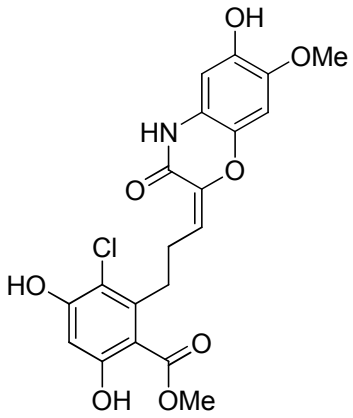

(*E*)-methyl 3-chloro-4,6-dihydroxy-2-(3-(6-hydroxy-7-methoxy-3-oxo-3,4-dihydro-2H-benzo[b][1,4]oxazin-2-ylidene)propyl)benzoate (17): Compound **13** (70.0 mg, 0.13 mmol) was subjected to the conditions used to generate **15**. Flash chromatography (SiO_2, 50% EtOAc in hexanes) gave **17** as a white amorphous solid (36.0 mg, 62%): ^{1}H NMR (Acetone, 400 MHz) δ 9.46 (s, 1H), 6.66 (s, 1H), 6.54 (s, 1H), 6.50 (s, 1H), 5.70 (t, *J* = 8.0, 1H), 3.95 (s, 3H), 3.82 (s, 3H), 3.24 – 3.21 (m, 2H), 3.00 (dd, *J* = 7.9, 15.9, 2H); ^{13}C NMR (Acetone, 126 MHZ) δ 171.6, 162.4, 158.9, 158.3, 144.0, 143.4, 142.8, 142.4, 136.0, 120.1, 119.7, 115.0, 107.9, 103.0, 103.0, 101.3, 56.9, 52.8, 33.0, 27.4; ESI-HRMS 434.0645 ($M - H^+$, $C_{20}H_{18}ClNO_8$ requires 434.0643).

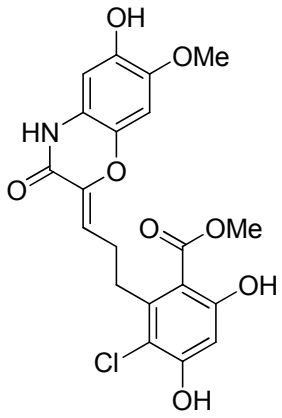

(Z)-methyl 3-chloro-4,6-dihydroxy-2-(3-(6-hydroxy-7-methoxy-3-oxo-3,4-dihydro-2H-benzo[b][1,4]oxazin-2-ylidene)propyl)benzoate (18): Compound **14** (7.0 mg, 0.013 mmol) was subjected to the conditions used to generate **15**. Flash chromatography (SiO_2, 50% EtOAc

in hexanes) gave **18** as a white amorphous solid (3.2 mg, 57%): ^{1}H NMR (Acetone, 400 MHz) δ 9.37 (s, 1H), 6.59 (s, 1H), 6.43 (s, 1H), 6.37 (s, 1H), 5.88 (t, *J* = 7.8, 1H), 3.85 (s, 3H), 3.69 (s, 3H), 3.16 – 3.06 (m, 2H), 2.49 – 2.42 (m, 2H); ^{13}C NMR (Acetone, 126 MHZ) δ 171.5, 162.4, 158.7, 157.1, 144.0, 144.0, 143.4, 143.0, 135.1, 119.2, 114.8, 113.6, 108.1, 103.2, 103.1, 101.4, 56.8, 52.9, 32.1, 25.3; ESI-HRMS 434.0635 ($M - H^+$, $C_{20}H_{18}ClNO_8$ requires 434.0643).

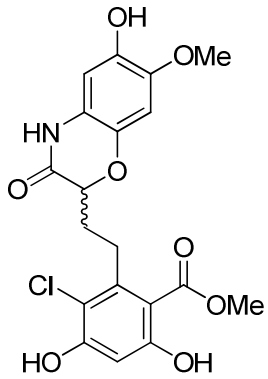

(±) Methyl 3-chloro-4,6-dihydroxy-2-(2-(6-hydroxy-7-methoxy-3-oxo-3,4-dihydro-2H-benzo[b][1,4]oxazin-2-yl)ethyl)benzoate (19): Palladium on carbon (10 mol%) was added to a stirred solution of mixed isomers **11** and **12** (60.0 mg, 0.12 mmol) in EtOAc (10 mL). Hydrogen was bubbled through the reaction mixture and then the reaction stirred under H_2 atmosphere for 12 h. The reaction was filtered through a plug of celite and the resulting filtrate was concentrated and purified by flash chromatography (SiO_2, 30% hexanes in EtOAc) to give **19** as an amorphous white solid (42.4 mg, 85%): ^{1}H NMR (Acetone, 400 MHz) δ 9.38 (s, 1H), 6.70 (s, 1H), 6.55 (s, 1H), 6.49 (s, 1H), 4.59–4.50 (m, 1H), 3.93 (s, 3H), 3.82 (s, 3H), 3.42–3.18 (m, 2H), 2.18–2.08 (m, 2H); ^{13}C NMR (Acetone, 126 MHZ) δ 171.4, 166.9, 162.3, 158.6, 144.0, 143.3, 142.8, 136.3, 121.5, 114.8, 108.2, 103.6, 103.4, 103.0, 78.0, 56.9, 52.8, 30.7, 29.1; ESI-HRMS 424.0783 ($M + H^+$, $C_{19}H_{18}ClNO_8$ requires 424.0799). Chiral HPLC with 15% EtOAc in hexanes

provided the pure enantiomers: **(+)-21**: $[\alpha]_D$ +137.1 (*c* = 0.24, $CHCl_3$); **(−)-22**: $[\alpha]_D$ -164.9 (*c* = 0.24, $CHCl_3$).

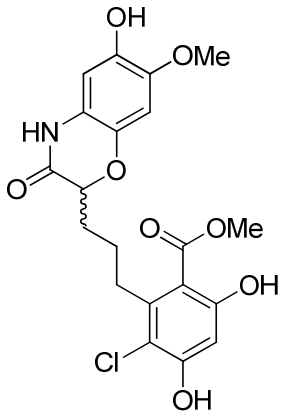

(±) Methyl 3-chloro-4,6-dihydroxy-2-(3-(6-hydroxy-7-methoxy-3-oxo-3,4-dihydro-2H-benzo[b][1,4]oxazin-2-yl)propyl)benzoate (20): Following the same procedure used to generate **19**, an E/Z mixture of **13** and **14** (106.9 mg, 0.20 mmol) were introduced to the conditions mentioned above. The resulting filtrate was concentrated and purified by flash chromatography (SiO_2, 30% hexanes in EtOAc) to give **20** as an amorphous white solid (49.0 mg, 85%): ^{1}H NMR (Acetone, 400 MHz) δ 9.32 (s, 1H), 6.68 (s, 1H), 6.54 (s, 1H), 6.49 (s, 1H), 4.47 (dd, *J* = 4.4, 8.2, 1H), 3.94 (s, 3H), 3.80 (s, 3H), 3.17–3.05 (m, 2H), 2.01–1.91 (m, 2H), 1.90–1.78 (m, 2H); ^{13}C NMR (Acetone, 126 MHZ) δ 171.6, 167.3, 162.4, 158.7, 144.2, 144.0, 142.8, 136.3, 121.6, 114.7, 107.9, 103.6, 102.9, 102.9, 77.6, 56.8, 52.8, 32.8, 31.0, 25.9; ESI-HRMS 438.0969 ($M + H^+$, $C_{20}H_{20}ClNO_8$ requires 438.0956). Chiral HPLC with 15% EtOAc in hexanes provided the pure enantiomers: **(+)** $[\alpha]_D$ +11.7 (*c* = 0.115, $CHCl_3$); **(−)** $[\alpha]_D$ -14.7 (*c* = 0.115, $CHCl_3$).

Anti-proliferation assay: MCF-7 and SKBr3 cells were maintained in a 1:1 mixture of Advanced DMEM/F12 (Gibco) supplemented with non-essential amino acids, L-glutamine (2 mM), streptomycin (500 μg/mL), penicillin (100 units/mL), and 10% FBS. Cells were grown to confluence in a humidified atmosphere (37 °C, 5% CO_2), seeded (2000/well, 100 μL) in 96-well plates, and allowed to attach overnight. Compound or geldanamycin at varying concentrations in DMSO (1% DMSO final concentration) was added, and cells were returned to the incubator for 72 h. At 72 h, the number of viable cells was determined using an MTS/PMS cell proliferation kit (Promega) per the manufacturer's instructions. Cells incubated in 1% DMSO were used as 100% proliferation, and values were adjusted accordingly. IC_{50} values were calculated from separate experiments performed in triplicate using GraphPad Prism.

ATPase assay: Recombinant yHsp90 was overexpressed and purified.[30, 31] The assay was run using optimized conditions previously reported and the P_iPer™ Phosphate Assay Kit (Molecular Probes #P-22061). Proper dilutions were made using the provided manufacturer's instructions. Assay solutions and conditions were taken directly from the optimized conditions previously published.[30] Each well contained a final volume of 100 μL. Wells were mixed by pipette and then shaken for approximately 30 s. Plates were then covered and incubated at 42 ºC while shaken for 2 h. Absorbance was measured at 563 nm and IC_{50} values were calculated using GraphPad Prism. Each compound was tested in triplicate on three separate occasions.

Western blot analysis: MCF-7 cells were cultured as described previously[28] and treated with various concentrations of drug, GDA in DMSO (1% DMSO final concentration), or vehicle (DMSO) for 24 h. Cells were harvested in cold PBS and lysed in RIPA lysis buffer containing 1

mM PMSF, 2 mM sodium orthovanadate, and protease inhibitors on ice for 1 h. Lysates were clarified at 1400 g for 10 min at 4 ºC. Protein concentrations were determined by using the Pierce BCA assay kit per the manufacturer's instructions. Equal amounts of protein (20 µg) were electrophoresed under reducing conditions, transferred to a nitrocellulose membrane, and immunoblotted with the corresponding specific antibodies. Membranes were incubated with an appropriate horseradish peroxidase-labeled secondary anti-body, developed with chemiluminescent substrate, and visualized.

II.7 References

1. Freeman, B. C.; Morimoto, R. I., The human cytosolic molecular chaperones Hsp90, Hsp70 (Hsc70) and Hdj-1 have distinct roles in recognition of a non-native protein and protein refolding. *EMBO J.* **1996,** 15, 2969-2979.

2. Walter, S.; Buchner, J., Molecular chaperones - cellular machines for protein folding. *Angew. Chem., Int. Ed.* **2002,** 41, 1098-1113.

3. Schneider, C.; Sepp-Lorenzino, L.; Nimmesgern, E.; Ouerfelli, O.; Danishefsky, S.; Rosen, N.; Hartl, F. U., Pharmacologic shifting of a balance between protein refolding and degradation mediated by Hsp90. *Proc. Natl. Acad. Sci. USA* **1996,** 93, 14536-14541.

4. Schumacher, R. J.; Hansen, W. J.; Freeman, B. C.; Alnemri, E.; Litwack, G.; Toft, D. O., Cooperative action of Hsp70, Hsp90, and DnaJ proteins in protein renaturation. *Biochemistry* **1996,** 35, 14889-14898.

5. Whitesell, L.; Mimnaugh, E. G.; De Costa, B.; Myers, C. E.; Neckers, L. M., Inhibition of heat shock protein HSP90-pp60v-src heteroprotein complex formation by benzoquinone

ansamycins: essential role for stress proteins in oncogenic transformation. *Proc. Natl. Acad. Sci. USA* **1994,** 91, 8324-8328.

6. Schulte, T. W.; Akinaga, S.; Soga, S.; Sullivan, W.; Stensgard, B.; Toft, D.; Neckers, L. M., Antibiotic radicicol binds to the N-terminal domain of Hsp90 and shares important biological activities with geldanamycin. *Cell Stress Chaperones* **1998,** 3, 100-108.

7. Binder, R. J.; Blachere, N. E.; Srivastava, P. K., Heat shock protein-chaperoned peptides but not free peptides introduced into the cytosol are presented efficiently by major histocompatibility complex I molecules. *J. Biol. Chem.* **2001,** 276, 17163-17171.

8. Hanahan, D.; Weinberg, R. A., The hallmarks of cancer. *Cell* **2000,** 100, 57-70.

9. Maloney, A.; Workman, P., HSP90 as a new therapeutic target for cancer therapy: The story unfolds. *Expert Opin. Biol. Ther.* **2002,** 2, 3-24.

10. Neckers, L., Using natural product inhibitors to validate Hsp90 as a molecular target in cancer. *Curr. Top. Med. Chem.* **2006,** 6, 1163-1171.

11. Chaudhury, S.; Welch, T. R.; Blagg, B. S., Hsp90 as a target for drug development. *ChemMedChem* **2006,** 1, 1331-1340.

12. Hadden, M. K.; Lubbers, D. J.; Blagg, B. S., Geldanamycin, radicicol, and chimeric inhibitors of the Hsp90 N-terminal ATP binding site. *Curr. Top. Med. Chem.* **2006,** 6, 1173-1182.

13. Roe, S. M.; Prodromou, C.; O'Brien, R.; Ladbury, J. E.; Piper, P. W.; Pearl, L. H., Structural basis for inhibition of the Hsp90 molecular chaperone by the antitumor antibiotics radicicol and geldanamycin. *J. Med. Chem.* **1999,** 42, 260-266.

14. Moulin, E.; Zoete, V.; Barluenga, S.; Karplus, M.; Winssinger, N., Design, synthesis, and biological evaluation of HSP90 inhibitors based on conformational analysis of radicicol and its analogues. *J. Am. Chem. Soc.* **2005,** 127, 6999-7004.

15. Kwon, H. J.; Yoshida, M.; Fukui, Y.; Horinouchi, S.; Beppu, T., Potent and specific inhibition of p60v-src protein kinase both in vivo and in vitro by radicicol. *Cancer Res.* **1992,** 52, 6926-6930.

16. Agatsuma, T.; Ogawa, H.; Akasaka, K.; Asai, A.; Yamashita, Y.; Mizukami, T.; Akinaga, S.; Saitoh, Y., Halohydrin and oxime derivatives of radicicol: synthesis and antitumor activities. *Bioorg. Med. Chem.* **2002,** 10, 3445-3449.

17. Ikuina, Y.; Amishiro, N.; Miyata, M.; Narumi, H.; Ogawa, H.; Akiyama, T.; Shiotsu, Y.; Akinaga, S.; Murakata, C., Synthesis and antitumor activity of novel O-carbamoylmethyloxime derivatives of radicicol. *J. Med. Chem.* **2003,** 46, 2534-2541.

18. Porter, J. R.; Ge, J.; Lee, J.; Normant, E.; West, K., Ansamycin inhibitors of Hsp90: Nature's prototype for anti-chaperone therapy. *Curr. Top. Med. Chem.* **2009,** 9, 1386-1418.

19. Thepchatri, P.; Eliseo, T.; Cicero, D. O.; Myles, D.; Snyder, J. P., Relationship among ligand conformations in solution, in the solid state, and at the Hsp90 binding site: geldanamycin and radicicol. *J. Am. Chem. Soc.* **2007,** 129, 3127-3134.

20. Lee, Y. S.; Marcu, M. G.; Neckers, L., Quantum chemical calculations and mutational analysis suggest heat shock protein 90 catalyzes trans-cis isomerization of geldanamycin. *Chem. Biol.* **2004,** 11, 991-998.

21. Chiosis, G.; Huezo, H.; Rosen, N.; Mimnaugh, E.; Whitesell, L.; Neckers, L., 17AAG: Low target binding affinity and potent cell activity-finding an explanation. *Mol. Cancer Ther.* **2003,** 2, 123-129.

22. Schulte, T. W.; Neckers, L. M., The benzoquinone ansamycin 17-allylamino-17-demethoxygeldanamycin binds to HSP90 and shares important biologic activities with geldanamycin. *Cancer Chemother. Pharmacol.* **1998,** 42, 273-279.

23. Jez, J. M.; Chen, J. C. H.; Rastelli, G.; Stroud, R. M.; Santi, D. V., Crystal structure and molecular modeling of 17-DMAG in complex with human Hsp90. *Chem. Biol.* **2003,** 10, 361-368.

24. Onuoha, S. C.; Mukund, S. R.; Coulstock, E. T.; Sengerova, B.; Shaw, J.; McLaughlin, S. H.; Jackson, S. E., Mechanistic Studies on Hsp90 Inhibition by Ansamycin Derivatives. *J. Mol. Biol.* **2007,** 372, 287-297.

25. Onodera, H.; Kaneko, M.; Takahashi, Y.; Uochi, Y.; Funahashi, J.; Nakashima, T.; Soga, S.; Suzuki, M.; Ikeda, S.; Yamashita, Y.; Rahayu, E. S.; Kanda, Y.; Ichimura, M., Conformational significance of EH21A1-A4, phenolic derivatives of geldanamycin, for Hsp90 inhibitory activity. *Bioorg. Med. Chem. Lett.* **2008,** 18, 1588-1591.

26. Zhang, M.-Q.; Gaisser, S.; Nur-E-Alam, M.; Sheehan, L. S.; Vousden, W. A.; Gaitatzis, N.; Peck, G.; Coates, N. J.; Moss, S. J.; Radzom, M.; Foster, T. A.; Sheridan, R. M.; Gregory, M. A.; Roe, S. M.; Prodromou, C.; Pearl, L.; Boyd, S. M.; Wilkinson, B.; Martin, C. J., Optimizing natural products by biosynthetic engineering: Discovery of nonquinone Hsp90 inhibitors. *J. Med. Chem.* **2008,** 51, 5494-5497.

27. Shen, G.; Wang, M.; Welch, T. R.; Blagg, B. S. J., Design, synthesis, and structure-activity relationships for chimeric inhibitors of Hsp90. *J. Org. Chem.* **2006,** 71, 7618-7631.

28. Clevenger, R. C.; Blagg, B. S. J., Design, synthesis, and evaluation of a radicicol and geldanamycin chimera, radamide. *Org. Lett.* **2004,** 6, 4459-4462.

29. Shen, G.; Blagg, B. S. J., Radester, a novel inhibitor of the Hsp90 protein folding machinery. *Org. Lett.* **2005,** 7, 2157-2160.

30. Avila, C.; Kornilayev, B. A.; Blagg, B. S., Development and optimization of a useful assay for determining Hsp90's inherent ATPase activity. *Bioorg. Med. Chem.* **2006,** 14, 1134-1142.

31. Richter, K.; Muschler, P.; Hainzl, O.; Buchner, J., Coordinated ATP hydrolysis by the Hsp90 dimer. *J. Biol. Chem.* **2001,** 276, 33689-33696.

32. Immormino, R. M.; Metzger IV, L. E.; Reardon, P. N.; Dollins, D. E.; Blagg, B. S. J.; Gewirth, D. T., Different poses for ligand and chaperone in inhibitor-bound Hsp90 and GRP94: implications for paralog-specific drug design. *J. Mol. Biol.* **2009,** 388, 1033-1042.

33. Bartha, B. B.; Ajtai, K.; Toft, D. O.; Burghardt, T. P., ATP sensitive tryptophans of hsp90. *Biophys. Chem.* **1998,** 72, 313-321.

Chapter III

Design and Synthesis of Proposed Grp94 Selective Inhibitors

III.1 Introduction to Grp94

The complexity, localization, and uniqueness of each protein dictates the need for multiple chaperone systems.[1] Furthermore, each cellular organelle maintains unique roles and must regulate its own proteostasis. Thus, the endoplasmic reticulum (ER) contains its own chaperoning network required for the development and trafficking of secretory and membrane bound proteins.[2] As such, the ER contains a resident member of the Hsp90 family, glucose-regulated protein 94 kDa (Grp94).[3, 4] Grp94 was first identified in 1977, upon observation that glucose depletion of Rous sarcoma virus transformed chick embryo fibroblasts resulted in the over expression of a ~94 kDa protein, which was subsequently named Grp94.[5] Research groups have since shown that Grp94 exhibits activities unrelated to glucose levels, resulting in numerous aliases including gp96, endoplasmin, Tra-1, or Hsp108.[6]

Similar to other Hsp90 isoforms, Grp94 is ubiquitously expressed in humans. As shown in Figure 21, secretory tissues maintain an especially high level of Grp94 expression.[7] As expected, introduction of stress to the ER results in the induction of the resident heat shock response, the unfolded-protein response (UPR).[8] Similar to the cytosol's ubiquitin-proteasome pathway, the ER maintains a protein degradation mechanism, referred to as endoplasmic reticulum-associated protein degradation (ERAD).[9, 10] Although Grp94 induction is a well accepted hallmark of ER stress, the functional role of Grp94 is poorly understood, with the only well-studied role for Grp94 being related to immunity.[8, 11-13] Interestingly, inhibition of other proteins involved in ER proteostasis results in a global induction of the cellular heat shock response; however, Grp94 silencing fails to induce either the UPR or the cytosolic HSR.[14, 15]

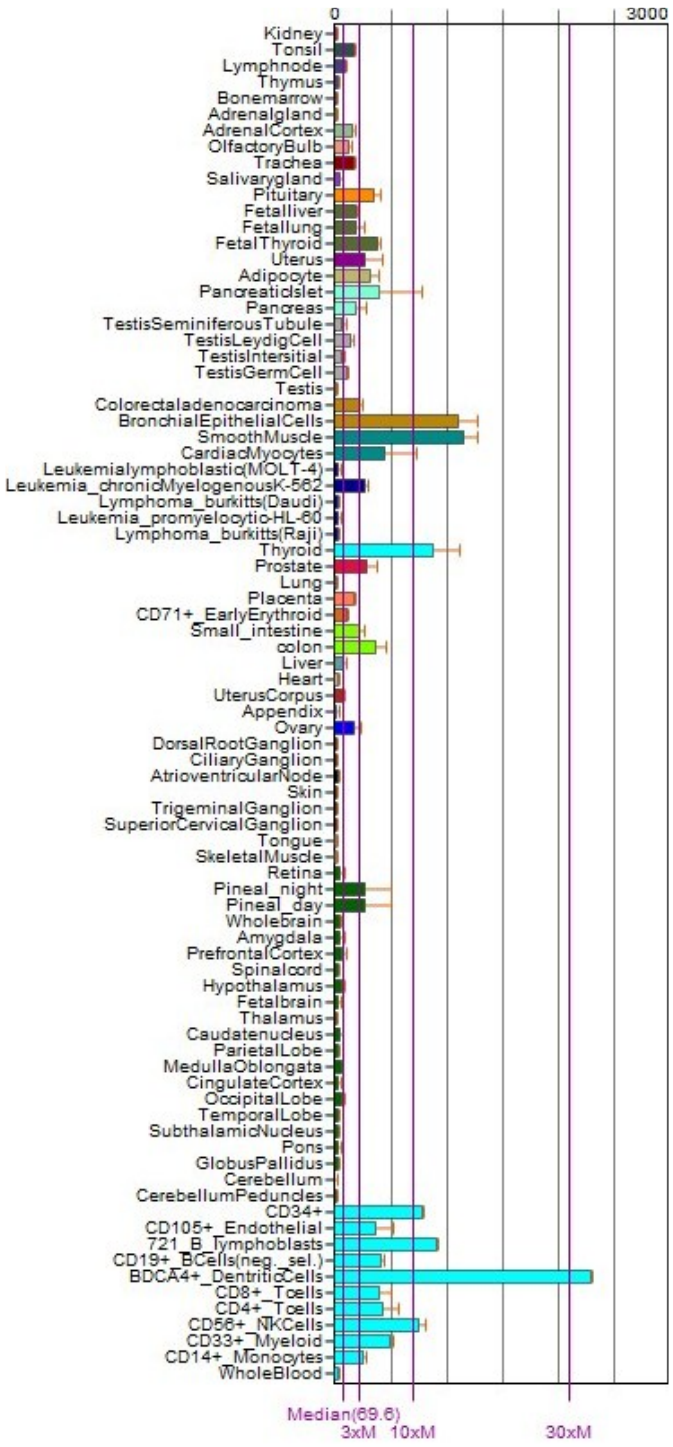

Figure 21. Grp94 expression profile in *H. sapiens*.[7]

The function of Grp94 is becoming less enigmatic, as its significance in cellular homeostasis and disease progression has recently attracted the attention of numerous researchers.

III.2 Structure

As mentioned in Chapter I, Grp94 exists as a soluble, obligate homodimer; comprised of an N-terminal domain (NTD), charged-linker (CL), middle domain (MD), and a C-terminal dimerization domain (CTD).[6, 16-19] Although the NTD possesses the characteristic Bergerat-fold ATP-binding pocket, interactions between both the NTD and MD cooperate to provide the requisite ATP-hydrolysis activity.[20, 21] Residence in the ER is maintained through a C-terminal tetrapeptide KDEL sequence, which is recognized by the KDEL retrieval receptor for sequestration.[22] The structure of the full-length canine ortholog of Grp94 has been solved in

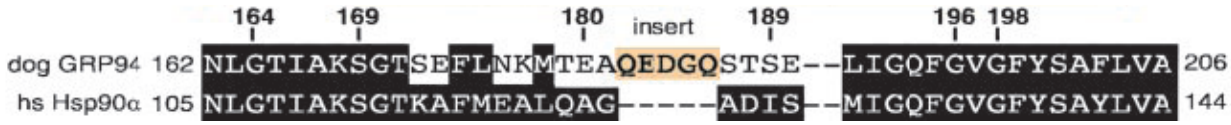

Figure 22. Primary sequence alignment of canine Grp94 and hHsp90α depicting the 5-amino acid insertion at residues 182–186.[6]

addition to various Grp94 truncates with N-terminal ligands.[6, 16-19, 23] However, the sites of interaction of both co-chaperones and partner proteins for Grp94 remain unknown.

Most noteably, Grp94 exhibits a 5-amino acid insertion (QEDGQ) at residues 182–186, which is not present in other Hsp90 isoforms (Figure 22).[6] This insertion causes a dramatic effect on the secondary and tertiary organization of Grp94, especially within the N-terminal binding pocket. As a consequence, the architecture of the binding pocket is unique. Therefore, it is not surprising that mechanistic and regulatory disparities between Hsp90 and Grp94 have been reported for specific ligands.[6, 16, 17, 19, 23]

III.3 Cellular Functions of Grp94

Research that ablates Grp94 levels has indicated the chaperone to be essential for the development of plants,[24] nematodes,[14] fruit flies,[25] and mice.[15] However, its function is non-essential to the growth of mammalian cell cultures, as Grp94 siRNA experiments demonstrate cell lines to grow normally and maintain the ability to differentiate.[11, 14] Furthermore, Grp94 is essential only to metazoans, as it is not expressed in unicellular organisms, with the exception of *Leishmania*.[21] Recent literature has revealed numerous intracellular proteins that are dependent upon Grp94 for proper maturation and biological activity.[8] Whereas cytosolic Hsp90 maintains roles in cell-cycle regulation and signaling, Grp94 mediates cell-to-cell communication through the chaperoning of secretory and membrane proteins. Thus, therapies that target Grp94 may represent promising chemotherapeutics for the treatment of pathological conditions that rely upon intercellular communication networks.[8, 12, 26-28]

GRP94 client proteins	IP	GRP94 KO/RNAi	GRP94 drug inhibition
Native proteins			
ADAMTS9 (Koo and Apte, 2010)	+	+	+
Apolipoprotein B (Linnik and Herscovitz, 1998)	+		
Cartilage oligomeric matrix protein (Hecht *et al.*, 2001)	+		
Collagen (Ferreira *et al.*, 1994)	+		
EGF-R (Supino-Rosin *et al.*, 2000)			+
ErbB2 (Chavany *et al.*, 1996)	+		+
Golgi apparatus casein kinase (Brunati *et al.*, 2000)	+		
Ig chains (Melnick *et al.*, 1992; Tramentozzi *et al.*, 2008)	+		
IGF-I (Ostrovsky *et al.*, 2010)		+	
IGF-II (Wanderling *et al.*, 2007; Ostrovsky *et al.*, 2009)	+	+	+
IFN-γ (Vandenbroeck *et al.*, 2006)	+		
IL-12p80 (Alloza *et al.*, 2004; MvLaughlin *et al.*, 2008)	+	+	+
Insulin receptor IRS-1 (Saitoh *et al.*, 2002)			+
Integrins CD11a, CD18, CD49d, α4, β7, αL, β2 (Randow and Seed, 2001; Liu and Li, 2008)		+	
MHC class II (Schaiff *et al.*, 1992)	+		
Bile-salt dependent lipase (Nganga *et al.*, 2000)		+	+
Thrombospondin (Kuznetsov *et al.*, 1997)	+		
Thyroglobulin (Kuznetsov *et al.*, 1997)	+		
TLR1, TLR2, TLR4 (Randow and Seed, 2001; Liu and Li, 2008)	+	+	
TLR9 (Yang *et al.*, 2007)	+	+	
WFS1 (Kakiuchi *et al.*, 2009)	+		
Mutant client proteins			
α-1-antitrypsin (Schmidt and Perlmutter, 2005)	+		
Protein C (Katsumi *et al.*, 1996)	+		
HSV glycoprotein (Ramakrishnan *et al.*, 1995)	+		

Figure 23. Known Grp94 client proteins and method of determination.[8]

As shown in Figure 23, Grp94 is responsible for a variety of proteins implicated in cancer (IRS-1, IGF-I, IGF-II, integrins) and in immunological conditions (TLRs, integrins, IFN-γ).[8] Most intriguing about the list of clients is the selectivity with which Grp94 operates, even within families of proteins, such as TLRs and integrins. This suggests that the ability to target Grp94 may result in disease modification with a lower side-effect profile, as fewer clients appear to be dependent upon Grp94 than Hsp90. Therefore, Grp94 isoform selective inhibitors represent novel biological tools and potential chemotherapies for diseases.

III.4 Known Ligands: Non-Selective and Selective

Amino acids 35-274 of Grp94 exhibit high homology to fragments 9-236 and 1-220 of human cytosolic Hsp90 and yeast Hsp90 (yHsp90), respectively. This domain comprises the N-

terminal nucleotide binding pocket and mediates the binding of structurally unrelated compounds, including ATP, GDA, and RDC. Co-crystallization has shown all three natural products bind to the same Bergarat-type ATP-binding pocket, which is comprised of α-helices positioned around a platform of β-sheets.[6, 17, 18, 23] Grp94 exhibits complete conservation of the requisite amino acids responsible for ligand binding to this pocket. While the inherent ATPase activity and conformational equilibrium is comparable for Grp94 and other Hsp90 isoforms,[20, 21] the regulation of conformational reorganization seems mechanistically unique and ligand specific.

III.4.1 *Endogenous Ligand: ATP*

Similar to all other members of the GHKL family of ATP binding proteins, Grp94 binds ATP in a unique bent conformation.[17] However, Grp94 exhibits a weak binding affinity for ATP, which is ~100-fold lower than that observed for cytosolic Hsp90.[16, 17] In addition, unlike other Hsp90s which bind ADP ~5–10-fold tighter than ATP, Grp94 binds both ATP and ADP with similar affinities ($K_d \approx 5\mu M$).[16-18] With the exception of lid reorganization (discussed below), the structures of Grp94 in complex with nucleotides closely resemble the structures of Grp94 bound to N-terminal inhibitors.

Rationale for Grp94's weak affinity for nucleotides is two-fold. Firstly, the 5-amino acid insertion in Grp94's primary sequence results in a sterically unfavorable orientation of Gly196 (Gly121 in Hsp90), which diminishes ATP affinity (Figure 24).[6] Thus, Grp94 must undergo a large conformational reorganization, which

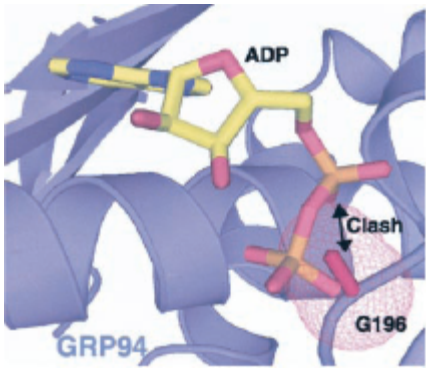

Figure 24. Depiction of the steric clash between Grp94 Gly196 and the phosphate region of ADP.[6]

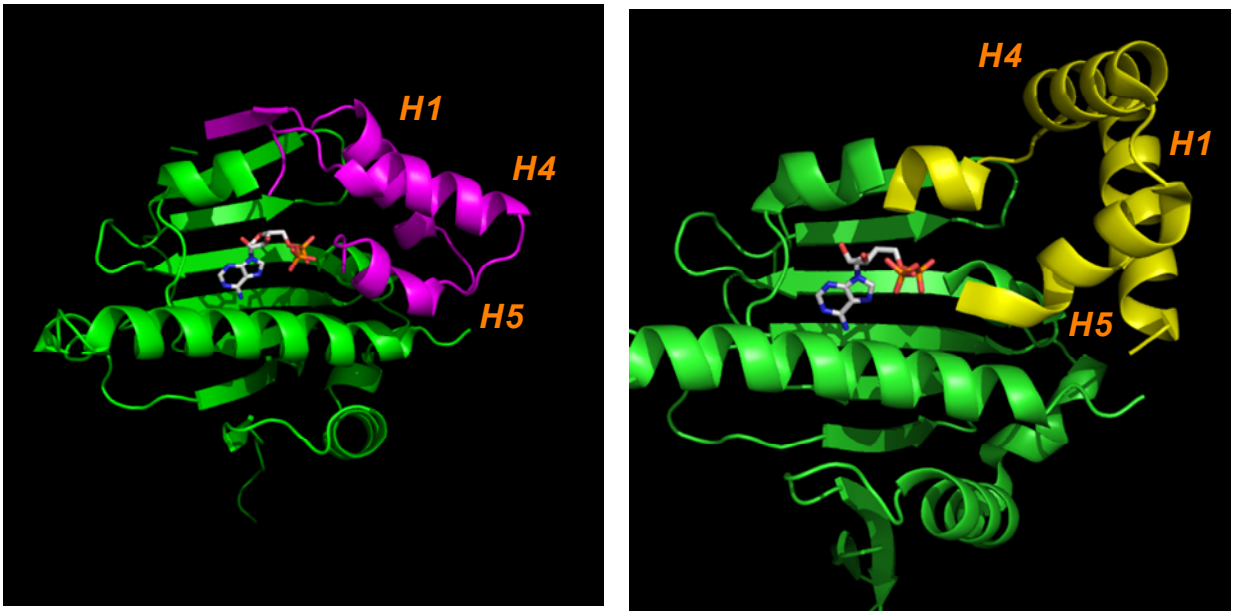

Figure 25. Co-crystal structure comparison of ADP bound to yHsp90N (left) and dGrp94N (right). Helices 1-4-5 are labeled and depicted in magenta (Hsp90) and yellow (Grp94).

includes a ~30˚ outward rotation of helices 1-4-5 into an open conformation in order to accommodate ATP (Figure 25).[17] Secondly, examination of the electrostatics of the Grp94 ligand binding pocket revealed an acidic and negative surface potential in the phosphate binding region, resulting in electrostatic repulsion between the negatively charged phosphates of the nucleotide and the protein (Figure 26).[23] This is in contrast to the phosphate binding region in yHsp90, in which basic groups compliment the phosphate charges. Thus, electrostatic repulsion between Grp94 and nucleotides may further facilitate the rotation of helices 1-4-5, providing the requisite energy for conformational reorientation.[23] Therefore, the extensive remodeling of helices 1-4-5 due to electrostatic repulsion and rotation appear to relieve congestion and may be responsible for the low affinity of Grp94 for ATP. Furthermore, research has shown both of these attributes are necessary to result in an open conformation, as delineated in the discussion of GDA in section III.4.2.

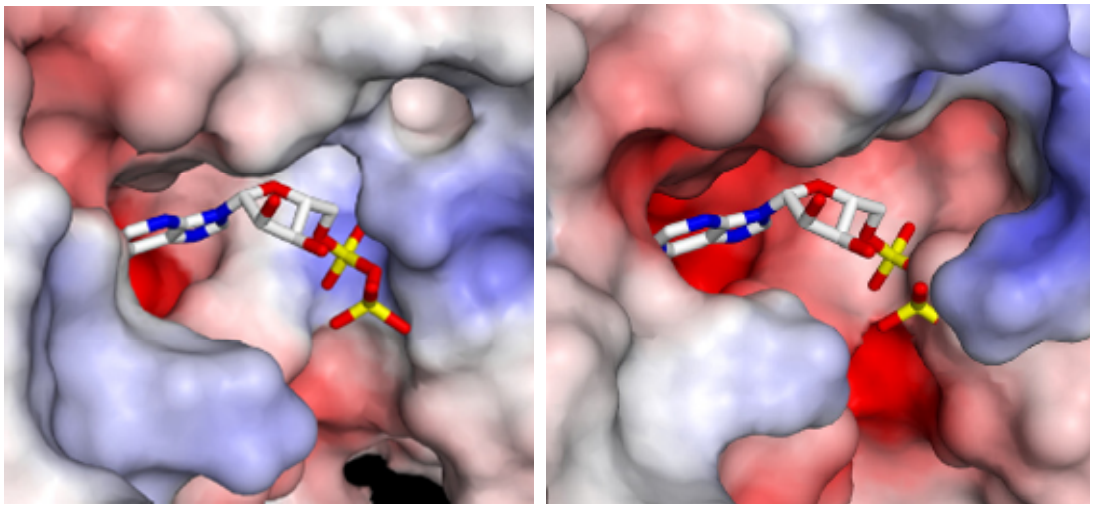

Figure 26. Co-crystal structure comparison depicting the nature of the phosphate binding region between yHsp90N (left) and dGrp94N (right).[23]

Upon binding ATP, the open conformation of the N-terminal "lid" (helices 1-4-5) of Grp94 results in exposure of hydrophobic regions necessary for N-terminal dimerization.[17] This is in contrast to other Hsp90 isoforms, which undergo lid closure upon binding ATP prior to dimerization (Figure 25).[29] Therefore, the mechanistic regulation of N-terminal dimerization represents a key difference between Grp94 and Hsp90.[18]

The aforementioned observations suggest Grp94 to be more sensitive to N-terminal ligand structure, but capable of reorganizing to accommodate various functionalities. Although the affinity of Grp94 for ATP is low, the ATPase activity is on par with Hsp90β.[21] The amount of reorganization exhibited by Grp94 has not been observed in other Hsp90 isoforms, which provides a mechanistic anomaly that may be exploitable in the design of isoform selective inhibitors.

III.4.2 *Geldanamycin*

Geldanamycin was originally identified in 1994[30] as an inhibitor of cytosolic Hsp90 and co-crystal structures of GDA·yHsp90 were reported shortly thereafter in 1999.[31] As a result of these seminal publications, much has been learned about the Hsp90 family, including the

existence of four isoforms in the human genome.[32] These disclosures and subsequent studies revealed GDA to be a *pan*-inhibitor of all four Hsp90 paralogs, albeit with varying affinities. Neckers and colleagues uncovered GDA's inhibitory activity of Grp94 in 1996.[33] Subsequently, through competition binding studies, Neckers *et al.* demonstrated GDA to bind Grp94 (~1 μM) with a lower efficiency than Hsp90α or Hsp90β (170 nM);[34] however, rationale for the observed selectivity was lacking. The GDA·Grp94 co-crystal structure was not available until 2009, in which a collaborative publication between the Gewirth laboratory at Hauptman-Woodward Medical Research Institute and our laboratory disclosed the structure.[23] This structure has been critical to understanding the mechanistic regulation of Grp94 by GDA.

Once again, Gly196 plays a critical role in ligand binding and may explain the lower affinity of GDA for Grp94. Prior to co-crystallization, GDA was modeled into the N-terminal ATP-binding pocket of apo-Grp94. These modeling studies revealed a steric clash between the macrocyclic amide of GDA and the backbone carbonyl oxygen of Gly196 in Grp94 (Figure 27).[23] Although this clash is similar to the predicted ATP clash, the co-crystal structure between dGrp94N and GDA reveals only moderate rearrangement of the flexible "lid" (Figure 28). Rationale for such a small perturbation of the lid can be proposed upon analysis of the electrostatic surface of the binding pocket.[23] Although GDA exhibits a polar quinone ring that binds in the phosphate binding region, it is considerably less polar than the phosphate moiety of bound nucleotides. Thus, the

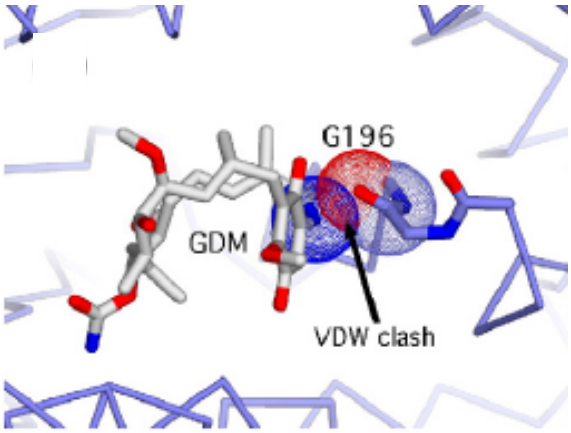

Figure 27. Depiction of the Gly196/GDA clash observed upon docking GDA into apo-Grp94.[23]

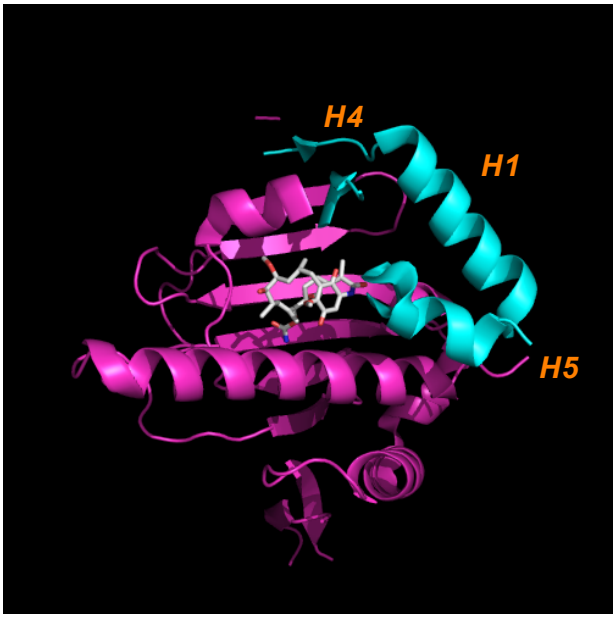

Figure 28. Co-crystal structure of GDA with dGrp94N. The mobile subdomain consisting of helices 1-4-5 is depicted in cyan.

lack of electrostatic repulsion allows for helices 1-4-5 to remain in a more compact conformation than that observed in the ADP·dGrp94N complex (Figure 25). Cytosolic Hsp90 can accommodate GDA through minor structural adjustments and the GDA·yHsp90 co-crystal structure is similar to that of ATP·yHsp90.

Similar to Hsp90, Grp94 binds GDA in a bent *cis*-amide conformation with the benzoquinone parallel to the ansamycin ring. Inspection of the remaining GDA and Grp94 interactions reveal similar networks as those observed with Hsp90, including direct water-mediated contacts between the carbamate group and Asp149; direct hydrogen bonds to Asp110, Lys114, Gly196, Gly198, and Phe 199; water mediated interactions between Leu104, Asn107, and Thr254; and multiple hydrophobic contacts between GDA and Met154, Leu163, Val197, and Phe199.[23] Considering the binding affinity data and co-crystal structure evidence, it is not surprising that GDA-derived analogs can be utilized to design isoform selective inhibitors. In fact, GDA-derived WX514 (Figure 29) exhibits a ~90-fold higher binding affinity for Hsp90 than Grp94.[34] However, the rationale for cytosolic selectivity exhibited by analogs of this class remains undisclosed.

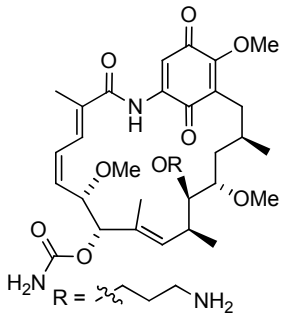

Figure 29. Structure of WX514, a selective inhibitor of cytosolic Hsp90.

III.4.3 *Isoform Selective Inhibitor: N-ethylcarboxamidoadenosine*

Studies regarding the adenosine receptors A_1 and A_2 in the 1980s resulted in significant knowledge pertinent towards understanding the adenosine receptor.[35, 36] However, upon identification of the adenosine A_2 receptor, a second class of proteins containing an adenosine A_2-like binding site was identified.[37] Subsequent studies revealed Grp94 to be a major contributor in adenosine A_2 ligand binding, exhibiting a binding affinity of ~200 nM for 5'-N-ethylcarboxamidoadenosine (NECA), a broad spectrum adenosine A_2 receptor agonist (Figure 30).[38] In fact, Grp94 was eventually identified as the prominent cellular target of NECA.[38] Furthermore, NECA was shown to exhibit no apparent binding affinity for Hsp90,[16] establishing NECA as the only known Grp94 selective inhibitor.

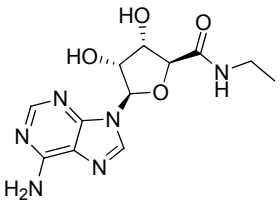

Figure 30. Structure of NECA.

In order to provide rationale for NECA's Grp94 binding selectivity, Gewirth and colleagues solved the NECA·dGrp94N and the RDC·dGrp94N co-crystal structures.[6] These structures provided a direct comparison between the Grp94 selective inhibitor, NECA, and a potent *pan*-Hsp90 inhibitor, RDC. Prior to solution of the co-crystal structures, it was unknown what role the 5-amino acid insertion in Grp94's primary sequence provided.

Analyses of the co-crystal structures, suggest a unique binding domain for Grp94, which is lacking in the RDC·yHsp90 structure, that interacts with the 5'-ethyl moiety of NECA.[6] As expected, the adenine moiety of NECA exhibits identical interactions to Grp94 as observed in ATP/ADP·Hsp90 complexes. This can be explained due to the complete conservation of requisite amino acids known to interact with nucleotides *via* direct and water-mediated hydrogen-bonding networks. The second domain that interacts with NECA is a unique structural

feature specific to Grp94, which is introduced by the 5-amino acid insertion in its primary sequence. The insertion occurs in the helix 1-4-5 subdomain and results in lengthening of helix 4 and two structural modifications.[6] Firstly, the orientations of Ala167 and Lys168 (Ala97 and Lys98 in Hsp90) are reorganized, which results in a volumetric increase of the second binding domain. This increase in volume can accommodate the 5'-ethyl moiety present in NECA. Secondly, the lengthening of helix-4 produces increased flexibility and a conformational re-orientation of helices 1-4-5, which may facilitate ligand binding.[6] As observed in Figure 31, NECA provides a direct hydrogen-bond with the backbone carbonyl of Asn162 in dGrp94 and the 5'-ethyl moiety is stabilized through van der Waals interactions with Val197 and Tyr200. This pocket is not present in yHsp90, and consequently it is not surprising that this type of "conformational switch" had not been previously observed in other Hsp90 isoforms. Furthermore, this pocket is present in apo-Grp94, suggesting that it is not ligand-induced, but rather inherent in nature.

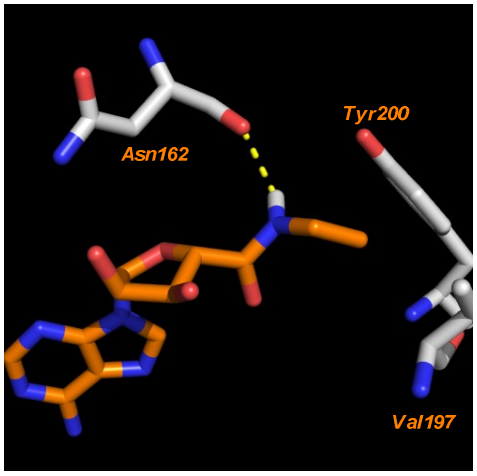

Figure 31. Interaction of NECA within the second binding domain unique to Grp94.

Rationale for the inability of NECA to bind Hsp90 can be postulated through molecular modeling studies. Since the adenine portion of NECA, ATP, and ADP bind to Grp94 and Hsp90 with identical interactions, positioning of the 5'-ethyl moiety of NECA is dictated by the adenine orientation. Thus, upon modeling NECA into yHsp90's N-terminal binding pocket, a clash between the 5'-ethyl group and the main chain carbonyl oxygen of yHsp90 Gly121 (Gly196 in Grp94) occurs.[6] The repercussions of protein remodeling to accommodate the ligand are detrimental, as remodeling of the protein would result

in net energy expenditure. Therefore, it can be hypothesized that the 5'-ethyl group of NECA is the sole factor responsible for the selective binding of NECA to Grp94.

Interestingly, these results suggest that the position of Gly196 in Grp94 maintains a discriminatory role towards ligand binding, as its orientation precludes the binding of endogenous nucleotides, but allows for the binding of NECA. This is in contrast to yHsp90, as the respective Gly121 allows binding of ATP/ADP, but prevents NECA binding. In total, the observations for ligand specificity and regulation provide evidence that Grp94 selective inhibitors can be designed; however, analogs based on the NECA scaffold have proved unsuccessful thus far.

III.5 Proposal of Grp94 Selective Inhibitors

As mentioned previously, the chimeric inhibitor radamide (RDA) was co-crystallized with both yHsp90N and dGrp94N.[23] Analysis of the two co-crystal structures revealed the resorcinol to bind similarly to both isoforms. However, the quinone moiety of RDA binds yHsp90 in a linear, *trans*-amide conformation; while upon binding Grp94, two unique bent conformations that project the quinone into the hydrophobic NECA 5'-binding pocket are observed (50% occupancy each). One conformation manifests a *cis*-amide orientation, while the second, orthogonal conformation contains a *trans*-amide (Figure 32). The quinone moiety of RDA exhibits distinct interactions with each protein, which provides a starting point for the rational design of Grp94 selective inhibitors. In fact, analysis of the RDA·yHsp90 co-crystal structure suggests the quinone to be involved in an intricate hydrogen-bonding network, whereas it's interaction with Grp94 is limited. This has led to speculation that the quinone may be dispensable for Grp94 binding, but obligatory for Hsp90 binding. Considering these

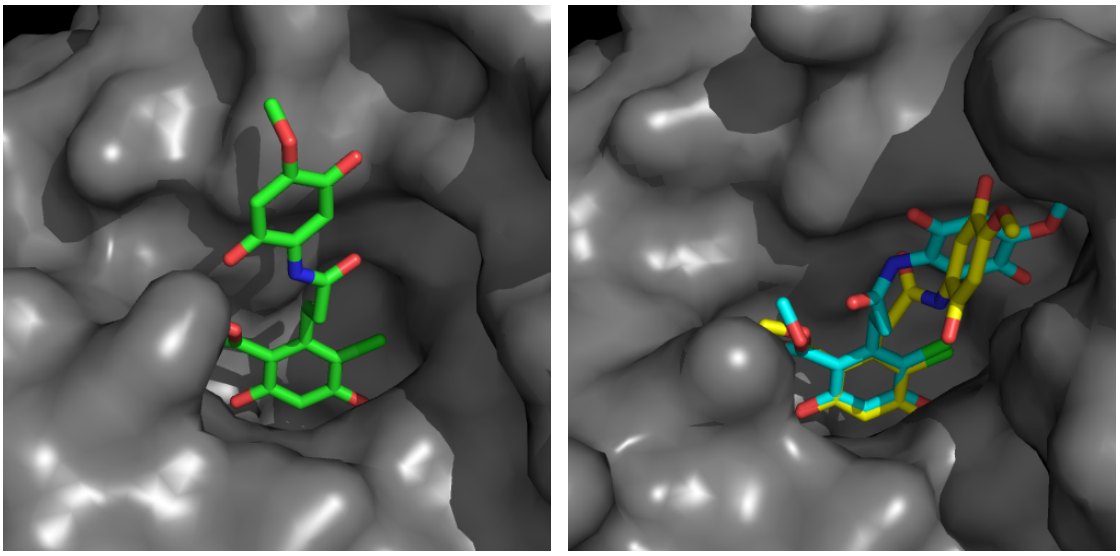

Figure 32. Co-crystal structures of RDA bound to yHsp90 (left) and Grp94 (right). The two RDA conformations populated when bound to Grp94 are depicted in cyan and yellow.

observations, two approaches were utilized to design Grp94 selective inhibitors: 1) manipulation of the quinone moiety; and 2) conformational constraint to incorporate a *cis*-amide bioisostere.

III.5.1 *Quinone Substitution*

The first series of analogs aimed at manipulating the substitution pattern of the quinone ring, and thus eliminating critical interactions required for binding Hsp90, but maintaining Grp94 inhibitory activity. Furthermore, analyses of the co-crystal structures suggested a more intricate

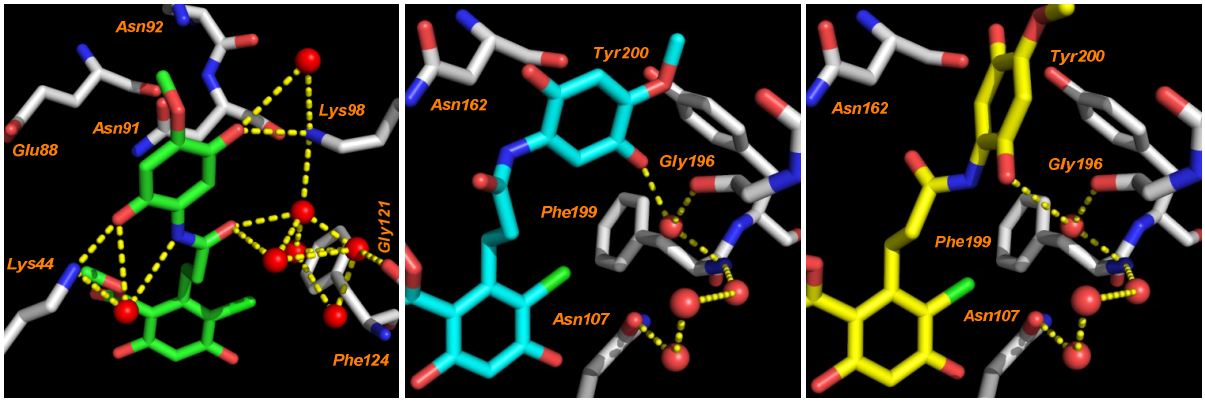

Figure 33. Quinone hydrogen bonding network comparison between yHsp90 (left), and the *cis*-amide (middle) and *trans*-amide (right) conformations of RDA that bind Grp94.

hydrogen-bonding network between the quinone and yHsp90 than that which was observed for the quinone (in either orientation) and Grp94 (Figure 33). Therefore, analogs **25**–**27** were proposed to systematically evaluate substituents of the RDA quinone ring. To design these analogs, the *trans*-amide conformation exhibited by RDA when bound to Grp94 was chosen as the design template, as this conformation represents the lowest energy and highest populated conformation of the amide in solution.

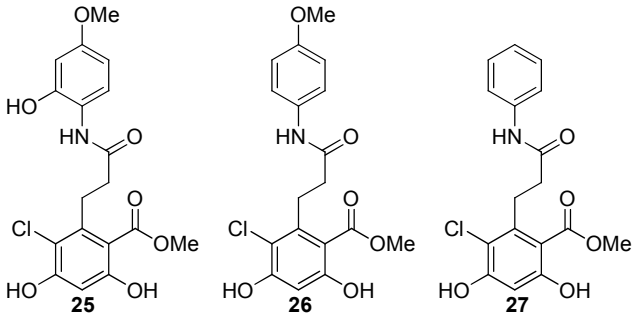

Figure 34. Proposed analogs which lack key functionalities for Hsp90 binding.

Removal of the 5-carbonyl (**25**, Figure 34) on the RDA quinone would eliminate hydrogen-bonding interactions between the carbonyl and Lys98 as observed in the yHsp90 structure. Interactions between Lys98 and the 5-carbonyl were also observed in the GDA·yHsp90 complex, which is critical to the binding affinity. Although this manipulation will also change the oxidation state of the 2-carbonyl, this should not affect interactions with Lys44, as the hydroquinone of RDA interacts similarly in the yHsp90 N-terminal binding pocket. Furthermore, the *trans*-amide conformation exhibited by RDA when bound to Grp94 suggests no apparent function of the 5-carbonyl (Figure 33). Thus, removal of this functionality should result in lower affinity for Hsp90, while unaffecting interactions with Grp94.

Further reduction of **25** *via* removal of the 2-oxo functionality provides analog **26**, which lacks the hydrogen bonding capability with Lys44 and Lys98 of yHsp90. This manipulation is also predicted to affect the hydrogen-bonding network of the ligand with Grp94, as this functionality is involved in hydrogen bonding with the backbone amides of Gly196 and Phe199.

However, the NECA·Grp94 co-crystal structure suggests this region of Grp94 to be hydrophobic in nature.[6] Therefore, this manipulation may still provide beneficial van der Waals and/or π-stacking interactions with Grp94. Lastly, removal of the 4-methoxy moiety will provide analog **27**, which eliminates all functionalities present on the RDA quinone. Development of this focused library allows for the rapid evaluation of the *des*-quinone hypothesis.

III.5.2 *Incorporation of a cis-Amide Bioisostere*

The second approach towards the design Grp94 selective inhibitors encompasses a bioisosteric replacement strategy. Previous evaluation of cRDA (Chapter II) revealed that chimeric analogs exhibiting a conformationally biased *cis*-amide moiety resulted in an improved binding affinity for Grp94. While the affinity for Hsp90 also improved, the ~110 nM affinity for Grp94 and ~5-fold improvement from RDA was most intriguing. However, the synthesis of cRDA was not amenable to facile SAR development. Upon evaluation of *cis*-amide bioisosteric replacements, imidazole was chosen for two reasons: 1) aldehyde **3**, utilized for the synthesis of RDA and cRDA, could be maintained as an advanced intermediate for the synthesis of a variety of analogs; and 2) optimized methodology had been previously reported, which enabled the rapid preparation of analogs in a straightforward manner with relatively inexpensive reagents.[39-41]

Closer analysis of the second Grp94 binding domain revealed the pocket to be hydrophobic in nature and to contain π-rich amino acids Phe199 and Tyr200, which are poised for π-stacking interactions. In agreement with the "dispensable quinone"

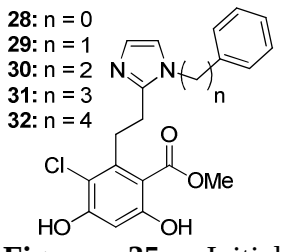

Figure 35: Initial imidazole analogs with varying linker length.

Table 5. Surflex binding scores of **28–32**.

Compound	Binding Score
28	4.80
29	5.94
30	-
31	-
32	-
RDA	3.82
cRDA	4.71

hypothesis, molecular modeling studies with imidazoles containing a pendent benzene ring (Figure 35) provided the desired interactions. Utilizing Surflex docking software,[42, 43] analogs **28**–**32** were docked to the RDA·Grp94 complex (PDB: 2GFD). As shown in Table 5, **28** and **29** were the only analogs that bound successfully to Grp94; and both exhibited better binding scores than RDA and cRDA. Furthermore, **28**–**32** failed to dock to the RDA·yHsp90 complex (PDB: 2FXS). Therefore, the first series of analogs synthesized consisted of an imidazole linkage flanked with a benzene ring attached with various linker lengths. Because of the flexible Grp94 lid region and inability of available modeling programs to consider this, linker lengths n = 3 and 4 were synthesized to confirm the docking results. The biological evaluation of these analogs will be described in detail in Chapter IV; however, analog **29** (n = 1) exhibited superior activity in the functional Grp94 inhibitory assay, which was in agreement with modeling studies. Therefore, functionalized analogs based upon **29** were designed for subsequent development.

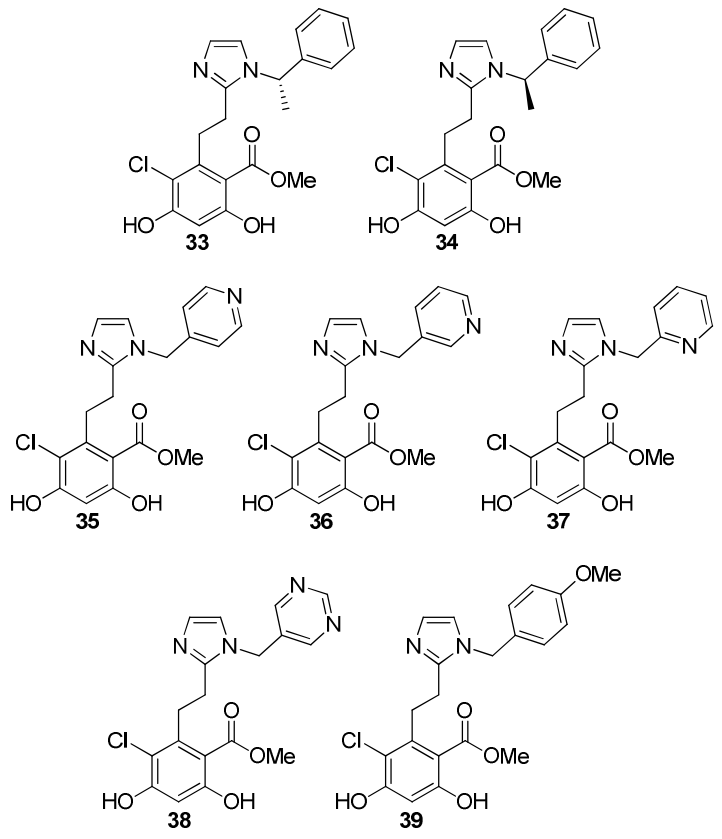

Figure 36. Imidazole analogs based upon **29**.

Analogs chosen for synthesis are depicted in Figure 36. Compounds **33** and **34** were designed to evaluate steric constraints and stereochemical

dependence. Analogs **35**–**38** were designed to assess the compatibility and optimal location of hydrogen bond acceptors. The exact binding orientation of the imadazole analogs remained unknown at the onset of analog development, however it was hypothesized that the presence of a hydrogen-bond acceptor may interact favorably with Tyr200 or the protein backbone, thus increasing affinity for Grp94. Furthermore, incorporation of a *cis*-amide bioisostere altered the projection angle towards the 5'-binding pocket present in Grp94. Thus, analogs **35**–**38** were devised to provide an evaluation of all possible locations, as hydrogen bonding is geometrically and directionally dependent. Additionally, analog **39** was designed to mimic the methyl ether present in RDA and cRDA, providing further information on the effects of hydrogen-bond donors, and to assess the spatial limitations of the binding pocket.

In parallel to the development of substituted analogs based on **29**, alkyl-imidazoles (**40**–**43**, Figure 37) were designed. These compounds were hypothesized to mimic NECA's 5'-ethyl functionality, which interacts with the Grp94 binding domain *via* van der Waals interactions with Val197 and Tyr200, rather than π-stacking interactions.

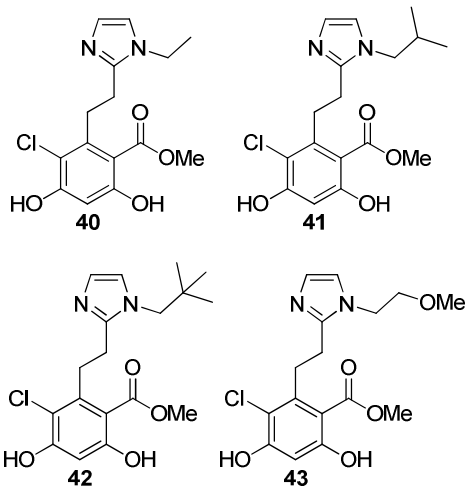

Figure 37. Alkyl-imidazoles.

III.6 Synthesis of Proposed Grp94 Selective Inhibitors

A key component of selecting the two aforementioned hypotheses for evaluation was the ability to utilize advanced intermediates previously reported by our laboratory. This allowed for the rapid evaluation of the two hypotheses in an efficient manner without significant scaffold development.

III.6.1 *Synthesis of des-Quinone Analogs*

Synthetically, analogs **25**–**27** were obtained in 3-steps from the previously disclosed aldehyde, **3** (Scheme 5).[44, 45] Commencing with a Pinnick oxidation, acid **44**[44, 46] was obtained in high yield and subsequently coupled with the necessary anilines through employment of EDCI/DMAP peptide coupling conditions. Facile removal of the *tert*-butyldimethylsilyl (TBS) protecting groups with tetra-*n*-butylammonium fluoride (TBAF) yielded the desired compounds **25**–**27**. Biological evaluation of these analogs is discussed in detail in Chapter IV.

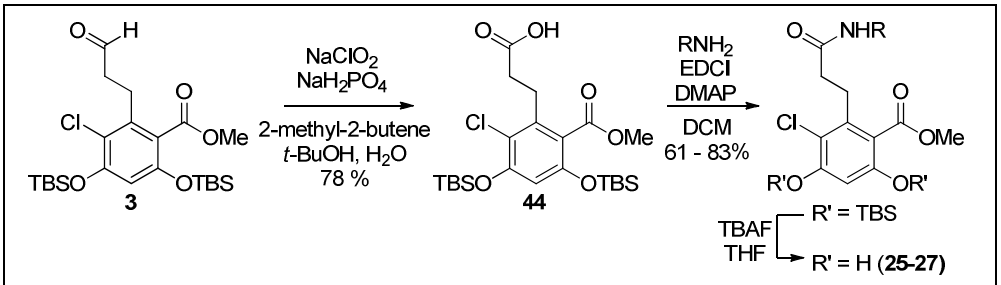

Scheme 5. Synthetic route to *des*-quinone analogs.

III.6.2 *Synthesis of Imidazole Bioisosteric Analogs*

The imidazole linked compounds were obtained in two steps from **3**. As shown in Scheme 6, aldehyde **3** was treated with primary amines, glyoxal, and ammonium bicarbonate,[39, 40] followed by subsequent TBS removal with TBAF to produce the desired compounds (**28–43**), in acceptable yields. Biological evaluation of these analogs is discussed in detail in Chapter IV.

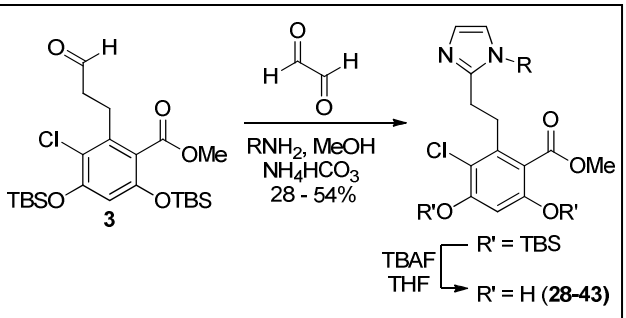

Scheme 6. Synthetic route to analogs **28–43**.

III.7 Concluding Remarks

In conclusion, analysis of RDA·yHsp90N, cRDA·hHsp90N, and RDA·dGrp94N co-crystal structures revealed ligand specific interactions, which were exploitable for isoform

selective inhibitors. Each of the 19 analogs designed provided information critical for the advancement of Grp94 selective inhibitors. Furthermore, the proposed analogs allow for an efficient evaluation of both the *des*-quinone and the *cis*-amide bioisostere hypotheses. Chapter IV will discuss the biological assays utilized to evaluate analogs **25**–**43** for isoform selectivity.

III.8 Methods and Experimentals

General procedure for analogs 25–27: Acid **44** (1 equiv.) was dissolved in anhydrous DCM at 25 ˚C. To the reaction flask was added 1-ethyl-3-(3-dimethylaminopropyl) carbodiimide) (EDCI, 3 equiv.) followed by 4-dimethylaminopyridine (DMAP, 3 equiv.). After dissolution, a 0.5 M solution of the required aniline (3 equiv.) in anhydrous DCM was added to the reaction flask. The reaction was stirred at 25˚ C until complete conversion of the acid was observed by TLC. Upon complete conversion, the reaction mixture was poured into H_2O and extracted with DCM. The organic layers were combined, dried with $MgSO_4$ and concentrated in vacuo. The resulting residue was redissolved in wet THF and tetra-n-butylammonium fluoride (TBAF, 4 equiv.) was added dropwise to the reaction flask at room temperature. After complete conversion of starting material, as observed by TLC, the reaction was quenched with saturated aqueous NH_4Cl and extracted with EtOAc. The organic layers were combined, dried with Na_2SO_4, and concentrated in vacuo. Purification conditions and yields for all compounds are described below:

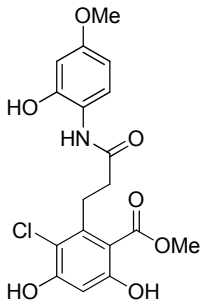

methyl 3-chloro-4,6-dihydroxy-2-(3-((2-hydroxy-4-methoxyphenyl)amino)-3-oxopropyl)benzoate (25): Purified by flash chromatography utilizing 95:5 (DCM:MeOH) as the eluent; Yield: 63 %; ^{1}H NMR ($CDCl_3$, 500 MHz) δ 9.27 (s, 1H), 7.19 (d, *J* = 8.8 Hz, 1H), 6.52 (s, 1H), 6.48 (d, *J* = 2.8 Hz, 1H), 6.41 (dd, *J* = 8.8 Hz, 2.8 Hz, 1H), 3.96 (s, 3H), 3.75 (s, 3H), 3.45–3.48 (m, 2H), 2.77–2.80 (m, 2H); ^{13}C NMR ($CDCl_3$, 125 MHz) δ 172.9, 171.4, 162.6, 159.4, 158.9, 151.1, 142.8, 123.9, 120.9, 115.0, 108.0, 106.3, 104.4, 103.3, 55.6, 53.0, 36.1, 30.6; ESI-HRMS *m/z* 394.0684 (M – H, $C_{18}H_{17}ClNO_7$ requires 394.0694).

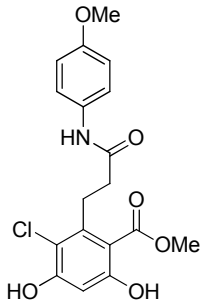

methyl 3-chloro-4,6-dihydroxy-2-(3-((4-methoxyphenyl)amino)-3-oxopropyl)benzoate (26): Purified by flash chromatography utilizing 97:3 (DCM:MeOH) as the eluent; Yield: 61 %; ^{1}H NMR (Acetone-D_6, 500 MHz) δ 10.98 (bs, 1H), 9.02 (s, 1H), 7.59 (d, *J* = 9.0 Hz, 1H), 6.87 (d, *J* = 9.0 Hz, 1H), 6.50 (s, 1H), 3.95 (s, 3H), 3.77 (s, 3H), 3.40–3.43 (m, 2H), 2.62–2.65 (m, 2H); ^{13}C NMR (Acetone-D_6, 125 MHz) δ 171.4, 170.4, 162.4, 158.6, 156.7, 143.3, 133.7, 121.6 (2C), 114.8, 114.6 (2C), 108.3, 103.1, 55.6, 52.9, 36.7, 29.1; ESI-HRMS *m/z* 378.0738 (M – H, $C_{18}H_{17}ClNO_6$ requires 378.0744).

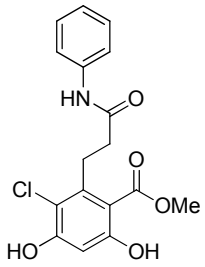

methyl 3-chloro-4,6-dihydroxy-2-(3-oxo-3-(phenylamino)propyl)benzoate (27): Purified by flash chromatography utilizing 90:10 (DCM:MeOH) as the eluent; Yield: 83 %; ^{1}H NMR ($CDCl_3$, 500 MHz) δ 11.16 (s, 1H), 7.46 (d, *J* = 7.9 Hz, 2H), 7.27 (t, *J* = 7.9 Hz, 2 Hz), 7.10 (s, 1H), 7.06 (t, *J* = 7.4 Hz, 1H), 6.53 (s, 1H), 6.05 (bs, 1H), 3.91 (s, 3H), 3.42–3.45 (m, 2H), 2.55–2.58 (m, 2H); ^{13}C NMR ($CDCl_3$, 125 MHz) δ 170.4, 169.9, 163.0, 156.2, 141.7, 137.8, 129.1 (2C), 124.4, 119.7 (2C), 113.9, 106.9, 103.0, 52.7, 36.7, 28.8; ESI-HRMS *m/z* 348.0629 (M – H, $C_{17}H_{15}ClNO_5$ requires 348.0639).

General procedure for compounds (28–43): Aldehyde **3** (1 equiv.) was dissolved in wet MeOH at 25˚ C. The required aniline/amine (1 equiv.) was added dropwise *via* a syringe to the reaction flask followed by addition of ammounim bicarbonate ($NH_3CH_2O_3$, 1 equiv.). Glyoxal (1 equiv.) was then added dropwise *via* a syringe and the reaction was allowed to stir at 25 ˚ C for 8 h. Upon complete conversion of the aldehyde, TBAF as observed by TLC, TBAF was added dropwise *via* syringe and the reaction was allowed to stir at 25 ˚C for ~30 min, upon which time, the reaction was quenched with sat. aq. NH_4Cl and extracted with EtOAc. The organic layers were combined, dried with Na_2SO_4, and concentrated in vacuo. All compounds were purified *via* flash chromatography utilizing 95:5 (DCM:MeOH) as the eluent. Yields for all compounds are provided below:

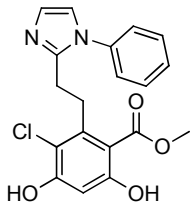

methyl 3-chloro-4,6-dihydroxy-2-(2-(1-phenyl-1H-imidazol-2-yl)ethyl)benzoate (28): Yield: 28%; ^{1}H NMR ($CDCl_3$, 400 MHz) δ 7.56 – 7.39 (m, 3H), 7.32 (d, *J* = 6.8, 2H), 7.14 (s, 1H), 7.05

(d, *J* = 1.0, 1H), 6.51 (s, 1H), 3.84 (s, 3H), 3.50 – 3.42 (m, 2H), 3.06 – 2.97(m, 2H); ^{13}C NMR ($CDCl_3$, 125 MHz) δ 171.0, 162.9, 158.2, 147.7, 141.4, 137.4, 129.6 (2C), 128.7, 127.0, 126.1 (2C), 121.1, 114.9, 105.7, 102.6, 52.53, 31.15, 26.20; ESI-HRMS *m/z* 371.0797 (M – H, $C_{19}H_{16}ClN_2O_4$ requires 371.0799).

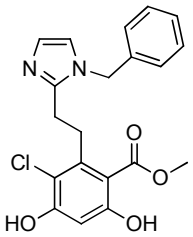

methyl 2-(2-(1-benzyl-1H-imidazol-2-yl)ethyl)-3-chloro-4,6-dihydroxybenzoate (29): Yield: 54%; ^{1}H NMR ($CDCl_3$, 400 MHz) δ 11.74 (bs, 1H), 7.37 – 7.29 (m, 3H), 7.09 – 7.07 (m, 3H), 6.88 (d, *J* = 1.4, 1H), 6.52 (s, 1H), 5.14 (s, 2H), 3.85 (s, 3H), 3.60 – 3.47 (m, 2H), 3.08 – 2.95(m, 2H); ^{13}C NMR ($CDCl_3$, 125 MHz) δ 171.0, 162.8, 159.6, 147.8, 141.2, 135.9, 129.1 (2C), 128.2, 126.7 (2C), 126.1, 120.3, 115.5, 105.0, 102.7, 52.6, 49.7, 30.9, 26.0; ESI-HRMS *m/z* 385.0953 (M – H, $C_{20}H_{19}ClN_2O_4$ requires 385.0955).

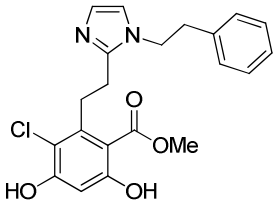

methyl 3-chloro-4,6-dihydroxy-2-(2-(1-phenethyl-1H-imidazol-2-yl)ethyl)benzoate (30): Yield: 51%; ^{1}H NMR ($CDCl_3$, 400 MHz) δ 7.35 – 7.22 (m, 3H), 7.07 (d, *J* = 6.9, 2H), 7.01 (s, 1H), 6.82 (s, 1H), 6.48 (s, 1H), 4.16 (t, *J* = 7.1, 2H), 3.90 (s, 3H), 3.53 – 3.40 (m, 2H), 3.04 (t, *J* = 7.1, 2H), 2.85 – 2.72 (m, 2H); ^{13}C NMR ($CDCl_3$, 125 MHz) δ 170.8, 162.8, 158.5, 147.3, 141.4, 137.2, 128.9 (2C), 128.7 (2C), 127.1, 126.4, 119.1, 115.0, 105.6, 102.7, 52.6, 47.4, 37.6, 30.8, 25.8; ESI-HRMS *m/z* 399.1115 (M – H, $C_{21}H_{20}ClN_2O_4$ requires 399.1112).

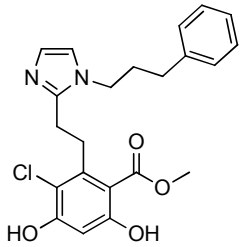

methyl 3-chloro-4,6-dihydroxy-2-(2-(1-(3-phenylpropyl)-1H-imidazol-2-yl)ethyl)benzoate (31): Yield: 48 %; ^{1}H NMR ($CDCl_3$, 400 MHz) δ 7.32 – 7.11 (m, 5H), 7.04 (s, 1H), 6.89 (s, 1H), 6.51 (s, 1H), 4.02 – 3.81 (m, 5H), 3.63 – 3.44 (m, 2H), 3.06 – 2.91 (m, 2H), 2.68 (t, *J* = 7.6, 2H), 2.22– 2.04 (m, 2H); ^{13}C NMR ($CDCl_3$, 125 MHz) δ 170.9, 162.8, 159.3, 147.2, 141.3, 140.2, 128.7 (2C), 128.3 (2C), 126.4, 126.2, 119.1, 115.4, 105.2, 102.8, 52.6, 45.3, 32.7, 32.2, 30.9, 25.9; ESI-HRMS *m/z* 413.1272 (M – H, $C_{22}H_{23}ClN_2O_4$ requires 413.1268).

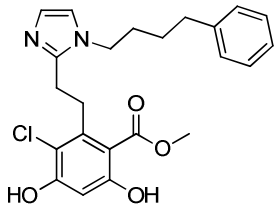

methyl 3-chloro-4,6-dihydroxy-2-(2-(1-(4-phenylbutyl)-1H-imidazol-2-yl)ethyl)benzoate (32): Yield: 37 %; ^{1}H NMR ($CDCl_3$, 400 MHz) δ 7.33 – 7.13 (m, 1H), 7.02 (d, *J* = 1.1, 1H), 6.85 (d, *J* = 1.2, 1H), 6.51 (s, 1H), 3.97 – 3.86 (m, 5H), 3.58 – 3.47 (m, 2H), 3.04 – 2.94 (m, 2H), 2.67 (t, *J* = 7.4, 2H), 1.80 (dt, *J* = 11.3, 7.1, 2H), 1.68 (dt, *J* = 15, 7.1, 2H); ^{13}C NMR ($CDCl_3$, 125 MHz) δ 171.0, 162.8, 159.4, 147.1, 141.4, 141.3, 128.5 (2C), 128.4 (2C), 126.1, 125.9, 119.2, 115.4, 105.1, 102.7, 52.6, 46.0, 35.3, 30.8, 30.4, 28.4, 25.9; ESI-HRMS *m/z* 427.1421 (M – H, $C_{23}H_{25}ClN_2O_4$ requires 427.1425).

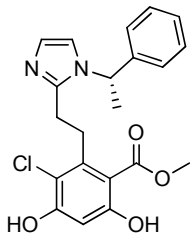

(S)-methyl 3-chloro-4,6-dihydroxy-2-(2-(1-(1-phenylethyl)-1H-imidazol-2-yl)ethyl)benzoate (33): Yield: 35 %; ^{1}H NMR ($CDCl_3$, 400 MHz) δ 7.28 – 7.17 (m, 3H), 7.01 (dd, *J* = 1.4, 1H), 6.97 (m, 3H), 6.42 (s, 1H), 5.36 (q, *J* = 7.0, 1H), 3.71 (s, 3H), 3.42 (m, 2H), 2.84 (t, *J* = 8.2, 2H), 1.74 (d, *J* = 7.0, 3H); ^{13}C NMR ($CDCl_3$, 125 MHz) δ 171.0, 162.8, 159.0, 147.5, 141.5, 141.4, 129.0 (2C), 127.9, 126.2, 125.6 (2C), 116.7, 115.3, 105.3, 102.7, 54.8, 52.5, 30.7, 26.2, 22.5; ESI-HRMS *m/z* 399.111 (M – H, $C_{21}H_{21}ClN_2O_4$ requires 399.1112).

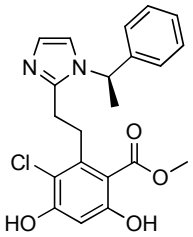

(R)-methyl 3-chloro-4,6-dihydroxy-2-(2-(1-(1-phenylethyl)-1H-imidazol-2-yl)ethyl)benzoate (34): Yield 42 %; ^{1}H NMR ($CDCl_3$, 400 MHz) δ 7.28 – 7.17 (m, 3H), 7.01 (dd, *J* = 1.4, 1H), 6.97 (m, 3H), 6.42 (s, 1H), 5.36 (q, *J* = 7.0, 1H), 3.71 (s, 3H), 3.42 (m, 2H), 2.84 (t, *J* = 8.2, 2H), 1.74 (d, *J* = 7.0, 3H); ^{13}C NMR ($CDCl_3$, 125 MHz) δ 171.0, 162.8, 159.0, 147.5, 141.5, 141.4, 129.0 (2C), 127.9, 126.2, 125.6 (2C), 116.7, 115.3, 105.3, 102.7, 54.8, 52.5, 30.7, 26.2, 22.5; ESI-HRMS *m/z* 399.111 (M – H, $C_{21}H_{21}ClN_2O_4$ requires 399.1112).

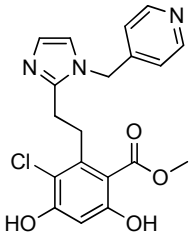

methyl 3-chloro-4,6-dihydroxy-2-(2-(1-(pyridin-4-ylmethyl)-1H-imidazol-2-yl)ethyl)benzoate (35): Yield: 40 %; ^{1}H NMR ($CDCl_3$, 400 MHz) δ 8.58 (dd, *J* = 4.5, 1.5, 2H), 7.13 (d, *J* = 1.4, 1H), 6.96 (d, *J* = 6.0, 2H), 6.92 (d, *J* = 1.4, 1H), 6.47 (s, 1H), 5.19 (s, 2H), 3.89 (s, 3H), 3.55 – 3.44 (m, 2H), 2.99 – 2.89 (m, 2H); ^{13}C NMR ($CDCl_3$, 125 MHz) δ 170.1, 162.5,

159.3, 150.1 (2C), 148.0, 145.8, 141.2, 127.2, 121.3 (2C), 120.3, 115.3, 105.4, 102.8, 52.6, 48.4, 31.0, 26.0; ESI-HRMS *m/z* 386.0912 (M – H, $C_{19}H_{18}ClN_3O_4$ requires 386.0908).

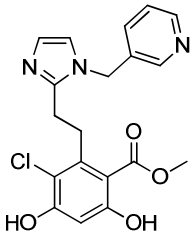

methyl 3-chloro-4,6-dihydroxy-2-(2-(1-(pyridin-3-ylmethyl)-1H-imidazol-2-yl)ethyl)benzoate (36): Yield 48 %; ^{1}H NMR ($CDCl_3$, 400 MHz) δ 8.59 (dd, *J* = 4.6, 1.7, 1H), 8.51 (d, *J* = 1.4, 1H), 7.40 – 7.30 (m, 2H), 7.11 (d, *J* = 1.3, 1H), 6.92 (d, *J* = 1.3, 1H), 6.50 (s, 1H), 5.20 (s, 2H), 3.90 (s, 3H), 3.58 – 3.49 (m, 2H), 3.01 – 2.92 (m, 2H); ^{13}C NMR ($CDCl_3$, 125 MHz) δ 170.5, 162.5, 158.8, 149.4, 148.0, 147.7, 141.4, 134.6, 132.1, 127.3, 124.1, 120.0, 115.1, 105.6, 102.9, 52.6, 47.1, 31.1, 26.1; ESI-HRMS *m/z* 386.0903 (M – H, $C_{19}H_{18}ClN_3O_4$ requires 386.0908).

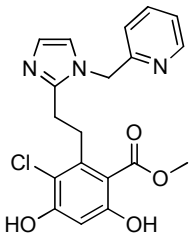

methyl 3-chloro-4,6-dihydroxy-2-(2-(1-(pyridin-2-ylmethyl)-1H-imidazol-2-yl)ethyl)benzoate (37): Yield: 45 %; ^{1}H NMR ($CDCl_3$, 400 MHz) δ 8.61 (d, *J* = 4.5, 1H), 7.69 (td, *J* = 7.7, 1.7, 1H), 7.26 (dd, *J* = 7.3, 5.2, 1H), 7.11 (d, *J* = 1.3, 1H), 6.98 (d, *J* = 1.3, 1H), 6.85 (d, *J* = 7.9, 1H), 6.49 (s, 1H), 5.29 (s, 2H), 3.88 (s, 3H), 3.58 – 3.45 (m, 2H), 3.06 – 2.91 (m, 2H); ^{13}C NMR ($CDCl_3$, 125 MHz) δ 170.8, 162.7, 158.6, 156.0, 149.7, 147.9, 141.3, 137.5, 127.0, 123.0, 120.7, 120.2, 115.1, 105.6, 102.8, 52.6, 51.2, 30.9, 26.0; ESI-HRMS *m/z* 386.0899 (M – H, $C_{19}H_{18}ClN_3O_4$ requires 386.0908).

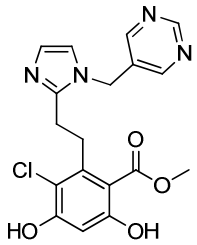

methyl 3-chloro-4,6-dihydroxy-2-(2-(1-(pyrimidin-5-ylmethyl)-1H-imidazol-2-yl)ethyl)benzoate (38): Yield; 45 %; ^{1}H NMR ($CDCl_3$, 400 MHz) δ 9.19 (s, 1H), 8.54 (s, 2H), 7.11 (d, *J* = 1.4, 1H), 6.91 (d, *J* = 1.4, 1H), 6.48 (s, 1H), 5.20 (s, 2H), 3.89 (s, 3H), 3.55 – 3.44 (m, 2H), 3.02 – 2.92 (m, 2H); ^{13}C NMR ($CDCl_3$, 125 MHz) δ 169.1, 161.4, 157.6, 157.5, 154.4 (2C), 146.7, 140.1, 128.9, 126.6, 118.7, 114.0, 104.8, 102.0, 51.6, 44.0, 30.1, 25.1; ESI-HRMS *m/z* 387.0861 (M – H, $C_{18}H_{17}ClN_4O_4$ requires 387.0860).

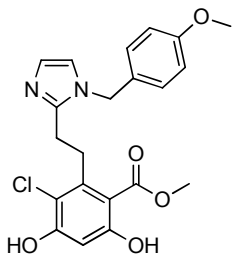

methyl 3-chloro-4,6-dihydroxy-2-(2-(1-(4-methoxybenzyl)-1H-imidazol-2-yl)ethyl)benzoate (39): Yield 33%; ^{1}H NMR ($CDCl_3$, 400 MHz) δ 7.19 (m, 3H), 7.10 (d, *J* = 1.3, 1H), 6.93 (m, 2H), 6.64 (s, 1H), 5.22 (s, 2H), 3.89 (s, 3H), 3.79 (s, 3H), 3.52 (dd, *J* = 9.0, 7.0, 2H), 3.10 (m, 2H); ^{13}C NMR ($CDCl_3$, 125 MHz) δ 171.2, 162.2, 160.6, 158.9, 147.5, 141.6, 129.7 (2C), 128.8, 123.9, 121.7, 115.1 (2C), 115.0, 108.2, 103.6, 55.6, 53.1, 50.1, 31.0, 26.1; ESI-HRMS *m/z* 415.1061 (M – H, $C_{21}H_{21}ClN_2O_5$ requires 415.1061).

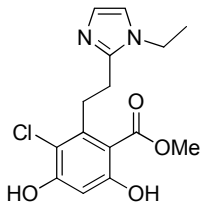

methyl 3-chloro-2-(2-(1-ethyl-1H-imidazol-2-yl)ethyl)-4,6-dihydroxybenzoate (40): Yield: 43 %; ^{1}H NMR (MeOH, 500 MHz) δ 6.91 (2, 1H), 6.77 (s, 1H), 6.12 (s, 1H), 3.82 (q, *J* = 7.3 Hz, 2H), 3.73 (s, 3H), 3.30–3.33 (m, 2H), 2.84–2.87 (m, 2H), 1.24 (t, *J* = 7.3 Hz, 3H); ^{13}C NMR (MeOH, 125 MHz) δ; 172.4, 163.1, 154.7, 148.6, 141.3, 135.1, 127.3, 119.9, 104.6, 101.3, 52.4, 41.6, 32.0, 27.3, 16.5; ESI-HRMS *m/z* 323.0797 (M – H, $C_{15}H_{16}ClN_2O_4$ requires 323.0799).

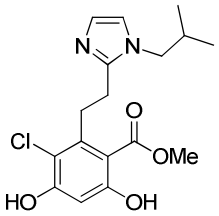

methyl 3-chloro-4,6-dihydroxy-2-(2-(1-isobutyl-1H-imidazol-2-yl)ethyl)benzoate (41): Yield: 42 %; ^{1}H NMR (MeOH, 500 MHz) δ 7.02 (s, 1H), 6.91 (s, 1H), 6.39 (s, 1H), 3.87 (s, 3H), 3.70 (d, *J* = 7.5 Hz, 2H), 3.32–3.37 (m, 2H), 2.96–2.99 (m, 2H), 1.92–2.05 (m, 1H), 0.91 (d, *J* = 6.7 Hz, 6H); ^{13}C NMR (MeOH, 125 MHz) δ 171.5, 161.1, 160.4, 148.7, 141.4, 126.9, 121.4, 115.6, 109.3, 103.6, 54.0, 52.8, 31.7, 31.2, 27.4, 20.1 (2C); ESI-HRMS *m/z* 351.1115 (M – H, $C_{17}H_{20}ClN_2O_4$ requires 351.1112).

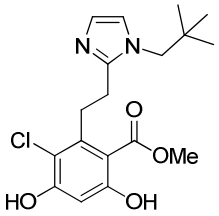

methyl 3-chloro-4,6-dihydroxy-2-(2-(1-neopentyl-1H-imidazol-2-yl)ethyl)benzoate (42): Yield: 35 %; ^{1}H NMR (MeOH, 500 MHz) δ 7.00 (s, 1H), 6.91 (s, 1H), 6.35 (s, 1H), 3.85 (s, 3H), 3.70 (s, 2H), 3.35–3.38 (m, 2H), 2.98–3.01 (m, 2H), 0.96 (s, 9H); ^{13}C NMR (MeOH, 125 MHz) δ 171.7, 162.1, 161.6, 149.5, 141.4, 126.6, 122.5, 116.5, 107.9, 103.8, 57.6, 52.7, 34.3, 31.7, 28.1 (3C), 27.8; ESI-HRMS *m/z* 365.1269 (M – H, $C_{18}H_{22}ClN_2O_4$ requires 365.1268).

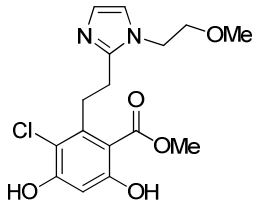

methyl 3-chloro-4,6-dihydroxy-2-(2-(1-(2-methoxyethyl)-1H-imidazol-2-yl)ethyl)benzoate (43): Yield: 39 %; ^{1}H NMR (MeOH, 500 MHz) δ 7.05 (d, *J* = 1.3 Hz, 1H), 6.88 (d, *J* = 1.2 Hz, 1H), 6.27 (s, 1H), 4.05 (t, *J* = 5.2 Hz, 2H), 3.85 (s, 3H), 3.60 (t, *J* = 5.2 Hz, 2H), 3.40–3.42 (m, 2H), 3.31 (s, 3H), 2.98–3.01 (m, 2H); ^{13}C NMR (MeOH, 125 MHz) δ 172.2, 165.1, 162.6, 149.4, 141.4, 127.1, 121.0, 118.1, 105.3, 104.4, 73.0, 59.2, 52.5, 46.7, 31.9, 27.4; ESI-HRMS *m/z* 353.0902 (M – H, $C_{16}H_{18}ClN_2O_5$ requires 353.0904).

III.9 References

1. Hartl, F. U.; Bracher, A.; Hayer-Hartl, M., Molecular chaperones in protein folding and proteostasis. *Nature* **2011,** 475, 324-332.

2. Buchberger, A.; Bukau, B.; Sommer, T., Protein quality control in the cytosol and the endoplasmic reticulum: Brothers in arms. *Mol. Cell* **2010,** 40, 238-252.

3. Kang, H. S.; Welch, W. J., Characterization and purification of the 94-kDa glucose-regulated protein. *J. Biol. Chem.* **1991,** 266, 5643-5649.

4. Little, E.; Ramakrishnan, M.; Roy, B.; Gazit, G.; Lee, A. S., The glucose-regulated proteins (GRP78 and GRP94): functions, gene regulation, and applications. *Crit. Rev. Eukaryot. Gene Expr.* **1994,** 4, 1-18.

5. Shiu, R. P.; Pouyssegur, J.; Pastan, I., Glucose depletion accounts for the induction of two transformation-sensitive membrane proteinsin Rous sarcoma virus-transformed chick embryo fibroblasts. *Proc. Natl. Acad. Sci. USA* **1977,** 74, 3840-3844.

6. Soldano, K. L.; Jivan, A.; Nicchitta, C. V.; Gewirth, D. T., Structure of the N-terminal domain of GRP94. *J. Biol. Chem.* **2003,** 279, 48330-48338.

7. http://biogps.gnf.org (August 9, 2011),

8. McLaughlin, M.; Vandenbroeck, K., The endoplasmic reticulum protein folding factory and its chaperones: new targets for drug discovery? *Br. J. Pharmacol.* **2011,** 162, 328-345.

9. Bernasconi, R.; Molinari, M., ERAD and ERAD tuning: disposal of cargo and of ERAD regulators from the mammalian ER. *Curr. Opin. Cell Biol.* **2010,** 23, 176-183.

10. Goeckeler, J. L.; Brodsky, J. L., Molecular chaperones and substrate ubiquitination control the efficiency of endoplasmic reticulum-associated degradation. *Diabetes Obes. Metab.* **2010,** 12 Suppl 2, 32-38.

11. Randow, F.; Seed, B., Endoplasmic reticulum chaperone gp96 is required for innate immunity but not cell viability. *Nat. Cell Biol.* **2001,** 3, 891-896.

12. Yang, Y.; Liu, B.; Dai, J.; Srivastava, P. K.; Zammit, D. J.; Lefrancois, L.; Li, Z., Heat shock protein gp96 is a master chaperone for toll-like receptors and is important in the innate function of macrophages. *Immunity* **2007,** 26, 215-226.

13. Verfaillie, T.; Garg, A. D.; Agostinis, P., Targeting ER stress induced apoptosis and inflammation in cancer. *Cancer Lett.* **2010**, [E pub] ahead of print, doi:10.1016/j.physletb.2003.10.071.

14. Eletto, D.; Dersh, D.; Argon, Y., GRP94 in ER quality control and stress responses. *Semin. Cell Dev. Biol.* **2010,** 21, 479-485.

15. Wanderling, S.; Simen, B. B.; Ostrovsky, O.; Ahmed, N. T.; Vogen, S. M.; Gidalevitz, T.; Argon, Y., GRP94 is essential for mesoderm induction and muscle development because it regulates insulin-like growth factor secretion. *Mol. Biol. Cell.* **2007,** 18, 3764-3775.

16. Rosser, M. F.; Nicchitta, C. V., Ligand interactions in the adenosine nucleotide-binding domain of the Hsp90 chaperone, GRP94. I. Evidence for allosteric regulation of ligand binding. *J. Biol. Chem.* **2000,** 275, 22798-22805.

17. Immormino, R. M.; Collins, D. E.; Shaffer, P. L.; Soldano, K. L.; Walker, M. A.; Gewirth, D. T., Ligand-induced conformational shift in the N-terminal domain of GRP94, an Hsp90 chaperone. *J. Biol. Chem.* **2004,** 279, 46162-46171.

18. Dollins, D. E.; Warren, J. J.; Immormino, R. M.; Gewirth, D. T., Structures of GRP94-nucleotide complexes reveal mechanistic differences between the Hsp90 chaperones. *Mol. Cell* **2007,** 28, 41-56.

19. Dollins, D. E.; Immormino, R. M.; Gewirth, D. T., Structure of unliganded GRP94, the endoplasmic reticulum Hsp90. Basis for nucleotide-induced conformational change. *J. Biol. Chem.* **2005,** 280, 30438-30447.

20. Frey, S.; Leskovar, A.; Reinstein, J.; Buchner, J., The ATPase cycle of the endoplasmic chaperone Grp94. *J. Biol. Chem.* **2007,** 282, 35612-35620.

21. Ostrovsky, O.; Makarewich, C. A.; Snapp, E. L.; Argon, Y., An essential role for ATP binding and hydrolysis in the chaperone activity of GRP94 in cells. *Proc. Natl. Acad. Sci. USA* **2009,** 106, 11600-11605.

22. Munro, S.; Pelham, H. R., A C-terminal signal prevents secretion of luminal ER proteins. *Cell* **1987,** 48, 899-907.

23. Immormino, R. M.; Metzger IV, L. E.; Reardon, P. N.; Dollins, D. E.; Blagg, B. S. J.; Gewirth, D. T., Different poses for ligand and chaperone in inhibitor-bound Hsp90 and GRP94: implications for paralog-specific drug design. *J. Mol. Biol.* **2009,** 388, 1033-1042.

24. Ishiguro, S.; Watanabe, Y.; Ito, N.; Nonaka, H.; Takeda, N.; Sakai, T.; Kanaya, H.; Okada, K., SHEPHERD is the Arabidopsis GRP94 responsible for the formation of functional CLAVATA proteins. *EMBO J.* **2002,** 21, 898-908.

25. Maynard, J. C.; Pham, T.; Zheng, T.; Jockheck-Clark, A.; Rankin, H. B.; Newgard, C. B.; Spana, E. P.; Nicchitta, C. V., Gp93, the Drosophila GRP94 ortholog, is required for gut epithelial homeostasis and nutrient assimilation-coupled growth control. *Dev. Biol.* **2010,** 339, 295-306.

26. Lee, A. S., The glucose-regulated proteins: Stress induction and clinical applications. *Trends Biochem. Sci.* **2001,** 26, 504-510.

27. Lawson, B.; Brewer, J. W.; Hendershot, L. M., Geldanamycin, an Hsp90/GRP94-binding drug, induces increased transcription of endoplasmic reticulum (ER) chaperones via the ER stress pathway. *J. Cell. Physiol.* **1998,** 174, 170-178.

28. Huang, Q. Q.; Sobkoviak, R.; Jockheck-Clark, A. R.; Shi, B.; Mandelin, A. M., 2nd; Tak, P. P.; Haines, G. K., 3rd; Nicchitta, C. V.; Pope, R. M., Heat shock protein 96 is elevated in rheumatoid arthritis and activates macrophages primarily via TLR2 signaling. *J. Immunol.* **2009,** 182, 4965-4973.

29. Prodromou, C.; Panaretou, B.; Chohan, S.; Siligardi, G.; O'Brien, R.; Ladbury, J. E.; Roe, S. M.; Piper, P. W.; Pearl, L. H., The ATPase cycle of Hsp90 drives a molecular 'clamp' via transient dimerization of the N-terminal domains. *EMBO J.* **2000,** 19, 4383-4392.

30. Whitesell, L.; Mimnaugh, E. G.; De Costa, B.; Myers, C. E.; Neckers, L. M., Inhibition of heat shock protein HSP90-pp60v-src heteroprotein complex formation by benzoquinone ansamycins: essential role for stress proteins in oncogenic transformation. *Proc. Natl. Acad. Sci. USA* **1994,** 91, 8324-8328.

31. Roe, S. M.; Prodromou, C.; O'Brien, R.; Ladbury, J. E.; Piper, P. W.; Pearl, L. H., Structural basis for inhibition of the Hsp90 molecular chaperone by the antitumor antibiotics radicicol and geldanamycin. *J. Med. Chem.* **1999,** 42, 260-266.

32. Sreedhar, A. S.; Kalmar, E.; Csermely, P.; Shen, Y.-F., Hsp90 isoforms: Functions, expression and clinical importance. *FEBS Lett.* **2004,** 562, 11-15.

33. Chavany, C.; Mimnaugh, E.; Miller, P.; Bitton, R.; Nguyen, P.; Trepel, J.; Whitesell, L.; Schnur, R.; Moyer, J.; Neckers, L., p185erbB2 binds to GRP94 in vivo. Dissociation of the p185erbB2/GRP94 heterocomplex by benzoquinone ansamycins precedes depletion of p185erbB2. *J. Biol. Chem.* **1996,** 271, 4974-7.

34. Snader, K. M.; Neckers, L. M.; Vishnuvajjala, B. R.; Saudville, E. A.; Xu, W.; Rosser, M. E.; Nicchitta, C.; Isaacs, J. A. Geldanamycin Derivatives Useful For the Treatment of Cancer. WO 02/36574, 2001.

35. Stone, T. W.; Ceruti, S.; Abbracchio, M. P., Adenosine receptors and neurological disease: neuroprotection and neurodegeneration. *Handb. Exp. Pharmacol.* **2009**, (193), 535-587.

36. Fishman, P.; Bar-Yehuda, S.; Synowitz, M.; Powell, J. D.; Klotz, K. N.; Gessi, S.; Borea, P. A., Adenosine receptors and cancer. *Handb. Exp. Pharmacol.* **2009**, (193), 399-441.

37. Hutchison, K. A.; Fox, I. H., Purification and characterization of the adenosine A2-like binding site from human placental membrane. *J. Biol. Chem.* **1989,** 264, 19898-19903.

38. Hutchison, K. A.; Nevins, B.; Perini, F.; Fox, I. H., Soluble and membrane-associated human low-affinity adenosine binding protein (adenotin): properties and homology with mammalian and avian stress proteins. *Biochemistry* **1990,** 29, 5138-5144.

39. Nakajima, T. Method for Producing 2-Alkylimidazole and 2-Alkyimidazole Obtained Thereby. Int. patent #CO7D 233/58, 2007.

40. Zhouhua, Z.; Zhengqiang, X.; Kun, Z.; Huanbin, L. Method for Preparing 2-Propyl Imidazole. CN20091272449 20091019 2010.

41. Arduengo III, A. J.; Gentry Jr., F. P.; Taverkere, P. K.; Simmons III, H. E. Process For Manufacture of Imidazoles. US 6,177575 B1, 2001.

42. Jain, A. N., Surflex: Fully automatic flexible molecular docking using a molecular similarity-based search engine. *J. Med. Chem.* **2003,** 46, 499-511.

43. Jain, A. N., Surflex-Dock 2.1: Robust performance from ligand energetic modeling, ring flexibility, and knowledge-based search. *J. Comput. Aided Mol. Des.* **2007,** 21, 281-306.

44. Clevenger, R. C.; Blagg, B. S. J., Design, synthesis, and evaluation of a radicicol and geldanamycin chimera, radamide. *Org. Lett.* **2004,** 6, 4459-4462.

45. Duerfeldt, A. S.; Brandt, G. E. L.; Blagg, B. S. J., Design, synthesis, and biological evaluation of conformationally constrained cis-amide Hsp90 inhibitors. *Org. Lett.* **2009,** 11, 2353-2356.

46. Hadden, M. K.; Blagg, B. S. J., Synthesis and evaluation of radamide analogues, a chimera of radicicol and geldanamycin. *J. Org. Chem.* **2009,** 74, 4697-4704.

Chapter IV

Evaluation of Proposed Grp94 Selective Inhibitors

IV.1 Biological Roles of Grp94: Implications for Grp94 Inhibition

As discussed previously, glucose-regulated protein 94 kDa (Grp94) was first identified as an induction product resulting from glucose deprivation.[1] Subsequent studies identified Grp94 as the endoplasmic reticulum (ER) paralog of heat shock protein 90 kDa (Hsp90). Although potent Hsp90 inhibitors have been developed, no isoform selective inhibitors have been identified, other than NECA, which has proven to be an unacceptable starting point for small molecule development. The highly homologous N-terminal binding domain has led the general research community to consider isoform selective inhibitors as an impractical venture. However, analyses of the co-crystal structures has revealed obvious structural and mechanistic differences, specifically between Grp94 and cytosolic Hsp90 that can be exploited for inhibitor design. Identification of a selective Grp94 inhibitor would result in a paradigm shift for Hsp90 inhibition and help elucidate biological roles of Grp94. Recently, siRNA, immunoprecipitation, and combinatorial Hsp90/Grp94 ATPase disruption has implicated Grp94 in cancer and the innate and adaptive immune responses. Thus, small molecule selective Grp94 inhibitors have become desirable.

IV.1.1 Grp94 and Cancer

The ER manifests its own response to cellular stress, a major component of which is the unfolded-protein response (UPR).[2] Much like the heat shock response (HSR), which results in induction of cytosolic chaperones; activation of the UPR increases the concentration of resident ER chaperones.[2] Therefore, not surprisingly, Grp94 levels are elevated in numerous malignancies.[3] Known client proteins of Grp94, discussed in Chapter III, implicate Grp94 in the

maturation and trafficking of secretory and membrane bound proteins.[4] Specific clients of Grp94 that exhibit known roles in cancer progression include the insulin receptor substrate-1 (IRS-1), insulin-like growth factors I and II (IGF-1 and IGF-II), and integrins.[4]

IRS-1 is constitutively activated in numerous solid tumors including breast cancers, leiomyomas, Wilms' tumors, rhabdomyosarcomas, liposarcomas, leiomyosarcomas, and adrenal cortical carcinomas.[5, 6] Tyrosine phyosphorylation of IRS-1 results in activation of the phospoinositide 3-kinase (PI3K) and mitogen-activated protein (MAP) kinase pathways; two pathways tied to oncogenesis.[7-9] Furthermore, IRS-1 was found to play a key role in the constitutively activated β-catenin/Wnt signaling pathway, which contributes to transformation and cancer progression.[5, 10] Blockade of the phosphorylation sites, through phenylalanine mutations, results in IRS-1 inactivation and a subsequent reduction in tumor growth.[11] Recently, studies by Saitoh and colleagues have identified IRS-1 as a Grp94-dependent client protein[12] and established Grp94 as a promising option for regulating aberrant IRS-1 function.

Another important class of client proteins dependent upon Grp94 is the integrin family.[13, 14] Intriguingly, not all integrins are Grp94-dependent, including β_1 integrins which are Grp94 independent.[15] This intra-class specificity is a unique feature of Grp94 and further suggests Grp94 inhibition to yield a more acceptable toxicity profile than inhibitors targeting cytosolic Hsp90. Integrins mediate adhesion between cells and their surrounding environment including other cell types or the extra cellular matrix. Thus, it is not surprising that integrins regulate cell signaling, morphology, motility, and influence the cell cycle; all of which are features critical to intitiation, progression and metastasis of solid tumors.[16] Therefore, indirect disruption of integrin formation, through Grp94 inhibition, represents a promising therapeutic venue.

Of the client proteins dependent upon Grp94 for cancer progression, IGF-1 and IGF-II are the most studied. Argon and colleagues have demonstrated the dependence of IGFs upon Grp94 and showed that upon Grp94 knockdown, pro-IGF intermediates are targeted for endoplasmic reticulum-associated degradation (ERAD) and mature IGF-I and IGF-II are not formed.[17-20] Under normal cellular conditions, IGFs are tightly regulated, as the IGF signaling pathway is pro-growth and anti-apoptotic. However under stressed conditions aberrant IGF signaling triggers a cascade of molecular events that can result in malignancy.[21] Additionally, IGFs are known to activate signaling cascades through IRS-1 binding,[22] thus intertwining two Grp94 clients to cancer progression.

Grp94 involvement in multiple facets of oncogenesis provides an impetus for the development of small molecule inhibitors. Development of selective inhibitors may elucidate a novel anti-cancer target and thus provide a new class of cancer chemotherapeutics.

IV.1.2 Grp94 and Inflammation

Beyond its role in the initiation and progression of cancer, Grp94 has been demonstrated to maintain an intricate role in immunomodulation.[4, 23] Client proteins of Grp94 implicated in aberrant immuno-activity include major histocompatibility complex II (MHC II),[24] Toll-like receptors (TLR),[14, 25] integrins,[13, 14] interferon-γ (IFN-γ),[26] and the p40 subunit of the interleukin-12 (IL-12)[27, 28] family of cytokines. While all of these clients maintain roles in immunity, the affect on TLR activity has been most pursued.

TLRs are a component of the innate immune system responsible for recognizing foreign molecules present in the cellular milieu.[29] Upon recognition of foreign material, TLRs trigger intracellular signaling cascades, which lead to immunoresponse through gene transcription. Immunoprecipitation and Grp94 knockout models have demonstrated the dependence of TLR1,

TLR2, TLR4 and TLR9 upon Grp94.[13, 14] Inhibition of Grp94's function leads to TLR retention in the ER and decreased surface presentation. Expression levels of TLR mRNA remains unaffected by Grp94 inhibition, suggesting Grp94 is responsible for trafficking TLRs to the cell membrane.[4] Thus, Grp94 represents a relevant therapeutic target for disease states in which an exaggerated response to infection is evident including sepsis, rheumatoid arthritis, asthma and chronic autoimmune disorders.[4, 29]

IV.2 Biological Evaluation of Proposed Grp94 Isoform Selective Inhibitors

After synthesizing the proposed Grp94 isoform selective inhibitors described in Chapter III, our attention turned towards their evaluation. With no established protocol for the identification of Grp94 inhibitors, prior studies guided our desire to evaluate such analogs.

IV.2.1 Anti-proliferative Activity

Previous reports have demonstrated Grp94 to be essential for embryonic development, but unlike cytosolic Hsp90, non-essential for mammalian cell culture viability.[14, 30] Considering this observation, compounds **25–43** were evaluated against MCF-7 and SKBr3 cell lines, two breast cancer cell lines sensitive to Hsp90 inhibition. Thus, if analogs **25–43** exhibit Hsp90 inhibitory activity, cell death will be apparent. As shown in Table 6, none of the analogs designed to be selective Grp94 inhibitors exhibited cytotoxicity against MCF-7 or SKBr3 cell lines at concentrations as high as 50 μM. This mimics the activity of NECA, a known Grp94 selective inhibitor, which was discussed in Chapter III. As a control, cRDA (Chapter II) is included in Table 6, which manifests low micromolar activity against both MCF-7 and SKBr3 cells lines. This preliminary study provided the foundation for collaboration with the Nicchitta laboratory at Duke University to evaluate the inhibitors in a functional Grp94 assay.

Table 6. Anti-proliferative and Toll-trafficking results for compounds **25–43**. IC_{50} values expressed in μM concentrations.

Compound	MCF-7	SKBr3	Grp94
25	>50	>50	>50
26	>50	>50	12.6 ± 1.0
27	>50	>50	>50
28	>50	>50	3.8 ± 0.2
29	>50	>50	0.03 ± 0.02
30	>50	>50	ND
31	>50	>50	ND
32	>50	>50	ND
33	>50	>50	ND
34	>50	>50	ND
35	>50	>50	>50
36	>50	>50	0.4 ± 0.3
37	>50	>50	2.3 ± 1.6
38	>50	>50	0.6 ± 0.1
39	>50	>50	0.2 ± 0.2
40	>50	>50	1.1 ± 0.7
41	>50	>50	0.3 ± 0.1
42	>50	>50	0.4 ± 0.1
43	>50	>50	16.5 ± 1.2
cRDA	6.3 ± 0.9	7.8 ± 0.2	8.5 ± 2.2
NECA	>50	>50	1.1 ± 0.2

ND = not determined; compound exhibited <50% inhibition at 5 μM.

IV.2.2 Inhibition of Toll-trafficking: A Grp94 Functional Assay

As discussed previously, TLRs are dependent upon Grp94 for their trafficking to the cell membrane. In collaboration with the Nicchitta laboratory, we developed a functional Grp94 assay utilizing human embryonic kidney cells (HEK293) stably transfected to express the Toll receptor, the *Drosphilia melanogaster* ortholog of human interleukin-1 receptor (Figure 38). This receptor is of the same superfamily as the human TLR2 and TLR4 receptors, establishing it as a viable surrogate for monitoring TLR expression. In the presence of functional Grp94, the Toll receptor is trafficked to the cell membrane; however, in the absence of functional Grp94, the Toll receptor is sequestered intracellulary and not present on the cell membrane.

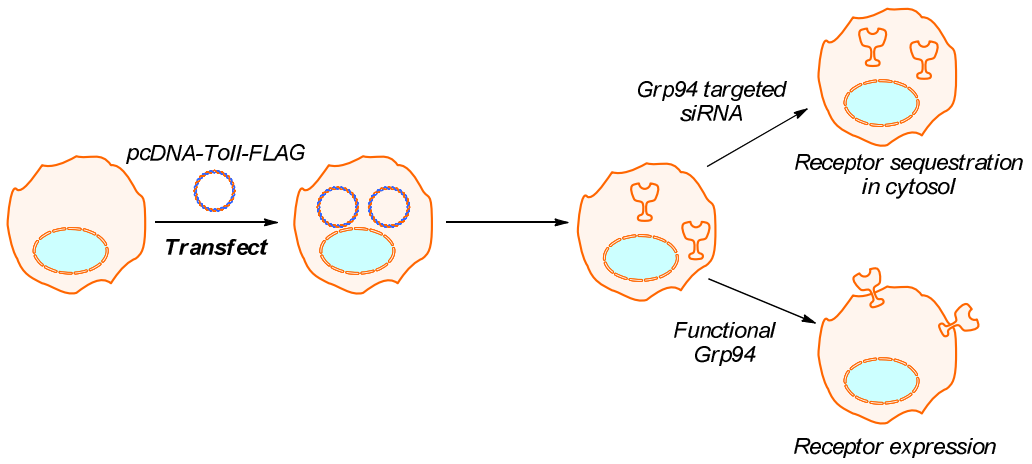

Figure 38. Functional Grp94 assay description. HEK293 cells stably transfected with Toll are exposed to Grp94 target siRNA or small molecules and the presence of Toll expression is measured by confocal microscopy.

As expected, treatment of stably transfected HEK293 cells with Grp94 targeted siRNA resulted in inhibition of Toll membrane presentation (Figure 39). Therefore, we proposed that a similar affect would be manifested by a small molecule Grp94 inhibitor. As shown in Table 6, **26**, **28**, **29** and **36–43** exhibited inhibition of Toll-trafficking, indicative of Grp94 inhibition.

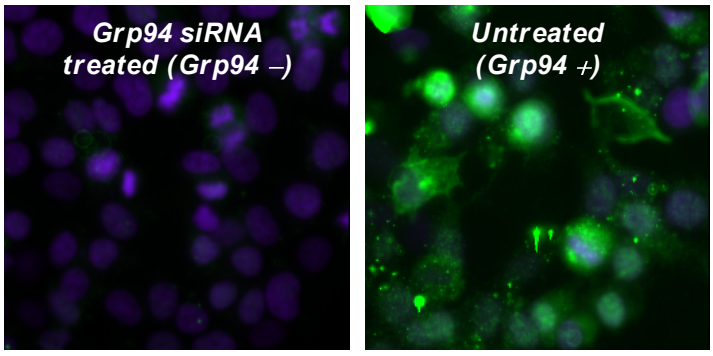

Figure 39. Results of functional Grp94 Toll-trafficking assay. Cells treated with Grp94 targeted siRNA (left) and untreated cells (right).

***des*-Quinone Analogs**

As discussed in Chapter III, the *des*-quinone RDA analogs (**25–27**, Figure 40) were designed to systematically evaluate the necessity of each moiety on the quinone ring for Hsp90 inhibition. It was hypothesized that the functionalities on the quinone ring are necessary for Hsp90 inhibition and removal of such critical hydrogen-bonding functionalities should provide Grp94 selective inhibitors.

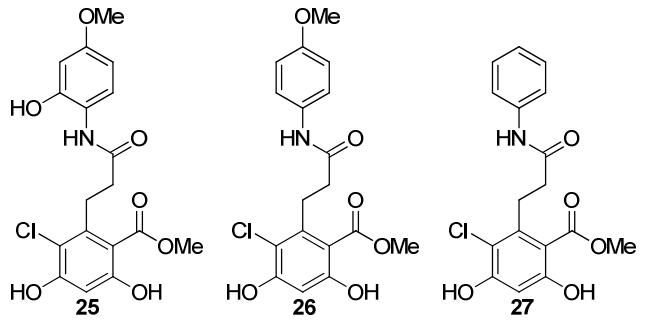

Figure 40. Proposed analogs which lack key functionalities for yHsp82 binding.

As predicted, removal of the 5-carbonyl of RDA's quinone ring (**25**), eliminated Hsp90 inhibitory activity up to concentrations as high as 50 μM. However, elimination of the 5-carbonyl failed to produce a Grp94 inhibitor, as shown in Table 6. Subsequent removal of the 2-carbonyl (**26**) introduced micromolar Grp94 inhibition. A representative depiction of the confocal microscopy results for **26**, is shown in Figure 41. As can be observed, Toll-expression on the cellular membrane is inhibited in a dose-dependent manner. Although the IC_{50} value suggested by the graphic is 1–5 μM, it should be noted that IC_{50} calculations are conducted using at least 10 separate images, each containing 10–20 cells per concentration.

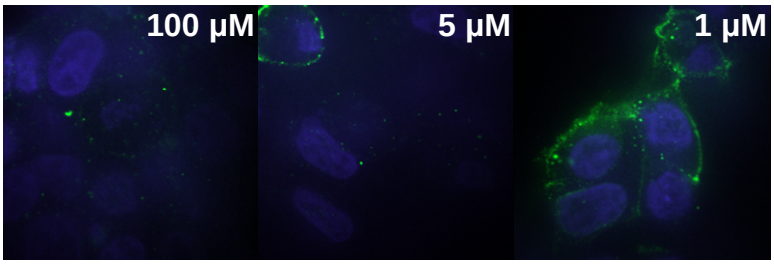

Figure 41. Representative confocal microscopy results for **26** in the Toll-trafficking assay.

Further manipulation of the RDA quinone ring *via* removal of the 4-methyl ether provided analog **27**. Interestingly, **27** exhibited neither Hsp90 nor Grp94 inhibitory activity at concentrations as high as 50 μM. These results suggest that, for analogs based upon *seco*-RDA, the 4-methyl ether, or surrogate hydrogen-bond acceptor, is necessary for Grp94 inhibition. Furthermore, the lack of activity for **25**, suggests the presence of the 2-hydroxy group, to inhibit the necessary conformation required for binding Grp94. The 4-methoxy functionality is proposed to hydrogen-bond with the free phenol of Tyr200 in the Grp94

N-terminal nucleotide-binding pocket. This is speculative, as docking studies with this compound failed. This modeling failure was expected however, because in order to accommodate the interaction with Tyr200 the lid region of Grp94 must be displaced, which cannot be accomplished in the static representation of the protein in AutoDock[31] or Surflex[32, 33] modeling programs. Thus, to develop this class of Grp94 selective inhibitors further, analogs exploiting the interactions and spatial constraint of the 4-position will be synthesized. Additionally, it would be advantageous to acquire the co-crystal structure of **26**, to account for the proposed lid displacement and provide a viable structure for subsequent modeling studies.

Imidazole cis-Amide Bioisostere Analogs

The second hypothesis discussed in Chapter III was that *cis*-amide bioisosteric replacement of the amide bond, displayed by RDA, would provide selective Grp94 inhibitors. This proposal was a result of the analyses of RDA·yHsp90N and RDA·dGrp94N co-crystal structures. Furthermore, the binding data acquired for cRDA, demonstrates that *cis*-amide constraint results in a higher binding affinity for recombinant Grp94. Thus, an imidazole linkage was hypothesized to provide a synthetically accessible scaffold capable of producing relevant analogs to test this hypothesis. The first series of analogs synthesized were **28–32**, which incorporated a phenyl substituted imidazole connected through varying tether linkages (Figure 42). As observed in Table 6, only linker lengths of zero (**28**) and one (**29**) yielded significant Grp94 inhibition, with compound **29**, exhibiting low-nanomolar activity. This was in agreement with the initial Surflex docking studies reported in Chapter III, which suggest linker lengths of n = 0 or 1 exhibit superior Grp94 binding. Compound **29** was hypothesized to project

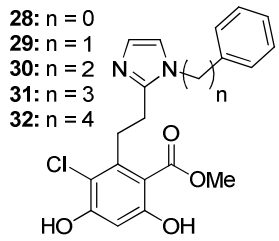

Figure 42: Initial imidazole analogs with varying linker length.

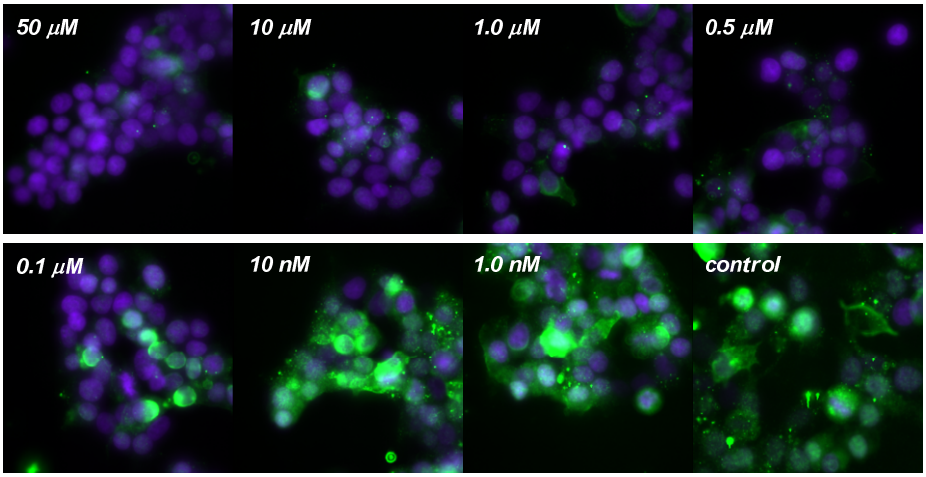

Figure 43. Representative confocal microscopy results for **29** in the Toll-trafficking assay.

into the NECA binding pocket and π-stack with either Phe199 or Tyr200. The confocal microscopy results for **29** are shown in Figure 43. Due to the superior Grp94 inhibitory activity, an expanded concentration range was evaluated. Thus, compound **29** served as our lead compound for further SAR development, leading to analogs **33–39** (Figure 44) and **40–43** (Figure 45).

As demonstrated in Table 6, steric bulk is not accommodated around the linker as introduction of a (*S*, **33**) or (*R*, **34**) methyl group dramatically decreased activity.

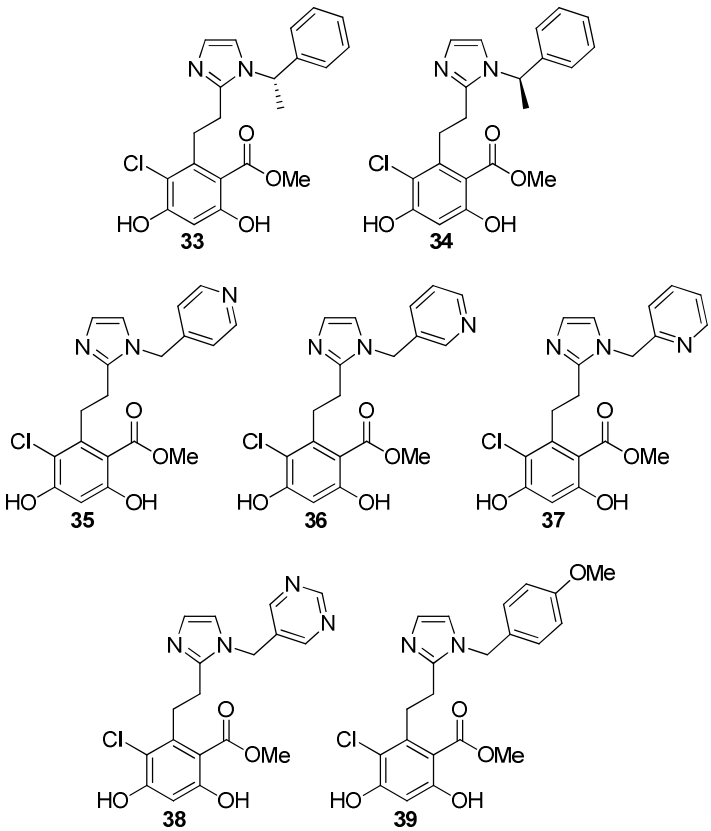

Figure 44. Imidazole analogs based upon **29**.

This result was not surprising, as addition of a chiral center alters the position of the aromatic ring. Thus, the proposed π-stacking interactions with Phe199 and/or Tyr200 become hindered. Compound **35** also failed to elicit Grp94 inhibition even though it was hypothesized to hydrogen-bond with Tyr200 similar to **26**. This was not entirely unexpected as electron-poor 4-pyridyl systems exhibit dramatically different properties than electron-rich anisoles; however, the inability of **35** to exhibit Grp94 inhibition suggests a different binding mode for the linear *des*-quinone analogs than the constrained imidazole class of inhibitors. This coincides with the alternative binding modes exhibited by *trans*- and *cis*-RDA when bound to Grp94, and suggests two exploitable scaffolds that can be optimized for Grp94 inhibition. Thus, the *trans*-RDA conformation should be used as a model for *des*-quinone analogs. Likewise, the *cis*-RDA conformation serves as a relevant model for development of the imidazole series. Furthermore, the pyridine analogs **36–38**, provide additional SAR data demonstrating the *m*-pyridine (**36**) to exhibit ~5-fold higher Grp94 inhibitory activity compared to the *o*-pyridine, **37**. Addition of an extra hydrogen-bond acceptor to yield pyrimidine **38** resulted in similar activity to **36**, which suggests no additional hydrogen-bonding contacts are gained through the incorporation of an additional heteroatom. The Grp94 inhibitory activity manifested by **36–38** is hypothesized to occur from beneficial binding interactions between the heterocyclic nitrogen and the protein backbone amides provided by Gly196 or Phe199, as shown in Figure 33 in Chapter III.

Incorporation of a *p*-methoxy group yielded the second-most active compound of this series, which manifests a Grp94 inhibitory IC_{50} value of ~200 nM. Assuming a similar binding mode to **29**, this suggests exploitable space surrounding the 4-position. Thus, future analogs will aim to discern the size of this cavity.

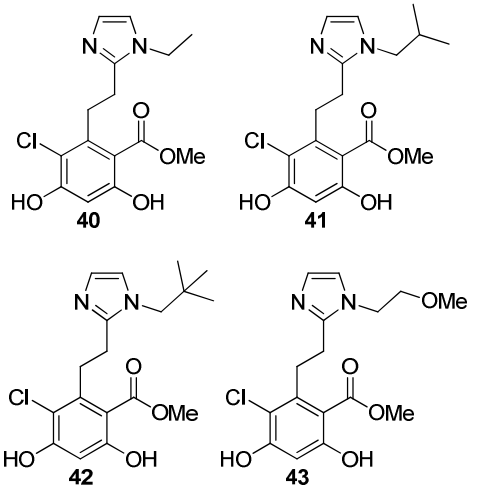

Figure 45. Alkyl-imidazoles

After evaluation of the synthesized benzylated imidazole analogs, compounds **40–43** (Figure 45), were evaluated in anti-proliferation and Toll-trafficking assays. As observed in Table 6, all of the analogs were active, with **41** exhibiting the most potent Grp94 inhibition. However, none of the aliphatic analogs exhibited activity comparable to **29**. This suggests that π-stacking interactions outweigh hydrophobic interactions and contribute to the potency observed for **29**. Considering the results from the Toll-trafficking assay, compound **29** was selected as a lead compound for further evaluation and was re-named KU-NG-1.

IV.3 Biological Profile of KU-NG-1

IV.3.1 Western Blot Confirmation for Lack of Hsp90 Inhibition

Although no cytotoxicity was observed for KU-NG-1 up to 100 μM, Western blot analysis was conducted on MCF-7 cell lysates treated with KU-NG-1 to confirm the lack of Hsp90 inhibition. As shown in Figure 46, no dose-dependent client protein degradation was observed upon treatment with KU-NG-1, as indicated by Akt and Raf levels. Furthermore, no induction of Hsp90 or Hsp70 occurred, which is a hallmark of Hsp90 N-terminal inhibition, as will be dicussed in detail in Chapter V. Actin concentration is independent of Hsp90 and serves as a control.

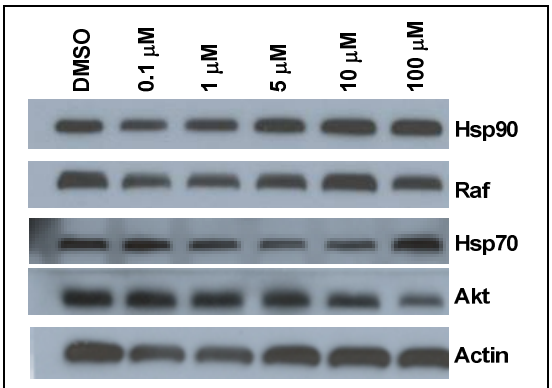

Figure 46. Western blot analysis of MCF-7 cell lysates after treatment with KU-NG-1.

IV.3.2 NCI Cell Panel Profile

Although Randow and Seed demonstrated a lack of dependency of immune cell-lines upon Grp94, very little evidence existed for transformed cell lines. Our preliminary anti-proliferative studies conducted with MCF-7 and SKBr3 breast cancer cells lines confirmed Randow and Seed's findings; however, Grp94 expression is known to correlate with tumor growth and progression. Therefore, KU-NG-1 was submitted to the National Cancer Institute (NCI) for evaluation against 60 cell-panel cytotoxicity assay in an attempt to elucidate the affect of Grp94 inhibition against various malignant cell cultures. As shown in Figure 47, none of the cell-lines exhibited sensitivity to a 10 μM treatment of KU-NG-1. This confirms Randow and Seed's findings and provides evidence that cell culture viability, in general, is independent upon Grp94.

Interestingly, however, overexpression of Grp94 in numerous malignancies has been shown. For instance, breast cancer carcinomas (HBL-100, MDA-MB-231, MCF-7, T47D, MDA-MB-453 and SkBR3) exhibit a ~3–5-fold increase of Grp94 in comparison to normal breast tissue. Furthermore, in conditions deprived of glucose, which mimics conditions observed in a poorly vascularized tumor, a 9-fold induction of Grp94 was observed.[34] Additionally, ductal and lobular invasive breast carcinomas show an increase in Grp94.[35] A similar increase in Grp94 expression is noted in gastric,[36] pancreatic,[37] colon,[38] lung,[39] esophageal[40-42] and oral[43] malignancies; with Grp94 overexpression often correlating with poor prognosis. Thus, the expression pattern of Grp94 specific to tumors suggests a role for cancer progression and metastasis, even though transformed cell cultures lack dependency upon Grp94.

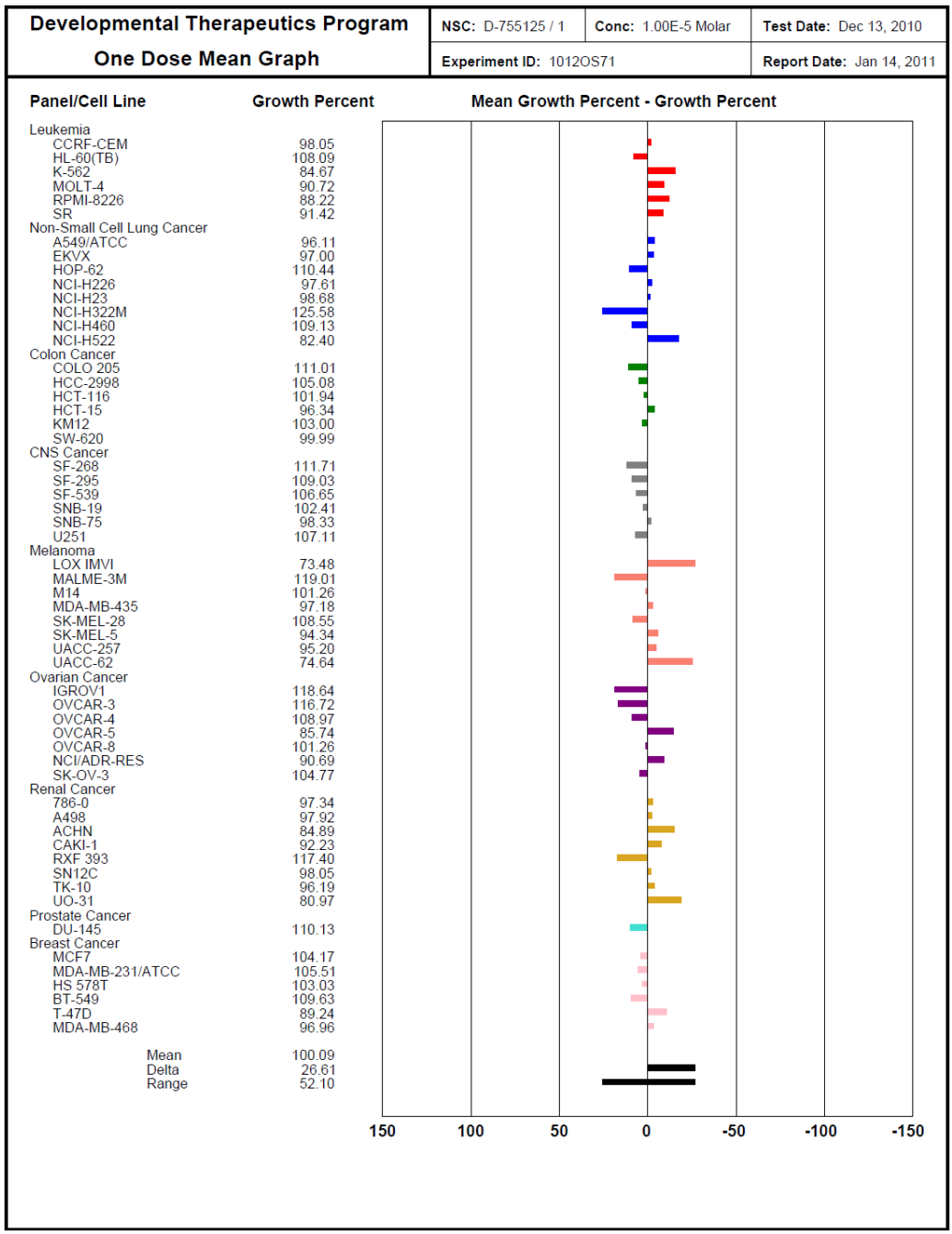

Figure 47. NCI 60 cell-panel cytotoxicity results for KU-NG-1.

As discussed previously, Grp94 is responsible for the biological maturation of signaling molecules and secretory proteins, both of which are more important to a three-dimensional tumors than a cell-culture monolayer. This may provide an explanation for the apparent dependence upon Grp94 for tumor growth and invasion even though cell cultures demonstrate

lack of dependence. Therefore, in order to validate Grp94 as a promising anti-cancer target, three-dimensional tumor models must be utilized to fully understand the role of Grp94 in cancer biology. Recent research suggests the three-dimensional tumor environment to influence drug sensitivity.[44, 45] Additionally, specific signaling pathways are dependent upon the three-dimensional phenotype,[45] thus providing rationale that artificial monolayer cell-cultures may not suffice for the evaluation of Grp94 inhibitors as anti-cancer chemotherapeutic agents.

IV.3.3 Binding Data for KU-NG-1

In collaboration with Daniel Gewirth at the Hauptman-Woodward Medical Research Institute, the binding affinity of KU-NG-1 for recombinant Grp94 and Hsp90 was obtained utilizing isothermal calorimetry (ITC) and tryptophan fluorescence quenching (TFQ) techniques. In the ITC experiments, the binding affinity of KU-NG-1 was determined for the N-terminal truncates of canine Grp94 (dGrp94N) and human Hsp90 (hHsp90). These truncates have been shown to bind ligands in a similar fashion and with similar binding affinities as their full-length counterparts. Furthermore, dGrp94N exhibits ~98% homology with hGrp94N and is an accepted surrogate for biochemical studies.[46] Figure 48 shows representative binding curves for ITC experiments. As observed, KU-NG-1 shows reproducible binding curves for both dGrp94N and hHsp90N. Surprisingly, KU-NG-1 binds hHsp90N with a ~2-fold higher binding affinity than dGrp94N, as shown in Table 7. To confirm this observation, binding affinity was also determined with TFQ utilizing full-length dGrp94 and hHsp90. As shown in Figure 49 and Table 7, the results verified a ~2-fold higher binding affinity for hHsp90 in comparison to dGrp94.

Table 7. Binding affinity data for KU-NG-1 and Grp94 and hHsp90.

Protein	Method	Affinity
dGrp94N	ITC	1.6 μM
hHsp90N	ITC	0.8 μM
dGrp94	TFQ	0.25 μM
hHsp90	TFQ	0.10 μM

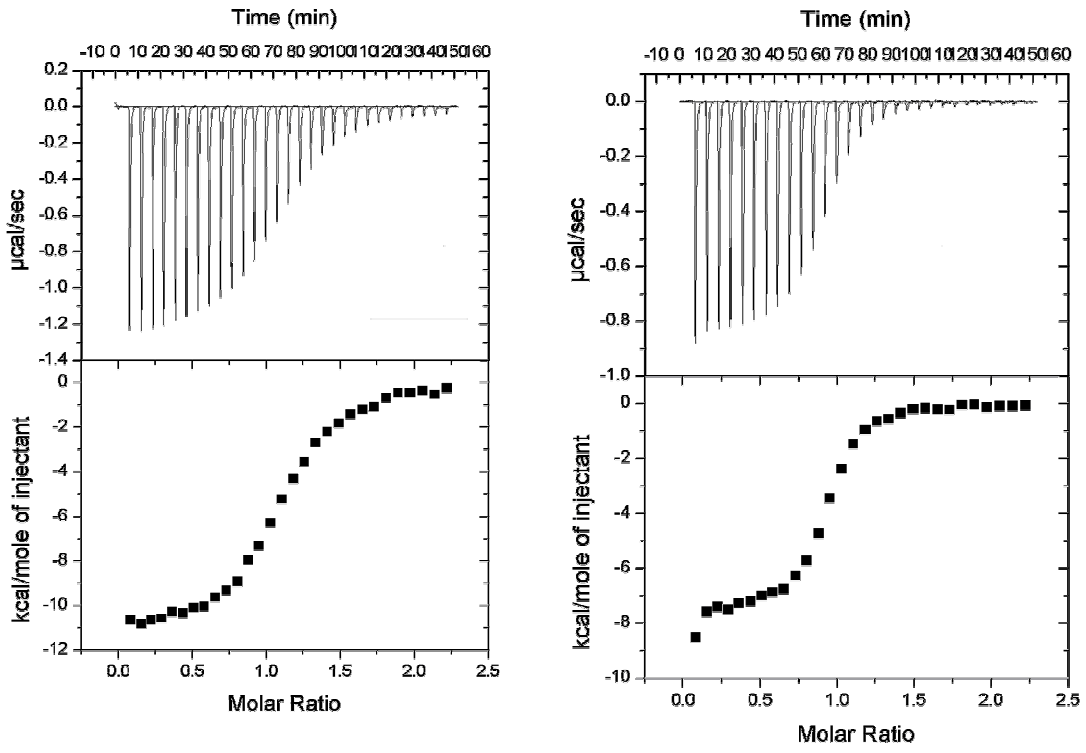

Figure 48. Representative ITC binding curves for KU-NG-1 binding to dGrp94N (left) and hHsp90N (right).

Considering the preliminary evaluation of KU-NG-1, which demonstrated selective Grp94 inhibitory activity, we were surprised by the binding affinity results. The observed binding affinities may provide information about the physiologically relevant form of Grp94, as purified recombinant Grp94 may not represent a viable model for the species present under physiological conditions. Interactions between Grp94, co-chaperones, and/or co-factors in cells may result in a conformation of Grp94 more conducive to N-

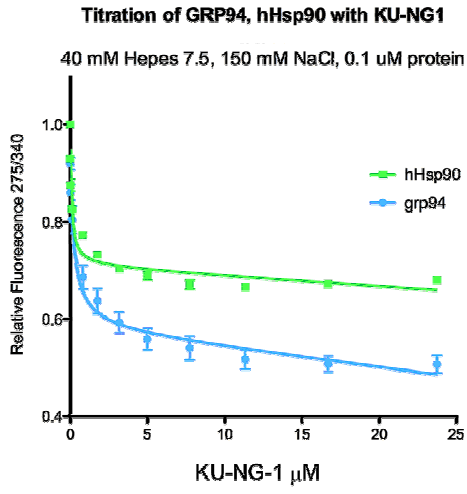

Figure 49. TFQ KU-NG-1 titration results for Grp94 and hHsp90.

terminal ligand binding; a conformation which is not populated in recombinant assays. Likewise, KU-NG-1 binds tightly to recombinant Hsp90; however it may not bind to the heteroprotein complex exhibited by Hsp90 in transformed cells. Thus, the binding data paired with KU-NG-1's cellular profile suggests a complex-induced selectivity. Although Grp94 has been shown to interact with co-chaperones and co-factors (unpublished data), no heteroprotein complexes have been identified or isolated. Therefore, studies that could verify this complex-induced selectivity are not currently possible with recombinant assays.

A second hypothesis for the observed discrepancy is that Grp94 inhibitors may exhibit a slow-tight binding profile due to the necessity for lid displacement. The binding studies completed to date were conducted on a short time scale, and do not account for time-dependent inhibition. Thus, necessary studies are ongoing and will address this hypothesis.

IV.4 Future Directions and Concluding Remarks

The development of a Grp94 isoform selective inhibitor represents an uncharted territory, and therefore the utility of such an inhibitor has yet to be demonstrated. To date, all experiments identifying Grp94 dependent processes or client proteins have been conducted with Grp94 targeted siRNA or unselective Hsp90 inhibitors. Thus, the biological profile for Grp94 results from disruption of the protein at the pre-transcriptional level, or after combinatorial disruption of both Hsp90 and Grp94. Considering the complex array of cellular responsibilities for Grp94 and the complex network involved with the mature chaperone, the only true mechanism to determine the utility of Grp94 inhibition is through the design of small molecule selective inhibitors.

Analysis of the Grp94 ATPase cycle can be utilized to explain the discrepancy between the binding and cellular data. Upon binding client proteins, alterations in the tertiary structure arise, including changes to the N-terminal binding domain.[47] Thus, it is plausible that the

conformation of the N-terminal binding pocket conducive to inhibitor binding is not revealed until client protein binding. Furthermore, conformations of the Grp94 N-terminal binding pocket may be client specific. Thus, Grp94 inhibitory scaffolds may disrupt specific clients, while not affecting others. For example, the conformation of Grp94 N-terminal binding pocket induced upon binding TLR binding may not be reciprocated upon the binding of IGFs, thus, an inhibitor such as KU-NG-1 may only bind and inhibit the conformation of Grp94 necessary for TLR trafficking. This leads to the proposal that small molecule Grp94 inhibitors can not only be designed, but can be manipulated to exhibit client specific affects.

As discussed in this chapter, we believe the first small molecule Grp94 inhibitor has been identified. Utilizing structure-based design techniques in parallel with conformational constraints, we have identified two scaffolds exhibiting Grp94 inhibition, as demonstrated through a novel Toll-trafficking assay. Development of a class of imidazole isosteres yielded nanomolar compounds, one of which, KU-NG-1, manifests ~ 30 nM activity.

Collaborations with the Gewirth laboratory have produced a co-crystal structure for KU-NG-1 bound to Grp94N, which is undergoing the final stages of refinement. Therefore, a clear picture of the interactions between KU-NG-1 and Grp94 will be available, expediting the structure-based development of novel compounds. The progression of Grp94 inhibitors relies opon the ability to develop relevant functional assays. Development of such assays will help analyze the proposal that client-induced conformation drives inhibitor binding, and may provide evidence that client specific inhibitors can be developed.

IV.5 Methods and Experimentals

Anti-proliferation Assay: MCF-7 and SKBr3 cells were maintained in a 1:1 mixture of Advanced DMEM/F12 (Gibco) supplemented with non-essential amino acids, L-glutamine (2

mM), streptomycin (500 μg/mL), penicillin (100 units/mL), and 10% FBS. Cells were grown to confluence in a humidified atmosphere (37 °C, 5% CO_2), seeded (2000/well, 100 μL) in 96-well plates, and allowed to attach overnight. Compound or geldanamycin at varying concentrations in DMSO (1% DMSO final concentration) was added, and cells were returned to the incubator for 72 h. At 72 h, the number of viable cells was determined using an MTS/PMS cell proliferation kit (Promega) per the manufacturer's instructions. Cells incubated in 1% DMSO were used as 100% proliferation, and values were adjusted accordingly. IC_{50} values were calculated from separate experiments performed in triplicate using GraphPad Prism.

Western Blot Analysis: MCF-7 cells were cultured as described previously[48] and treated with various concentrations of drug, GDA in DMSO (1% DMSO final concentration), or vehicle (DMSO) for 24 h. Cells were harvested in cold PBS and lysed in RIPA lysis buffer containing 1 mM PMSF, 2 mM sodium orthovanadate, and protease inhibitors on ice for 1 h. Lysates were clarified at 1400 g for 10 min at 4 ºC. Protein concentrations were determined by using the Pierce BCA assay kit per the manufacturer's instructions. Equal amounts of protein (20 μg) were electrophoresed under reducing conditions, transferred to a nitrocellulose membrane, and immunoblotted with the corresponding specific antibodies. Membranes were incubated with an appropriate horseradish peroxidase-labeled secondary anti-body, developed with chemiluminescent substrate, and visualized.

IV.6 References

1. Shiu, R. P.; Pouyssegur, J.; Pastan, I., Glucose depletion accounts for the induction of two transformation-sensitive membrane proteinsin Rous sarcoma virus-transformed chick embryo fibroblasts. *Proc. Natl. Acad. Sci. USA* **1977,** 74, 3840-3844.

2. Kapoor, A.; Sanyal, A. J., Endoplasmic reticulum stress and the unfolded protein response. *Clin. Liver Dis.* **2009,** 13, 581-590.

3. Fu, Y.; Lee, A. S., Glucose regulated proteins in cancer progression, drug resistance and immunotherapy. *Cancer Biol. Ther.* **2006,** 5, 741-744.

4. McLaughlin, M.; Vandenbroeck, K., The endoplasmic reticulum protein folding factory and its chaperones: new targets for drug discovery? *Br. J. Pharmacol.* **2011,** 162, 328-345.

5. Dearth, R. K.; Cui, X.; Kim, H. J.; Kuiatse, I.; Lawrence, N. A.; Zhang, X.; Divisova, J.; Britton, O. L.; Mohsin, S.; Allred, D. C.; Hadsell, D. L.; Lee, A. V., Mammary tumorigenesis and metastasis caused by overexpression of insulin receptor substrate 1 (IRS-1) or IRS-2. *Mol. Cell Biol.* **2006,** 26, 9302-9314.

6. Chang, Q.; Li, Y.; White, M. F.; Fletcher, J. A.; Xiao, S., Constitutive activation of insulin receptor substrate 1 is a frequent event in human tumors: therapeutic implications. *Cancer Res.* **2002,** 62, 6035-6038.

7. Brzezianska, E.; Pastuszak-Lewandoska, D., A minireview: The role of MAPK/ERK and PI3K/Akt pathways in thyroid follicular cell-derived neoplasm. *Front. Biosci.* **2011,** 16, 422-439.

8. Cakir, M.; Grossman, A. B., Targeting MAPK (Ras/ERK) and PI3K/Akt pathways in pituitary tumorigenesis. *Expert Opin. Ther. Targets* **2009,** 13, 1121-1134.

9. Meier, F.; Schittek, B.; Busch, S.; Garbe, C.; Smalley, K.; Satyamoorthy, K.; Li, G.; Herlyn, M., The RAS/RAF/MEK/ERK and PI3K/AKT signaling pathways present molecular targets for the effective treatment of advanced melanoma. *Front. Biosci.* **2005,** 10, 2986-3001.

10. Bommer, G. T.; Feng, Y.; Iura, A.; Giordano, T. J.; Kuick, R.; Kadikoy, H.; Sikorski, D.; Wu, R.; Cho, K. R.; Fearon, E. R., IRS1 regulation by Wnt/beta-catenin signaling and varied contribution of IRS1 to the neoplastic phenotype. *J. Biol. Chem.* **2010,** 285, 1928-1938.

11. Xia, W.; Voellmy, R., Hyperphosphorylation of heat shock transcription factor 1 is correlated with transcriptional competence and slow dissociation of active factor trimers. *J. Biol. Chem.* **1997,** 272, 4094-4102.

12. Saitoh, T.; Yanagita, T.; Shiraishi, S.; Yokoo, H.; Kobayashi, H.; Minami, S.-i.; Onitsuka, T.; Wada, A., Down-regulation of cell surface insulin receptor and insulin receptor substrate-1 phosphorylation by inhibitor of 90-kDa heat-shock protein family: Endoplasmic reticulum retention of monomeric insulin receptor precursor with calnexin in adrenal chromaffin cells. *Mol. Pharmacol.* **2002,** 62, 847-855.

13. Liu, B.; Li, Z., Endoplasmic reticulum HSP90b1 (gp96, grp94) optimizes B-cell function via chaperoning integrin and TLR but not immunoglobulin. *Blood* **2008,** 112, 1223-1230.

14. Randow, F.; Seed, B., Endoplasmic reticulum chaperone gp96 is required for innate immunity but not cell viability. *Nat. Cell Biol.* **2001,** 3, 891-896.

15. Morales, C.; Wu, S.; Yang, Y.; Hao, B.; Li, Z., Drosophila glycoprotein 93 Is an ortholog of mammalian heat shock protein gp96 (grp94, HSP90b1, HSPC4) and retains disulfide bond-independent chaperone function for TLRs and integrins. *J. Immunol.* **2009,** 183, 5121-5128.

16. Desgrosellier, J. S.; Cheresh, D. A., Integrins in cancer: biological implications and therapeutic opportunities. *Nat. Rev. Cancer* **2010,** 10, 890-890.

17. Eletto, D.; Dersh, D.; Argon, Y., GRP94 in ER quality control and stress responses. *Semin. Cell Dev. Biol.* **2010,** 21, 479-485.

18. Ostrovsky, O.; Ahmed, N. T.; Argon, Y., The chaperone activity of GRP94 toward insulin-like growth factor II is necessary for the stress response to serum deprivation. *Mol. Biol. Cell* **2009,** 20, 1855-64.

19. Ostrovsky, O.; Eletto, D.; Makarewich, C.; Barton, E. R.; Argon, Y., Glucose regulated protein 94 is required for muscle differentiation through its control of the autocrine production of insulin-like growth factors. *Mol. Cell Res.* **2010,** 1803, 333-341.

20. Wanderling, S.; Simen, B. B.; Ostrovsky, O.; Ahmed, N. T.; Vogen, S. M.; Gidalevitz, T.; Argon, Y., GRP94 is essential for mesoderm induction and muscle development because it regulates insulin-like growth factor secretion. *Mol. Biol. Cell.* **2007,** 18, 3764-3775.

21. Samani, A. A.; Yakar, S.; LeRoith, D.; Brodt, P., The role of the IGF system in cancer growth and metastasis: overview and recent insights. *Endocr. Rev.* **2007,** 28, 20-47.

22. Wu, A.; Tu, X.; Prisco, M.; Baserga, R., Regulation of upstream binding factor 1 activity by insulin-like growth factor I receptor signaling. *J. Biol. Chem.* **2005,** 280, 2863-2872.

23. Nicchitta, C. V.; Carrick, D. M.; Baker-Lepain, J. C., The messenger and the message: gp96 (GRP94)-peptide interactions in cellular immunity. *Cell Stress Chaperones* **2004,** 9, 325-331.

24. Schaiff, W. T.; Hruska, K. A., Jr.; McCourt, D. W.; Green, M.; Schwartz, B. D., HLA-DR associates with specific stress proteins and is retained in the endoplasmic reticulum in invariant chain negative cells. *J. Exp. Med.* **1992,** 176, 657-666.

25. Yang, Y.; Liu, B.; Dai, J.; Srivastava, P. K.; Zammit, D. J.; Lefrancois, L.; Li, Z., Heat shock protein gp96 is a master chaperone for toll-like receptors and is important in the innate function of macrophages. *Immunity* **2007,** 26, 215-226.

26. Vandenbroeck, K.; Martens, E.; Alloza, I., Multi-chaperone complexes regulate the folding of interferon-gamma in the endoplasmic reticulum. *Cytokine* **2006,** 33, 264-273.

27. Alloza, I.; Martens, E.; Hawthorne, S.; Vandenbroeck, K., Cross-linking approach to affinity capture of protein complexes from chaotrope-solubilized cell lysates. *Anal. Biochem.* **2004,** 324, 137-142.

28. McLaughlin, M.; Alloza, I.; Vandenbroeck, K., Different chaperone usage by IL-12 and IL-23 during their assembly reveals novel targets for intervention with cytokine secretion in neuroinflammation. *Neuroimmunol.* **2008,** 203, 268.

29. Zuany-Amorim, C.; Hastewell, J.; Walker, C., Toll-like receptors as potential therapeutic targets for multiple diseases. *Nat. Rev. Drug Discov.* **2002,** 1, 797-807.

30. Maynard, J. C.; Pham, T.; Zheng, T.; Jockheck-Clark, A.; Rankin, H. B.; Newgard, C. B.; Spana, E. P.; Nicchitta, C. V., Gp93, the Drosophila GRP94 ortholog, is required for gut epithelial homeostasis and nutrient assimilation-coupled growth control. *Dev. Biol.* **2010,** 339, 295-306.

31. Goodsell, D. S.; Morris, G. M.; Olson, A. J., Automated docking of flexible ligands: Applications of AutoDock. *J. Mol. Recognit.* **1996,** 9, 1-5.

32. Jain, A. N., Surflex: Fully automatic flexible molecular docking using a molecular similarity-based search engine. *J. Med. Chem.* **2003,** 46, 499-511.

33. Jain, A. N., Surflex-Dock 2.1: Robust performance from ligand energetic modeling, ring flexibility, and knowledge-based search. *J. Comput. Aided Mol. Des.* **2007,** 21, 281-306.

34. Gazit, G.; Lu, J.; Lee, A. S., De-regulation of GRP stress protein expression in human breast cancer cell lines. *Breast Cancer Res. Treat.* **1999,** 54, 135-146.

35. Hodorova, I.; Rybarova, S.; Solar, P.; Vecanova, J.; Prokopcakova, L.; Bohus, P.; Solarova, Z.; Mellova, Y.; Schmidtova, K., Gp96 and its different expression in breast carcinomas. *Neoplasma* **2008,** 55, 31-35.

36. Zheng, H. C.; Takahashi, H.; Li, X. H.; Hara, T.; Masuda, S.; Guan, Y. F.; Takano, Y., Overexpression of GRP78 and GRP94 are markers for aggressive behavior and poor prognosis in gastric carcinomas. *Hum. Pathol.* **2008,** 39, 1042-1049.

37. Pan, Z.; Erkan, M.; Streit, S.; Friess, H.; Kleef, J., Silencing of GRP94 expression promotes apoptosis in pancreatic cancer cells. *Int. J. Oncol.* **2009,** 35, 823-828.

38. Wang, X. P.; Qiu, F. R.; Liu, G. Z.; Chen, R. F., Correlation between clinicopathology and expression of heat shock protein 70 and glucose-regulated protein 94 in human colonic adenocarcinoma. *World J. Gastroenterol.* **2005,** 11, 1056-1059.

39. Wang, Q.; He, Z.; Zhang, J.; Wang, Y.; Wang, T.; Tong, S.; Wang, L.; Wang, S.; Chen, Y., Overexpression of endoplasmic reticulum molecular chaperone GRP94 and GRP78 in human lung cancer tissues and its significance. *Cancer Detect. Prev.* **2005,** 29, 544-551.

40. Wang, X. P.; Liu, G. Z.; Song, A. L.; Chen, R. F.; Li, H. Y.; Liu, Y., Expression and significance of heat shock protein 70 and glucose-regulated protein 94 in human esophageal carcinoma. *World J. Gastroenterol.* **2005,** 11, 429-432.

41. Langer, R.; Feith, M.; Siewert, J. R.; Wester, H. J.; Hoefler, H., Expression and clinical significance of glucose regulated proteins GRP78 (BiP) and GRP94 (GP96) in human adenocarcinomas of the esophagus. *BMC Cancer* **2008,** 8, 70.

42. Chen, X.; Ding, Y.; Liu, C. G.; Mikhail, S.; Yang, C. S., Overexpression of glucose-regulated protein 94 (Grp94) in esophageal adenocarcinomas of a rat surgical model and humans. *Carcinogenesis* **2002,** 23, 123-130.

43. Nomura, H.; Uzawa, K.; Yamano, Y.; Fushimi, K.; Ishigami, T.; Kato, Y.; Saito, K.; Nakashima, D.; Higo, M.; Kouzu, Y.; Ono, K.; Ogawara, K.; Shiiba, M.; Bukawa, H.; Yokoe, H.; Tanzawa, H., Network-based analysis of calcium-binding protein genes identifies Grp94 as a target in human oral carcinogenesis. *Br. J. Cancer* **2007,** 97, 792-801.

44. Fraley, S. I.; Feng, Y.; Krishnamurthy, R.; Kim, D. H.; Celedon, A.; Longmore, G. D.; Wirtz, D., A distinctive role for focal adhesion proteins in three-dimensional cell motility. *Nat. Cell Biol.* **2010,** 12, 598-604.

45. Nirmalanandhan, V. S.; Duren, A.; Hendricks, P.; Vielhauer, G.; Sittampalam, G. S., Activity of anticancer agents in a three-dimensional cell culture model. *Assay Drug Dev. Technol.* **2010,** 8, 581-590.

46. Dollins, D. E.; Warren, J. J.; Immormino, R. M.; Gewirth, D. T., Structures of GRP94-nucleotide complexes reveal mechanistic differences between the Hsp90 chaperones. *Mol. Cell* **2007,** 28, 41-56.

47. Wearsch, P. A.; Nicchitta, C. V., Interaction of endoplasmic reticulum chaperone GRP94 with peptide substrates is adenine nucleotide-independent. *J. Biol. Chem.* **1997,** 272, 5152-5156.

48. Clevenger, R. C.; Blagg, B. S. J., Design, synthesis, and evaluation of a radicicol and geldanamycin chimera, radamide. *Org. Lett.* **2004,** 6, 4459-4462.

Chapter V

The Design, Synthesis and Biological Evaluation of a Pro-mustard Irreversible Alkylator of Hsp90

V.1 Rationale for an Irreversible Hsp90 Alkylator

As discussed in Chapter I, numerous detriments exist with current Hsp90 inhibitors undergoing clinical evaluation. While many of these complications arise from *pan*-inhibition of all four Hsp90 isoforms, biological events, such as heat shock induction, are believed inherent to N-terminal Hsp90 inhibition. This is a consequence of heat shock factor-1 (HSF-1) release and subsequent binding to the heat shock element (HSE), which induces transcription of the heat shock genes.[1, 2] Under non-stressed conditions, Hsp90 binds HSF-1, preventing its function as a transcription factor (**1**, Figure 50).[3] In contrast, under stressed conditions, such as the accumulation of denatured proteins, HSF-1 is released from Hsp90 (**2**). Subsequent trimerization

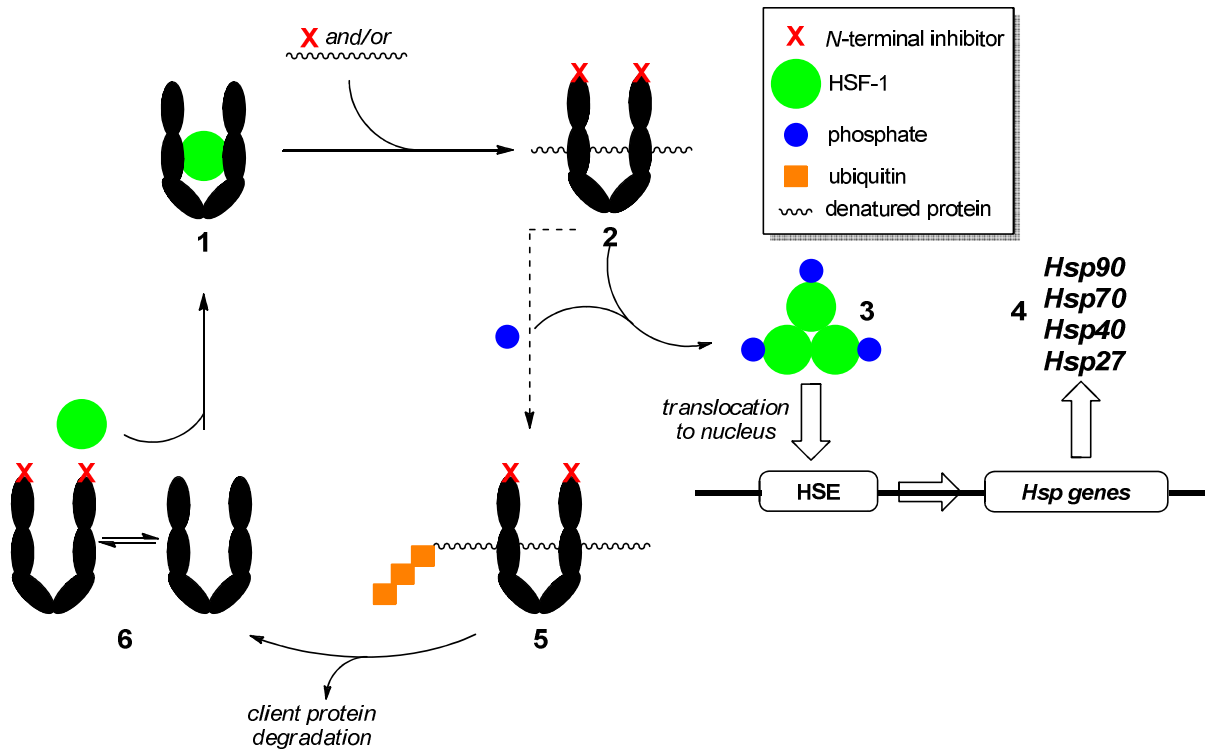

Figure 50. Heat shock factor-1 mediated induction of the heat shock response.

and phosphorylation of HSF-1 renders the active HSF-1 transcription factor (**3**).[2-4] This phosphorylated trimer translocates into the nucleus and binds the HSE to promote transcription of HSP genes (**4**).[2-4] N-terminal Hsp90 inhibitors also stimulate HSF-1 release, and induction of the heat shock response (HSR).[5] Thus, while client proteins are degraded upon Hsp90 inhibition (**5)**, the intracellular concentration of Hsp90 and various other anti-apoptotic chaperones (Hsp70, Hsp40 and Hsp27) are induced. This pro-survival response, specifically induction of the target protein, Hsp90, has resulted in dosing and scheduling issues with Hsp90 inhibitors in the clinic.[6] Therefore, a solution to this problem may lie in an Hsp90 inhibitor that results in synchronous degradation of the chaperone alongside client proteins. Although HSF-1 release and heat shock induction would still occur, a significant concentration of Hsp90 would succumb to proteasome degradation, culminating in an overall stagnant intracellular Hsp90 concentration.

V. 2 Design of 17-CEAG

Studies resulting from our laboratory and others have revealed the hydroquinone of GDA, as compared to the quinone, to exhibit greater activity against transformed cells.[7] This finding resulted in subsequent studies that identified NADH quinone oxidoreductase (NQO1) as the enzyme responsible for reduction of the quinone to the more active hydroquinone.[8-10] Xenobiotic metabolism is a secondary function of NQO1, as its primary biological role is to maintain a reduced antioxidant state of coenzyme Q (CoQ) in the mitochondrial electron transport chain.[11-13] Nonetheless, NQO1's secondary role in xenobiotic metabolism is one of importance, as numerous quinone containing molecules are known to undergo NQO1 mediated reduction.[14]

Previous studies have shown that 17-amino substitutions to the GDA scaffold maintain high affinity for Hsp90.[15, 16] The dependence of ansamycin analogs upon NQO1 for reduction, provided a novel approach towards the development of a mechanism-based irreversible Hsp90 inhibitor that contained a pro-mustard functionality, namely 17-chloroethylamino-17-demethoxygeldanamycin (17-CEAG, Figure 51). This compound was previously patented in 2006 for photolabeling purposes; however, alkylation studies were never disclosed.[17]

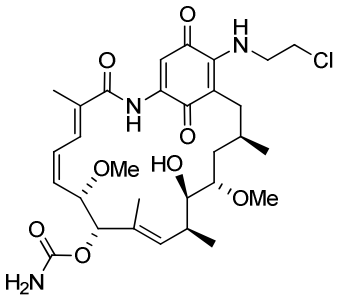

Figure 51. Structure of 17-CEAG.

In the quinone oxidation state, the pendent nitrogen lone-pair is delocalized into the quinone π-system. Upon reduction by NQO1 the electron-deficient quinone is transformed into an electron-rich hydroquinone. Thus, delocalization of the nitrogen lone pair is unfavorable, rendering the electrons reactive and available to displace the appended chlorine *via* an intramolecular S_N2 mechanism (Figure 52).[18, 19] The resulting aziridinium ion then provides the requisite functionality for Hsp90 alkylation upon binding.[18, 19] As expected, Surflex[20, 21] molecular modeling studies suggest the 17-CEAG aziridine to bind Hsp90 similarly to 17-AAG with the nucleophilic Lys44 poised for attacked onto the aziridinium (Figure 53). Once alkylated, the Hsp90 machinery should become ubiquitinylated and subsequently degraded by

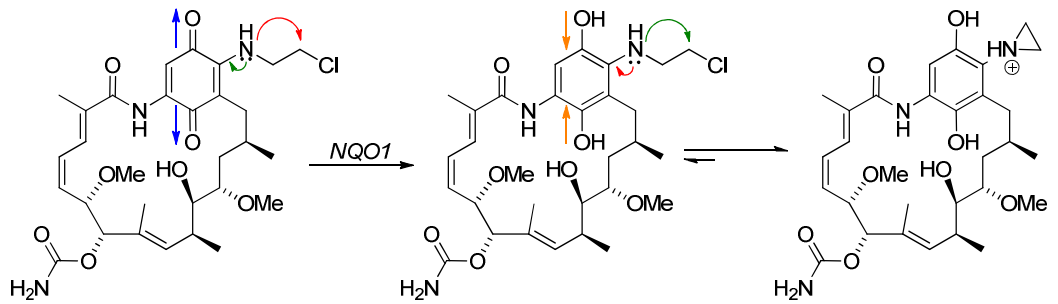

Figure 52. Reduction/activation of 17-CEAG *via* NQO1. Electron flow depicted by green (favorable) and red (unfavorable) arrows. Electronic nature of quinone oxygens depicted with electron withdrawal in blue and electron donation in orange.

the proteasome.[22] This degradation is proposed to counteract induction caused by HSF-1 release; thus, leading to a negligible change in Hsp90 concentration.

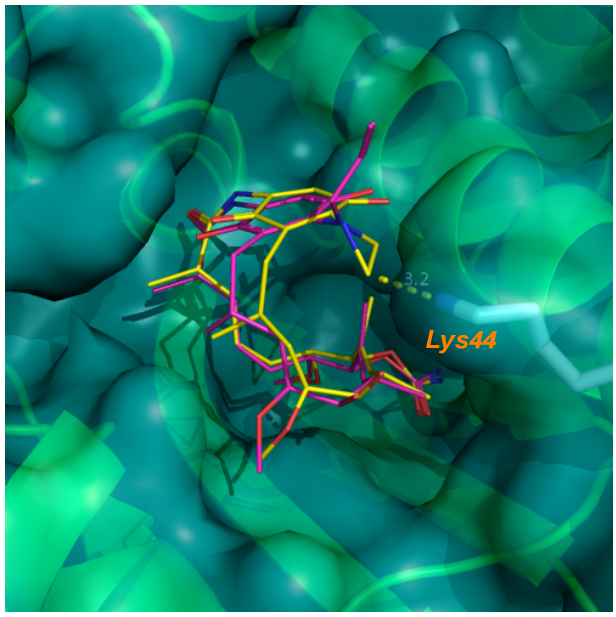

Figure 53. Overlay of 17-CEAG aziridine (yellow) and 17-AAG (magenta) in the N-terminal Hsp90 ATP-binding pocket.

V.3 Synthesis of 17-CEAG

In accordance with previous 17-amino-17-demethoxygeldanamycin derivatives,[23] 17-CEAG was synthesized in one step from GDA (Scheme 7). Upon treatment of GDA with 2-chloroethylamine hydrochloride and diisopropylethylamine (DIPEA) in dichloromethane (DCM) at room temperature, nucleophilic displacement of the 17-methyl ether resulted in the desired compound, 17-CEAG, in 90% yield.

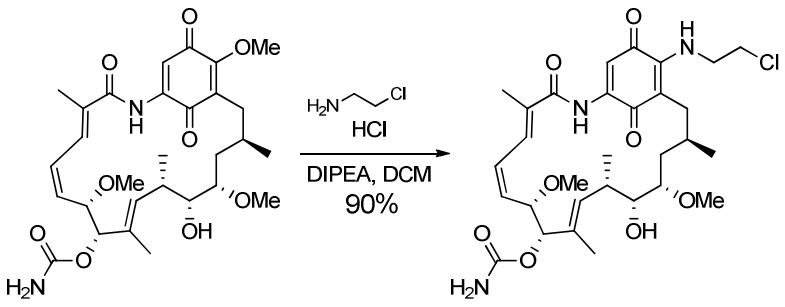

Scheme 7. Synthesis of 17-CEAG.

V.4 Biological Evaluation of 17-CEAG

Upon synthesis of 17-CEAG, biological evaluation was undertaken in collaboration with David Ross' laboratory at The University of Colorado Denver to elucidate the activity profile.

V.4.1 NQO1 Reduction Dependence

NQO1 (also known as DT-diaphorase) is an obligate 2-electron transfer flavoprotein that catalyzes the reduction of quinones to hydroquinones.[12-14, 24] In 1999, researchers at the National Cancer Institute (NCI) aimed to determine the metabolic fate of ansamycin-based Hsp90 inhibitors in hopes of elucidating toxicity issues associated with this class of inhibitors. Results suggested 17-AAG to be a substrate for NQO1 reduction.[8] Furthermore, the reduced form of 17-AAG, 17-AAGH_2, exhibited a 32-fold increase in growth inhibitory activity against various cell-lines.[8] These studies demonstrated that 17-amino substituted ansamycin analogs are substrates for NQO1.

In accordance with the studies completed at NCI, 17-CEAG was shown to be dependent upon NQO1 for reduction to 17-CEAGH_2 (Figure 54). Incubation of 17-CEAG with NADH in potassium phosphate buffer was not sufficient to reduce the parent compound, and only the quinone species was present by HPLC analysis. However, upon addition of NQO1 to the reaction mixture, rapid reduction occurred revealing near complete conversion to 17-CEAGH_2.

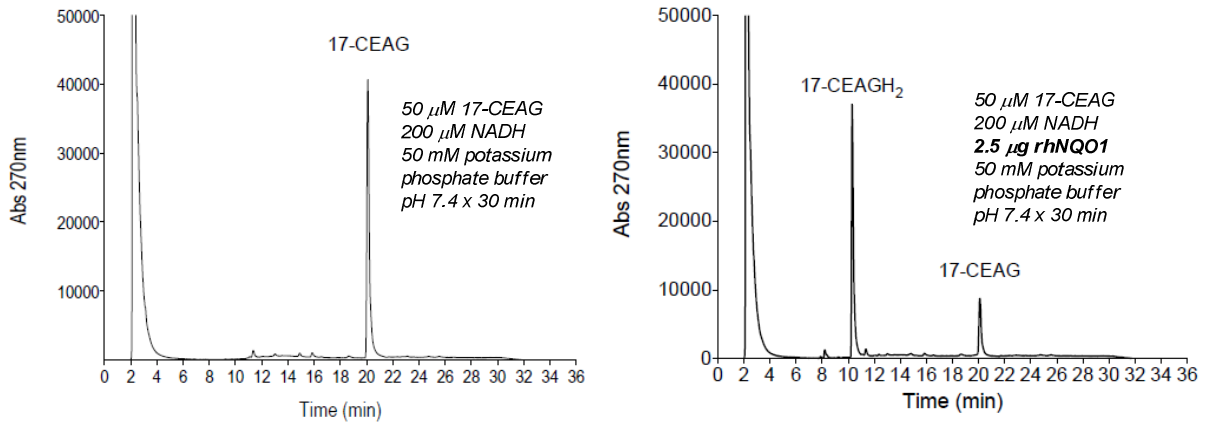

Figure 54. Dependence upon NQO1 for reduction of 17-CEAG to 17-CEAGH_2. Incubation of 17-CEAG without NQO1 (left) and incubation of 17-CEAG in the presence of NQO1 (right).

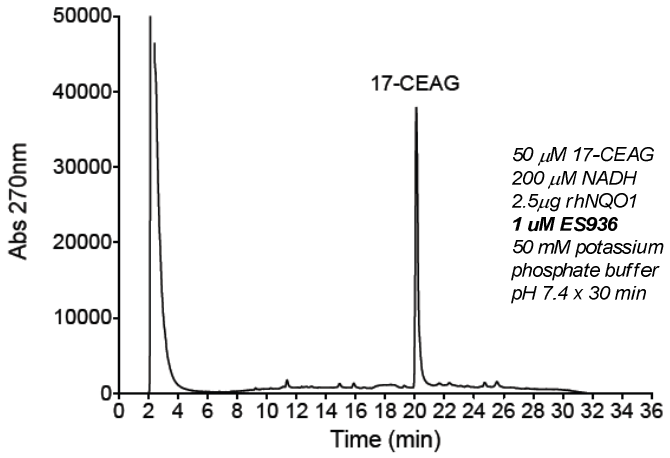

Figure 55. Affect of NQO1 inhibitor, ES936, on the reduction of 17-CEAG.

In order to further verify the dependence upon NQO1 for formation of 17-CEAGH_2, a small molecule irreversible NQO1 inhibitor, ES936, was incubated with NQO1 prior to addition of 17-CEAG. As observed in Figure 55, ES936 completely abolished the reduction of 17-CEAG, as only the quinone form was present. Results from these experiments clearly demonstrate that 17-CEAG is an NQO1 substrate and is dependent upon the reductase for conversion to 17-CEAGH_2.

V.4.2 Anti-proliferative Activity

Previous studies suggest mammalian cell cultures to be more sensitive to the hydroquinone form of ansamycins.[7] Furthermore, research has shown cell lines exhibiting higher concentrations of NQO1 are more sensitive to ansamycin treatment than cell lines deficient in NQO1.[25, 26] To parallel previously studies, 17-CEAG was evaluated for anti-proliferative activity against two isogenic cell lines: 1) MDA-468 breast cancer cells, which are NQO1 null as a consequence of a genetic polymorphism; and 2) MDA-468 (NQO1) cells which have been stably transfected to express high levels of NQO1.

Firstly, the intracellular concentration of each 17-CEAG species was measured *via* HPLC analysis. As shown in Figure 56, the only species present in NQO1 null cells was 17-CEAG. Additionally, the size of the peak in the HPLC trace demonstrates poor membrane permeabililty for the quinone species, consistent with previous studies. Other than improved binding

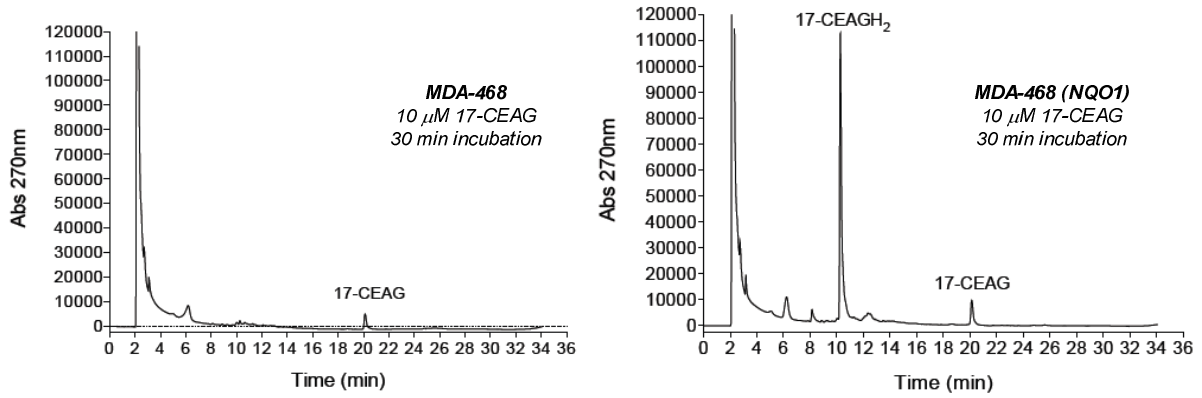

Figure 56. Oxidation state of 17-CEAG in MDA-468 (NQO1 null) cells (left) and MDA-468 (NQO1) cells (right).

interactions with the Hsp90 N-terminal binding pocket, superior intracellular sequestration and thus higher intracellular concentrations have been proposed as reasons for the improved activity manifested by hydroquinone ansamycin species.[7] Therefore, it was not surprising that cells expressing high levels of NQO1, exhibited a high intracellular concentration of 17-CEAGH$_2$, which further supports that ansamycin hydroquinone species are more efficiently sequestered intracellulary than the quinone counterparts.

Table 8. Anti-proliferation activity of 17-CEAG against MDA-468 and MDA-468 (NQO1) cell-lines.

Compound	**MDA-468** IC_{50} (μM)	**MDA-468 (NQO1)** IC_{50} (μM)
17-AAG	10.05	0.86
17-CEAG	4.53	0.37

MTT cytotoxicity assay

In addition, as observed in Table 8, 17-CEAG manifested ~12-fold higher anti-proliferative activity against MDA-468 (NQO1) cells than MDA-468 cells. This ~12-fold increase in activity was also observed upon treatment

of the cell-lines with 17-AAG, which is comparable to activity exhibited by other NQO1 dependent ansamycins.

V.4.3 Western Blot Analyses

To confirm cytotoxic activity resulted from Hsp90 inhibition, Western Blot analyses were conducted on MDA-468 (NQO1) cell lysates after treatment with 17-CEAG and 17-AAG, both in the presence and absence of NQO1 inhibitor ES936. As shown in Figure 57, Akt, a client of Hsp90, demonstrated a dose-dependent degradation in the presence of both 17-AAG and 17-CEAG, which is indicative of Hsp90 inhibition. As discussed previously, inhibition of Hsp90 with N-terminal inhibitors results in HSF-1 mediated heat shock induction. In the presence of a reversible Hsp90 inhibitor (17-AAG), dissociation of the inhibitor from Hsp90 occurs, allowing the chaperone to continue the protein folding cycle. Thus, no Hsp90 degradation occurs to counteract the HSF-1 mediated induction, which results in an overall increase in Hsp90

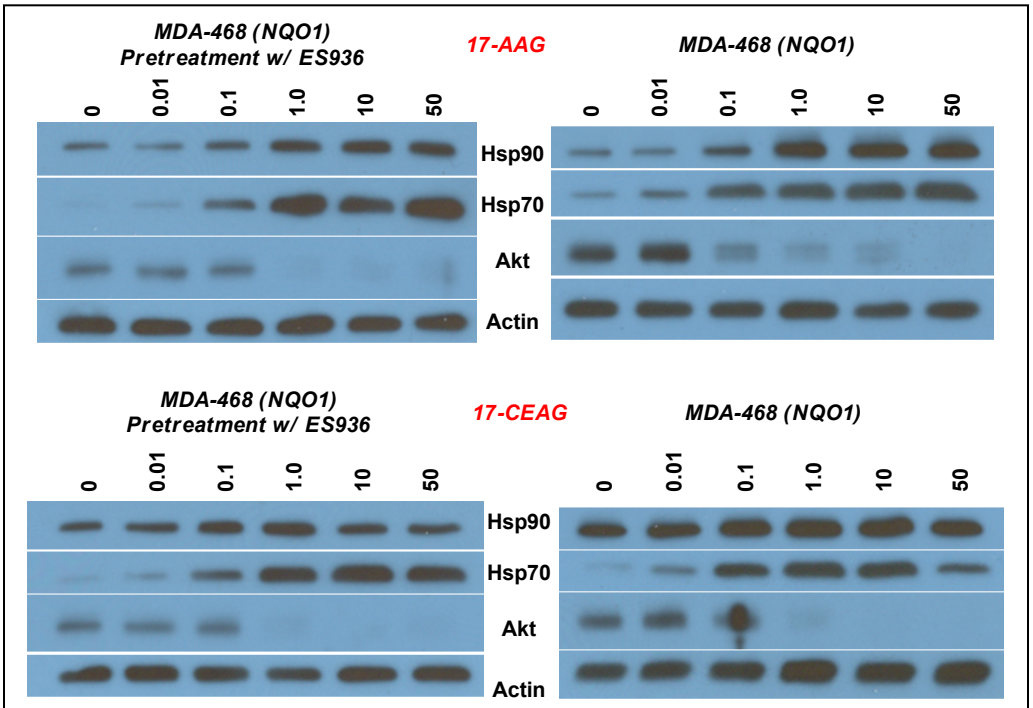

Figure 57. Western Blot analyses of MDA-468 (NQO1) cell lysates after treatment with 17-AAG and 17-CEAG; both in the presence and absence of ES936. Concentrations expressed as μM.

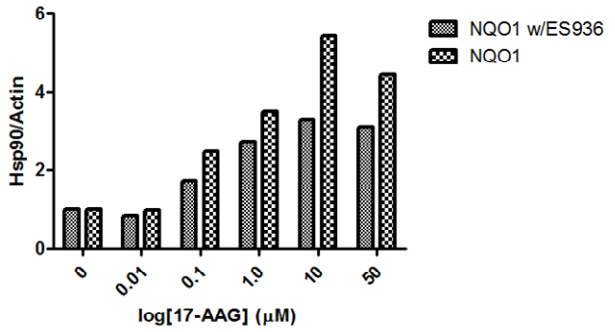

Figure 58. Densitometry results of the Western Blots from MDA-468 (NQO1) cell lines after treatment with 17-AAG.

concentration. This phenomenon is observed after treatment of MDA-468 (NQO1) cells with 17-AAG, and is illustrated in Figure 58. In contrast, upon treatment of MDA-468 (NQO1) cells with 17-CEAG, client protein degradation occurred at similar concentrations to 17-AAG (10–100 nM); however, Hsp90 levels remained constant (Figure 59) while Hsp70 levels increased. As expected, in the presence of ES936, Hsp90 induction is observed. This can be attributed to inhibition of NQO1, which mitigates the formation of 17-CEAGH_2, thus eliminating the alkylation of Hsp90. However, at high concentrations of 17-CEAG, occupation of NQO1 by 17-CEAG prevents inhibition of the enzyme by ES936. Thus, 17-CEAG reduction occurs and subsequent Hsp90 alkylation results in regression of Hsp90 concentration to control levels. Therefore, Western Blot analyses confirm the hypothesis that NQO1 dependent formation of 17-CEAGH_2 leads to Hsp90 alkylation and subsequent degradation, resulting in a negligible overall change in Hsp90 levels.

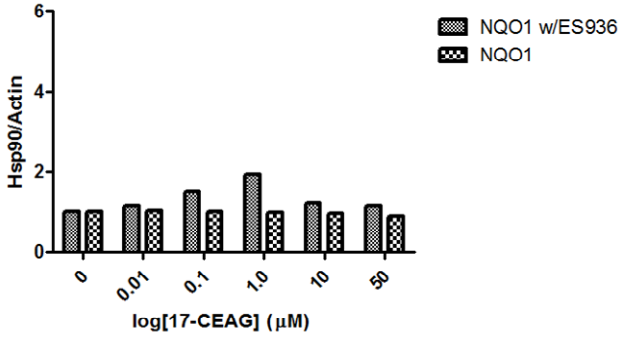

Figure 59. Densitometry results of the Western Blots from MDA-468 (NQO1) cell lines after treatment with 17-CEAG.

V.5 Future Studies and Concluding Remarks

Prior to publishing the profile for 17-CEAG, more studies are needed. Firstly, Hsp90 alkylation studies must be completed to ensure protein modification is occuring. Preliminary alkylation studies have failed; however condition optimization is ongoing with the Desaire Laboratory at The University of Kansas. Alkylation was hypothesized to be the rate-limiting experiment, as facile auto-oxidation back to the quinone species *in vitro* has been reported previously with 17-amino ansamycin inhibitors, which would mitigate the ability to alkylate the protein. Secondly, Western Blot analyses need to be conducted in the presence of a proteasome inhibitor, such as bortezomib to verify the mechanism of Hsp90 degradation upon alkylation. If Hsp90 alkylation leads to proteasome mediated degradation, then inhibition of the proteasome should reveal similar Hsp90 induction as seen with 17-AAG. Both of these studies are imperative in confirming the mechanism of action for 17-CEAG.

As discussed in this chapter, a pro-mustard ansamycin-based Hsp90 inhibitor has been designed and synthesized. Knowledge of NQO1 based reduction of this class of Hsp90 inhibitor has provided rationale for the development of 17-CEAG. Our studies have shown 17-CEAG to be dependent upon NQO1 for reduction to 17-CEAGH_2, dependent upon NQO1 for anti-proliferative activity, and to exhibit dose-dependent Hsp90 client protein degradation while failing to increase Hsp90 levels up to ~1.0 μM. Therefore, 17-CEAG has exhibited the biological profile proposed at the onset of studies and represents a promising lead for the first pro-mustard Hsp90 alkylating agent.

V.6 Methods and Experimentals

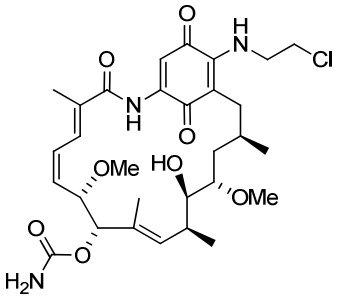

(4E,6Z,8S,9S,10E,12S,13R,14S,16R)-19-((2-chloroethyl)amino)-13-hydroxy-8,14-dimethoxy-4,10,12,16-tetramethyl-3,20,22-trioxo-2-azabicyclo[16.3.1]docosa-1(21),4,6,10,18-pentaen-9-yl carbamate (17-CEAG): To a solution of 2-chloroethylamine hydrochloride (105 mg, 0.9 mmol, 10 equiv.) and N.N-diisopropylethylamine (DIPEA, 151 mg, 1.17 mmol, 13 equiv.) in anhydrous DCM under argon at 25 ˚C, was added geldanamycin (GDA, 50 mg, 0.09 mmol). The reaction was stirred under argon at 25 ˚C for ~18 h. After complete conversion of GDA, as observed by TLC, the solvent was removed in vacuo and the residue subjected to flash chromatography utilizing 97:3 (DCM:MeOH) as the eluent. The desired product was isolated as a purple amorphous solid (49 mg, 90% yield). ^{1}H NMR ($CDCl_3$, 500 MHz) δ 9.09 (s, 1H), 7.29 (s, 1H), 6.94 (bd, *J* = 11.5 Hz, 1H), 6.56 (ddd, *J* = 11.5 Hz, 11.0 Hz, 1.0 Hz, 1H), 6.35 (bt, *J* = 5.0 Hz, 1H), 5.87 (bd, *J* = 9.5 Hz, 1H), 5.85 (bdd, *J* = 11.0 Hz, 10.0 Hz, 1H), 5.18 (s, 1H), 4.72 (bs, 2H), 4.30 (bd, *J* = 10.0 Hz, 1H), 4.03 (bs, 1H), 3.94–3.83 (m, 2H), 3.75–3.67 (m, 2H), 3.56 (ddd, *J* = 9.0 Hz, 6.5 Hz, 2.0 Hz, 1H), 3.43 (ddd, *J* = 9.0 Hz, 3.0 Hz, 3.0 Hz, 1H), 3.35 (s, 3H), 3.26 (s, 3H), 2.73 (dqd, *J* = 9.5 Hz, 7.0 Hz, 2.0 Hz, 1H), 2.70 (d, *J* = 14.0 Hz, 1H), 2.24 (dd, *J* = 14.0 Hz, 11.0 Hz, 1H), 2.01 (bs, 3H), 1.78 (d, *J* = 1.0 Hz, 3H), 1.80–1.75 (m, 2H), 1.75–1.68 (m, 1H), 1.00–0.96 (m, 6H); ^{13}C NMR ($CDCl_3$, 125 MHz) δ 183.8, 181.2, 168.3, 155.9, 144.7, 140.8, 135.9, 135.0, 133.6, 132.9, 127.0, 126.5, 110.0, 109.1, 81.6,

81.4, 81.2, 72.7, 57.1, 56.7, 46.9, 42.7, 35.1, 34.4, 32.4, 28.8, 23.0, 12.8, 12.6, 12.5; ESI–HRMS 630.2548 (M + Na, $C_{30}H_{42}ClN_3ONa$ requires 630.2558).

Western Blot Analyses: MDA468 or MDA468/NQ16 were maintained in RPMI 1640 media supplemented L-glutamine (2 mM), streptomycin (500 µg/mL), penicillin (100 units/mL), and 10% FBS. Cells were grown to confluence in a humidified atmosphere (37 °C, 5% CO2), seeded ($3x10^5$/well, 2 mL) in 6-well plates, and grown to 60% confluency prior to dosing. Cells were then treated with various concentrations of 17-CEAG or 17-AAG in DMSO (1% DMSO final concentration), or vehicle (DMSO) for 24 h. Cells were harvested in cold PBS and lysed in mammalian protein extraction reagent (MPER, Pierce) containing protease inhibitors (Roche) on ice for 1 h. Lysates were clarified at 14,000g for 15 min at 4° C. Protein concentrations were determined using the Pierce BCA protein assay kit per the manufacturer's instructions. Equal amounts of protein (5 µg) were electrophoresed under reducing conditions, transferred to a PVDF, and immunoblotted with the corresponding specific antibodies. Membranes were incubated with an appropriate horseradish peroxidase-labeled secondary antibody, developed with a chemiluminescent substrate, and visualized. Densitometry was performed using ImageJ "Gels" tool.

V.7 References

1. Soti, C.; Nagy, E.; Giricz, Z.; Vigh, L.; Csermely, P.; Ferdinandy, P., Heat shock proteins as emerging therapeutic targets. *Br. J. Pharmacol.* **2005,** 146, 769-780.

2. Voellmy, R., Feedback regulation of the heat shock response. *Handb. Exp. Pharmacol.* **2006**, (172), 43-68.

3. Powers, M. V.; Workman, P., Inhibitors of the heat shock response: biology and pharmacology. *FEBS Lett.* **2007,** 581, 3758-3769.

4. Xia, W.; Voellmy, R., Hyperphosphorylation of heat shock transcription factor 1 is correlated with transcriptional competence and slow dissociation of active factor trimers. *J. Biol. Chem.* **1997,** 272, 4094-4102.

5. Whitesell, L.; Bagatell, R.; Falsey, R., The stress response: Implications for the clinical development of Hsp90 inhibitors. *Curr. Cancer Drug Targets* **2003,** 3, 349-358.

6. Duerfeldt, A. S.; Blagg, B. S., Hsp90 inhibition: Elimination of shock and stress. *Bioorg. Med. Chem. Lett.* **2010,** 20, 4983-4987.

7. Maroney, A. C.; Marugan, J. J.; Mezzasalma, T. M.; Barnakov, A. N.; Garrabrant, T. A.; Weaner, L. E.; Jones, W. J.; Barnakova, L. A.; Koblish, H. K.; Todd, M. J.; Masucci, J. A.; Deckman, I. C.; Galemmo, R. A., Jr.; Johnson, D. L., Dihydroquinone ansamycins: Toward resolving the conflict between low in vitro affinity and high cellular potency of geldanamycin derivatives. *Biochemistry* **2006,** 45, 5678-5685.

8. Kelland, L. R.; Sharp, S. Y.; Rogers, P. M.; Myers, T. G.; Workman, P., DT-Diaphorase expression and tumor cell sensitivity to 17-allylamino, 17-demethoxygeldanamycin, an inhibitor of heat shock protein 90. *J. Natl. Cancer Inst.* **1999,** 91, 1940-1949.

9. Guo, W.; Reigan, P.; Siegel, D.; Zirrolli, J.; Gustafson, D.; Ross, D., Formation of 17-allylamino-demethoxygeldanamycin (17-AAG) hydroquinone by NAD(P)H:quinone oxidoreductase 1: role of 17-AAG hydroquinone in heat shock protein 90 inhibition. *Cancer Res.* **2005,** 65, 10006-10015.

10. Guo, W.; Reigan, P.; Siegel, D.; Zirrolli, J.; Gustafson, D.; Ross, D., The bioreduction of a series of benzoquinone ansamycins by NAD(P)H:quinone oxidoreductase 1 to more potent heat

shock protein 90 inhibitors, the hydroquinone ansamycins. *Mol. Pharmacol.* **2006,** 70, 1194-1203.

11. Dinkova-Kostova, A. T.; Talalay, P., NAD(P)H:quinone acceptor oxidoreductase 1 (NQO1), a multifunctional antioxidant enzyme and exceptionally versatile cytoprotector. *Arch. Biochem. Biophys.* **2010,** 501, 116-123.

12. Beyer, R. E.; Segura-Aguilar, J.; Di Bernardo, S.; Cavazzoni, M.; Fato, R.; Fiorentini, D.; Galli, M. C.; Setti, M.; Landi, L.; Lenaz, G., The role of DT-diaphorase in the maintenance of the reduced antioxidant form of coenzyme Q in membrane systems. *Proc. Natl. Acad. Sci. USA* **1996,** 93, 2528-2532.

13. Beyer, R. E.; Segura-Aguilar, J.; di Bernardo, S.; Cavazzoni, M.; Fato, R.; Fiorentini, D.; Galli, M. C.; Setti, M.; Landi, L.; Lenaz, G., The two-electron quinone reductase DT-diaphorase generates and maintains the antioxidant (reduced) form of coenzyme Q in membranes. *Mol. Aspects Med.* **1997,** 18 Suppl, S15-23.

14. Ross, D., Quinone reductases multitasking in the metabolic world. *Drug Metab. Rev.* **2004,** 36, 639-654.

15. Porter, J. R.; Ge, J.; Lee, J.; Normant, E.; West, K., Ansamycin inhibitors of Hsp90: Nature's prototype for anti-chaperone therapy. *Curr. Top. Med. Chem.* **2009,** 9, 1386-1418.

16. Ge, J.; Normant, E.; Porter, J. R.; Ali, J. A.; Dembski, M. S.; Gao, Y.; Georges, A. T.; Grenier, L.; Pak, R. H.; Patterson, J.; Sydor, J. R.; Tibbitts, T. T.; Tong, J. K.; Adams, J.; Palombella, V. J., Design, synthesis, and biological evaluation of hydroquinone derivatives of 17-amino-17-demethoxygeldanamycin as potent, water-soluble inhibitors of Hsp90. *J. Med. Chem.* **2006,** 49, 4606-15.

17. Xie, Q.; Wenkert, D.; Shen, Y.; Vande Woude, G. F.; Hay, R. Preparation of Geldanamycin and Derivatives to Inhibit Cancer Invasion and Identify Novel Targets. WO 2005095347 A1 20051013, 2005.

18. Beall, H. D.; Winski, S. I., Mechanisms of action of quinone-containing alkylating agents. I: NQO1-directed drug development. *Front. Biosci.* **2000,** 5, D639-648.

19. Hargreaves, R. H.; Hartley, J. A.; Butler, J., Mechanisms of action of quinone-containing alkylating agents: DNA alkylation by aziridinylquinones. *Front. Biosci.* **2000,** 5, E172-180.

20. Jain, A. N., Surflex: Fully automatic flexible molecular docking using a molecular similarity-based search engine. *J. Med. Chem.* **2003,** 46, 499-511.

21. Jain, A. N., Surflex-Dock 2.1: Robust performance from ligand energetic modeling, ring flexibility, and knowledge-based search. *J. Comput. Aided Mol. Des.* **2007,** 21, 281-306.

22. Marques, C.; Guo, W.; Pereira, P.; Taylor, A.; Patterson, C.; Evans, P. C.; Shang, F., The triage of damaged proteins: Degradation by the ubiquitin-proteasome pathway or repair by molecular chaperones. *FASEB J.* **2006,** 20, 741-743.

23. Tian, Z. Q.; Liu, Y.; Zhang, D.; Wang, Z.; Dong, S. D.; Carreras, C. W.; Zhou, Y.; Rastelli, G.; Santi, D. V.; Myles, D. C., Synthesis and biological activities of novel 17-aminogeldanamycin derivatives. *Bioorg. Med. Chem.* **2004,** 12, 5317-5329.

24. Tedeschi, G.; Chen, S.; Massey, V., DT-diaphorase. Redox potential, steady-state, and rapid reaction studies. *J. Biol. Chem.* **1995,** 270, 1198-1204.

25. Belinsky, M.; Jaiswal, A. K., NAD(P)H:quinone oxidoreductase1 (DT-diaphorase) expression in normal and tumor tissues. *Cancer Metastasis Rev.* **1993,** 12, 103-117.

26. Ross, D.; Kepa, J. K.; Winski, S. L.; Beall, H. D.; Anwar, A.; Siegel, D., NAD(P)H:quinone oxidoreductase 1 (NQO1): Chemoprotection, bioactivation, gene regulation and genetic polymorphisms. *Chem. Biol. Interact.* **2000,** 129, 77-97.